Biophysical Study of the Molecular Chaperone DnaK by Intramolecular FRET

David S. Rogawski

A thesis submitted for the degree of Master of Science
University of Otago
Dunedin, New Zealand
May 2010

Abstract

DnaK is a 70 kilodalton heat shock protein and molecular chaperone from *Escherichia coli* with an N-terminal nucleotide binding domain and C-terminal substrate binding domain. During chaperone function DnaK occupies at least two conformational states characterized by distinct biochemical properties and interdomain distances. Here we develop a method for fluorescent double labeling of DnaK, creating a reagent that reports DnaK's conformational shift via changes in Förster resonance energy transfer. We show that selective labeling can be accomplished by identifying a pair of cysteine residues whose local environments render one thiol several-fold more reactive than the other. Reactivity of cysteines introduced at various positions on the surface of DnaK was assayed using two different fluorescent dyes and two distinct assays. The fluorescent compound 7-diethylamino-3-(4'-maleimidylphenyl)-4-methylcoumarin reacted threefold faster to DnaK single-cysteine variant T136C/C15S than to S423C/C15S (rate constants of $0.124 \pm 0.003\ s^{-1}$ and $0.0433 \pm 0.0005\ s^{-1}$, respectively). This difference in reactivity was predictive of relative reactivity to Alexa Fluor 555 maleimide, for which we observed a twentyfold difference in reactivity between T136C and S423C (rate constants of $0.029 \pm 0.003\ s^{-1}$ and $0.00144 \pm 0.00004\ s^{-1}$, respectively). We prepared a variant of DnaK that contains two cysteines at positions 136 and 423 and showed that Alexa Fluor 594 maleimide reacts 13-fold faster to T136C in the nucleotide binding domain than to S423C in the substrate binding domain (rate constants of $0.048 \pm 0.005\ s^{-1}$ and $0.0036 \pm 0.0006\ s^{-1}$, respectively). Limited proteolysis demonstrated that DnaK T136C/S423C/C15S is capable of undergoing a nucleotide-dependent conformational change, suggesting it is functionally active.

We overcame low solubility of double-labeled DnaK T136C/S423C/C15S by optimizing buffer conditions and labeling with donor and acceptor fluorophores sequentially in the same reaction vessel. Our improved labeling method allowed us to make double-labeled protein that reports DnaK's conformational change with a 16% decrease in Alexa Fluor 555 donor fluorescence upon addition of adenosine triphosphate. We use Förster resonance energy transfer together with small angle x-ray scattering and limited proteolysis to show that therapeutically applicable heat shock protein 70 activity modulators interfere with DnaK's conformational shift.

Acknowledgments

I am immensely grateful to Helen Nicholson, Sue Butt, and the Otago School of Medical Sciences for generously providing me with three scholarships during my time in New Zealand. Thank you to all the friends I've made in the University of Otago Biochemistry Department. You have been engaging, supportive, and eager to listen always. Thanks Erika for graciously hosting me, my family, and the lab at your beautiful home, and Rich and Arta for the delicious meals and warm bed during my visit to the Stanford Synchrotron. Thank you Rich, Jerry, Jess, Sam, Malcolm, Rhesa, Anshul, Peter, Rob, Helen, Eleni, and Souness for making the lab such a fun place to work and think. I'm indebted to Emma for many helpful discussions.

I have grown leaps and bounds as a scientist working with Sigurd the past one and a half years. He has imparted in me a passion for protein dynamics and homeostasis and taught me an array of biophysical techniques. He has instilled in me a thirst for understanding and desire to share knowledge and research with others. Furthermore, he has taught me to be rigorous, creative, and open-minded, and further augmented my skills in designing well-controlled and informative experiments. No less importantly, I have learned from him the scientific virtues of humility and generosity.

Table of Contents

Figures

Tables

Abbreviations

115-7c	Hsp70 ATPase activator (Chang et al., 2008; Wisén and Gestwicki, 2008)
116-9e	Hsp70 ATPase inhibitor (Chang et al., 2008; Wisén and Gestwicki, 2008)
ATP	adenosine triphosphate
ADP	adenosine diphosphate
AF488	Alexa Fluor 488 maleimide
AF555	Alexa Fluor 555 maleimide
AF594	Alexa Fluor 594 maleimide
amp	ampicillin
APS	ammonium persulfate
bp	basepair
BME	β-mercaptoethanol
BSA	bovine serum albumin
CE12	Hsp70 ATPase inhibitor (Chang et al., 2008; Wisén and Gestwicki, 2008)
CHES	N-cyclohexyl-2-aminoethanesulfonic acid
chlor	chloramphenicol
CPM	7-diethylamino-3-(4'-maleimidylphenyl)-4-methylcoumarin
CV	column volumes
Da	Dalton
DEAE	diethylaminoethyl cellulose
DMF	dimethylformamide
DMSO	dimethyl sulfoxide
dNTPs	deoxyribonucleotide triphosphates
DTT	dithiothreitol
E	FRET efficiency
EDTA	ethylenediaminetetraacetic acid

FRET	Förster resonance energy transfer
FL	fluorescent labeling
FPLC	fast protein liquid chromatography
fwd	forward
GSH	reduced glutathione
HABA	4'-hydroxyazobenzene-2-carboxylic acid
HEPES	4-(2-hydroxyethyl)-1-piperazineethanesulfonic acid
IAEDANS	5-({2-[(iodoacetyl)amino]ethyl}amino)naphthalene-1-sulfonic acid
IPTG	isopropyl β-D-1-thiogalactopyranoside
kb	kilobase
kDa	kilodalton
LB	Luria broth
MB	methylene blue, Hsp70 ATPase inhibitor (Chang et al., 2008; Wisén and Gestwicki, 2008)
MES	2-(N-morpholino)ethanesulfonic acid
min	minutes
mP	milli-Polarization
MWCO	molecular weight cutoff
MY	myricetin, Hsp70 ATPase inhibitor (Chang et al., 2008; Wisén and Gestwicki, 2008)
OD_{600}	optical density at 600 nm
PIPES	piperazine-N,N′-bis(2-ethanesulfonic acid)
PMSF	phenylmethylsulfonyl fluoride
PMT	photomultiplier tube
PVDF	polyvinylidene fluoride
rcf	relative centrifugal force
rev	reverse

SAXS	small angle X-ray scattering
SDS	sodium dodecyl sulfate
SDS-PAGE	SDS polyacrylamide gel electrophoresis
SW02	Hsp70 ATPase activator (Chang et al., 2008; Wisén and Gestwicki, 2008)
TAE	tris-acetate-EDTA
TCA	trichloroacetic acid
TCEP	tris(2-carboxyethyl)phosphine
TEMED	tetramethylethylenediamine
smFRET	single molecule FRET
w/v	weight per volume

Chapter 1

Introduction

Molecular chaperones and the heat shock response

In common usage a human chaperone is "a person who for propriety accompanies one or more young unmarried women in public or in mixed company."[1] A molecular chaperone is a protein that assists other proteins to attain their functional three-dimensional conformation. Chaperone is an apt term in the biochemical sense because molecular chaperones prevent incorrect interactions between molecules with potential affinity for one another in the crowded cell environment. This thesis examines the mechanism whereby one chaperone, DnaK, binds to a large number of protein substrates to facilitate their *de novo* folding, repair, or degradation. DnaK is a member of the widely conserved heat shock protein 70 (Hsp70) family of molecular chaperones.

The traditional chaperone definition implies that chaperones are not required if a woman matures without exposing herself to the outside world; the same is true in the biochemical sense in that most purified proteins will adopt their native structure *in vitro* in the absence of molecular chaperones. In fact, the Anfinsen hypothesis states that the three-dimensional native structure of a protein is the unique most thermodynamically stable conformation of a protein and is determined solely by interactions among amino acids in the protein's primary sequence (Anfinsen, 1972). Why then are molecular chaperones required at all? The answer begins with the realization that protein native structures are stabilized by a variety of relatively weak noncovalent interactions, including ion pairing, hydrogen bonding, van der Waals interactions, and hydrophobic effects (Dill, 1990). Inside the cell, where protein concentration is often greater than 200 mg/ml (Brown, 1991), the same weak forces that stabilize protein native conformations can lead to incorrect protein interactions and aggregation. Common cell stressors further increase the risk of protein misfolding; for example, heat stress causes rapid and violent vibration of protein atoms leading to disruption of hydrogen bonds and hydrophobic interactions (Vogta et al., 1997). Another frequent stressor, reactive oxygen species, can cause amino acid modification, extensive changes in net electrical charge, covalently linked protein aggregates, and direct fragmentation of polypeptide chains (Davies, 1987). Even in the absence of stress, common cellular events create opportunities for protein misfolding. For instance, the N-terminal portion of a protein is made before the C-terminus, meaning that the partially synthesized N-terminal segment does not have C-terminal residues to interact with and is exposed in a partially folded, aggregation-prone state. This problem is solved in bacteria by the ribosomal-bound trigger

[1] "chaperone." Merriam-Webster Online Dictionary. 2007. http://merriam-webster.com (18 Apr. 2010).

factor chaperone, which cooperates with DnaK to protect nascent peptides from misfolding (Hoffman et al., 2010). Another cellular event in which inappropriate protein interactions are likely to occur is protein transport across membranes, a process during which proteins are typically unfolded or partially unfolded. Chaperones of the Hsp70 family have been shown to preserve the transport-competent state of presecretory proteins and function in initiation and completion of protein translocation (Zimmermann, 1998). Finally, many protein complexes found inside organelles, such as rubisco in chloroplasts, consist of subunits made inside the organelle bound to subunits made in the cytosol. Chaperones are required to bind these subunits and prevent incorrect interactions before complex assembly (Ellis, 1991).

Ron Laskey coined the term molecular chaperone in 1978 when describing nucleoplasmin, a nuclear protein important for proper assembly of DNA and histones into nucleosomes. Under physiological conditions, mixing DNA and histones results in an immediate precipitate, but Laskey discovered that if an excess of nucleoplasmin chaperone is first allowed to bind to histones, reducing their strong positive charge, then incorrect histone-DNA interactions are eliminated and soluble nucleosomes are formed. Additional experiments showed that under certain non-physiological conditions, soluble nucleosomes form without nucleoplasmin, demonstrating that histones and DNA by themselves contain sufficient information for nucleosome assembly and the role of the nucleoplasmin chaperone, rather than to actively direct nucleosome formation, is only to prevent incorrect ionic interactions between histones and DNA (Laskey et al., 1978).

Additional molecular chaperones were discovered by identifying certain proteins induced upon heat stress. This heat shock response has been identified in most organisms in which it has been sought with the exception of cold-adapted, stenothermal Antarctic fishes such as *Trematomus bernacchii* (Hoffman et al., 2000). The heat shock response was first studied in *Drosophila busckii*, in which high temperatures cause puffs to form on the salivary chromosomes. In the 1970s Tissieres and Mitchell connected puff formation to the induction of a small set of genes, and the molecular study of heat shock was born. The coding and regulatory sequences of heat shock genes are remarkably well conserved across kingdoms (Lindquist, 1986). Induction of heat shock genes has now been associated with a variety of stressors including alcohol, inhibitors of energy metabolism, heavy metals, oxidative stress, and fever and inflammation. Most heat shock proteins (Hsp) are molecular chaperones that protect vulnerable proteins or degrade damaged or aggregated proteins (Zylicz et al., 2001).

How chaperones actually assist protein folding is not fully understood. Some chaperones function as passive "holdases" that bind to areas of unfolded proteins and prevent aggregation. For example, oligomers of Hsp27 bind to misfolded or oxidized proteins and remodel them into intermediates fit for refolding by other chaperone systems (Mathew et al., 2009). Other chaperones are active "unfoldases" that by binding to hydrophobic regions of misfolded peptides induce local unfolding that helps overcome a kinetic barrier to the properly folded state. The remarkable GroEL/GroES chaperonin machine is the best understood example of the latter type of chaperone. The machine is a double-ringed structure weighing approximately one thousand kilodaltons (kDa) composed of fourteen 60 kDa GroEL subunits. In the binding-active conformation, the central cavity of each ring is open and the hydrophobic interior interacts with hydrophobic surfaces of a client protein. In some cases the protein-protein binding energy may be sufficient to partially or completely unfold the bound substrate, freeing it from a kinetic trap and allowing it to refold correctly (Zahn et al., 1996). Binding of ATP and GroES to the GroEL ring triggers a global conformational rearrangement causing release of substrate into a central hydrophilic cavity, encouraging burial of hydrophobic regions of the substrate and promoting folding to the native state. ATP hydrolysis permits release of GroES and newly folded substrate protein (Bukau and Horwich, 1998; Zu and Sigler, 1998). Other unfoldases include chaperones of the Hsp100 family, which dissolve insoluble protein aggregates and remodel damaged proteins by unfolding and translocating polypeptides through the central pore of a hexameric complex (Bukau et al., 2006).

While chaperones in the heat shock families act on a wide variety of substrates, function broadly in maintaining protein homeostasis, and do not provide specific structural information required for folding, a number of steric chaperones have been discovered that are required for native folding of a single protein. These include intramolecular chaperones, such as the propeptide of the protease subtilisin E that is essential for correct folding and is removed by autoproteolysis once the active conformation is attained (Pauwels et al., 2007). There are also intermolecular steric chaperones, such as those in many Gram-negative bacteria used to fold toxic enzymes that are secreted into the extracellular milieu. For example, the lipase secreted by *Burkholderia glumae* does not fold properly *in vitro* and requires a periplasmic lipase-specific foldase (Lif) to reach its active conformation (El Khattabi et al., 2000).

Here, however, we focus on the ubiquitous and promiscuous Hsp70 family of chaperones. In the 1970s C.P. Georgopolous discovered that bacteriophage lambda DNA

replication in *Escherichia coli* requires several bacterial genes, one of which he called *dnaK* (Georgopoulos, 1977). An *in vitro* system composed of purified protein components permitted identification of the molecular role of DnaK protein in lambda replication, along with its co-chaperones DnaJ and GrpE. λO protein binds to *ori*λ DNA sequences and recruits DnaB helicase attached to λP protein. The O-P-DnaB complex is stably bound to the *ori*λ and unable to move forward to unwind DNA. DnaJ and DnaK next bind and sequester λP, releasing DnaB to unwind DNA. GrpE then dissociates the DnaK-DnaJ-λP complex (Hoffmann et al., 1992). DnaK's binding and subsequent release of λP is illustrative of a general problem faced by broad spectrum molecular chaperones and DnaK in particular; that is, chaperone binds only transiently to substrate and must be able to readily release it. DnaK overcomes this challenge by undergoing a conformational change that dramatically alters its substrate binding affinity.

Hsp70 in physiology and disease

Depletion of DnaK and its co-chaperone DnaJ in *E. coli* cells causes aggregation of approximately 340 proteins (Deuerling et al., 2003), and co-immunoprecipitation experiments show that DnaK binds transiently to at least 5-10% of all newly made proteins and 20% of proteins larger than 30 kDa (Teter et al., 1999). In eukaryotes Hsp70 proteins account for 1-2% of total cellular protein (Zylicz et al., 2001) and are estimated to assist *de novo* folding of at least 10-20% of all cellular proteins (Mayer and Bukau, 2005). Beyond *de novo* folding, however, Hsp70 plays a role in an astonishing number of cellular processes. For instance, Hsp70s function in the ATP-dependent dissociation of clathrin from clathrin-coated vesicles involved in sorting cargo in eukaryotic cells (Rothman and Schmid, 1986). In addition, Hsp70 proteins assist in the translocation of peptides across membranes by preventing precursor aggregation, and there is some evidence that certain co-chaperones target substrates to specific cellular compartments. For example, the Hsp70 co-chaperone and J domain protein Djp1 in yeast has a C-terminal domain that interacts with peroxisomes (Hettema, 1998). Furthermore, Hsp70 chaperones interacts with and in general inactivate a large number of regulatory proteins including nuclear receptors, kinases, and transcription factors controlling cell homeostasis, growth, differentiation, and apoptosis. Hsp70 can be titrated away from these regulatory protein clients by stress-induced protein misfolding. In this way environmental, developmental, and pathological stressors influence signal transduction pathways via Hsp70 (Mayer and Bukau, 2005).

Hsp70 has been implicated in a large variety of human diseases and is becoming a hot topic in biomedical research with interest in Hsp70-based therapies on the rise. In humans there are 11 different genes located on different chromosomes that encode Hsp70 homologues, including the constitutively expressed version Hsc70 and various stress-inducible forms under control of the heat shock factor (HSF) (Zylicz et al., 2001). Hsp70s have been shown to be involved in cancer as well as a wide variety of protein folding and neurodegenerative diseases such as Alzheimer's, Parkinson's, Huntington's, and amyotrophic lateral sclerosis. In the case of cancer Hsp70s exacerbate disease by stabilizing mutant proteins with harmful effects on the cell, whereas in protein folding diseases Hsp70s typically work therapeutically by disassembling aggregates and degrading misfolded proteins (Mayer and Bukau, 2005).

Hsp70 is a negative regulator of apoptosis and transiently associates with cell cycle regulators like Cdk4, Wee-1, c-Myc, pRb, and p27/Kip1 in addition to kinases in mitogen-activated signal cascades (Zylicz et al., 2001). In caspase-dependent cell death, Hsp70 can inhibit the signal cascade at the pre-mitochondrial, mitochondrial, or post-mitochondrial levels by binding and sequestering signalling components such as c-Jun N-terminal Kinase and Apaf-1 (Lanneau et al., 2007). In cases where caspase activation does not occur, Hsp70 binds to apoptosis inducing factor (AIF), inhibiting AIF nuclear translocation and chromatin condensation (Ravagnan et al., 2001). Hsp70 can even rescue cells late in the apoptosis process by regulating folding and activity of caspase-activated DNase (CAD) (Sakahira and Nagata, 2002). Overexpression of Hsp70 provides resistance against apoptosis-inducing agents like tumor necrosis factor-α, staurosporin, and doxorubicin, and downregulation of Hsp70 increases susceptibility to these molecules (Mayer and Bukau, 2005). Overexpression of Hsp70 is often correlated with increased malignancy of tumors (Zylicz et al., 2001), while RNAi against Hsp70 inhibits growth of gastric cancer cells, induces cell cycle arrest and triggers apoptosis (Xiang et al., 2008). Lastly, Hsp70 has been shown to restore enzymatic activity of mutant proteins (Singh et al., 2010), possibly allowing cancer cells to proliferate despite DNA mutations and transcription errors. In sum, Hsp70 chaperones promote cell survival in cancer both by directly inhibiting apoptosis and by enhancing general proteostasis.

In neurodegenerative diseases characterized by excessive apoptosis, overexpression of Hsp70 can reduce or eliminate symptoms caused by a disease-related gene. Overexpression of Hsp70 rescues neurons from the toxic effects of intracellular accumulation of amyloid beta (Aβ), an early event associated with Alzheimer's disease (Magrané et al., 2004), and Hsp70

inhibits the self-assembly of Aβ aggregates *in vitro* when Hsp70 is added to Aß oligomers but not fibrils (Evans et al., 2006). Hsp70 overexpression is particularly therapeutic in models of Parkinson's Disease, a neurodegenerative disorder characterized by proteinacious inclusions within neurons called Lewy bodies, which are mainly composed of aggregated α-synuclein protein. Transgenic flies expressing α-synuclein display many features of human Parkinson's Disease including loss of dopaminergic neurons in adulthood, Lewy body formation, and locomotor dysfunction. Increasing the level of Hsp70, either with an Hsp70 transgene or by chemically activating the heat shock response, protects dopaminergic neurons from degenerative cell death. Interestingly, flies with increased Hsp70 expression still have α-synuclein inclusion bodies in their neurons, suggesting that Lewy bodies are inert while soluble α-synuclein is toxic, and Hsp70 protects cells from the soluble toxic form. There is evidence that Hsp70 protects cells from toxic α-synuclein by assisting its translocation into lysosomes for degradation and, in cooperation with its co-chaperone and E3 ubiquitin ligase CHIP, targeting α-synuclein to the proteasome for degradation. In addition, Hsp70 inhibits α-synuclein amyloid formation *in vitro*, apparently by "capping" prefibrillar species. This capping function may block the ability of α-synuclein to punch holes in membranes or keep α-synuclein soluble and accelerate its degradation via the proteasome or autophagy (Witt, 2010).

It is interesting to note that Hsp70 is required for the propagation of yeast prions, infectious proteins that cause existing polypeptides in the host organism to take on their own misfolded conformation. Endogenous cellular prion protein, PrP^{C}, is a primarily α-helical, membrane-bound, monomeric protein, whereas the disease-specific conformation PrP^{Sc} contains mostly β-sheets and forms insoluble aggregates. Hsp70 disassembles PrP^{Sc} aggregates, generating a form of the infectious prion that can seed further protein polymerization and propagate the prion cycle (Jones and Tuite, 2005).

Also striking is that Hsp70's role in disease extends beyond interactions with proteins, as a recent study revealed that Hsp70 inhibits lysosomal membrane permeabilization by binding to an endolysosomal anionic phospholipid bis(monoacylglycero)phosphate (BMP), a critical co-factor of acid sphingomyelinase (ASM). Hsp70's binding to BMP expedites BMP binding to ASM, thus stimulating ASM's activity. Recombinant Hsp70 maintains lysosomal stability in cells from patients with Niemann-Pick disease, a lysosomal storage disorder caused by mutations in the gene encoding ASM (Kirkegaard et al., 2010).

Finally, Hsp70 and other chaperones are becoming powerful tools in vaccine development. The presence of molecular chaperones on the cell surface and in various body fluids has led some researchers to hypothesize that chaperones have moonlighting functions as signal receptors and intercellular signals in immunological pathways (Henderson, 2010). Indeed, some chaperones are strong inducers of innate and antigen-specific immunity that activate dendritic natural killer cells (Segal et al., 2006). Recombinant Hsp70 stimulates human monocytes to produce pro-inflammatory cytokines by interacting with CD40, CD14, TLR2, and TLR4 (Henderson, 2010). Furthermore, Hsp70 can chaperone antigenic peptides and help elicit an adaptive cytotoxic T-lymphocyte response (Bolhassani and Rafati, 2008). For these reasons Hsp70 and other heat shock proteins are being explored as vaccine adjuvants that may enhance immunity to an antigen (Segal et al., 2006).

Because of Hsp70's role in many diseases, there is much interest in developing small molecules that target Hsp70 activity for use as research tools and therapies. In 2008 Jason Gestwicki and colleagues used a high-throughput screen to identify classes of compounds that modify Hsp70's ATPase activity and its ability to refold denatured firefly luciferase (Chang et al., 2008; Wisén and Gestwicki, 2008). Certain dihydropyrimidines stimulate Hsp70 activity whereas phenothiazine compounds inhibit Hsp70 activity. Hsp70 inhibitors were later found to increase proteasome-dependent tau degradation in cells and mouse brain tissue, while Hsp70 activators maintained tau levels. An even larger degree of tau clearance was achieved with Hsp70 overexpression in concert with Hsp70 inhibition (Jinwal et al., 2009). In addition, levels of the Akt survival kinase can be decreased by inhibiting the ATPase activity of Hsp70, and Hsp70 inhibitors can rapidly and selectively kill cancer cells that require Akt for survival. Interestingly, an even greater cytotoxic effect is observed when Hsp70 inhibition is combined with overexpression of Hsp70 (Koren et al., 2009). These counterintuitive findings can be explained if overexpression of Hsp70 increases the number of Hsp70-tau or Hsp70-Akt complexes, and inhibition of Hsp70 leads to degradation of Hsp70's substrate rather than unsuccessful refolding. Although a direct interaction between Hsp70 and the inhibitor MB has been confirmed by NMR spectroscopy (Jinwal et al., 2009), we do not know the location of binding for any of the Hsp70 activity modulators other than it does not appear to be the substrate binding groove (Chang et al., 2008). These studies are rapidly heightening interest in combining genetic and pharmacologic manipulation of Hsp70 to treat a variety of diseases.

Hsp70/DnaK structure and allosteric interdomain communication

Hsp70 is the most highly conserved protein among all organisms on earth. Bacterial DnaK is 46% identical to human Hsp70 (Gupta and Golding, 1993), so studies of DnaK have been used to inform our understanding of eukaryotic versions of Hsp70 and vice versa. Hsp70s have an N-terminal ca. 45-kDa nucleotide binding domain (NBD) and C-terminal ca. 25-kDa substrate binding domain (SBD) connected by a short, flexible, hydrophobic linker. The NBD has two equally large lobes (domains I and II) each divided further into two separate topological domains (A and B) (Figure 1). There is a deep cleft between domains IB and IIB, at the base of which nucleotide binds in complex with one Mg^{2+} and two K^{+} ions. Nucleotide is stabilized by β- and γ-phosphate-binding loops and hydrophobic interactions with adenosine (Flaherty et al., 1990).

The SBD consists of a sandwich of β-sheets connected by four loops, helices that form a lid to capture substrate peptides, and an unstructured C-terminal region. Unfolded client proteins are bound by a deep flexible hydrophobic binding pocket between loops $L_{1,2}$ and $L_{3,4}$ and a hydrophobic arch composed of a methionine and alanine. The lid composed of helix B closes the substrate binding pocket through a salt bridge and two hydrogen bonds to loops $L_{3,4}$ and $L_{5,6}$ (Mayer and Bukau, 2005).

A)

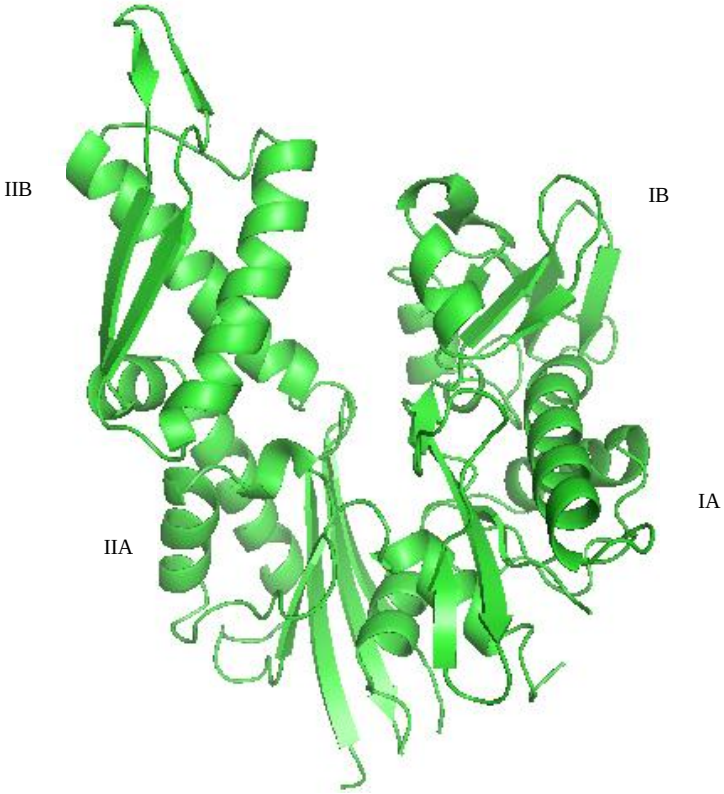

B)

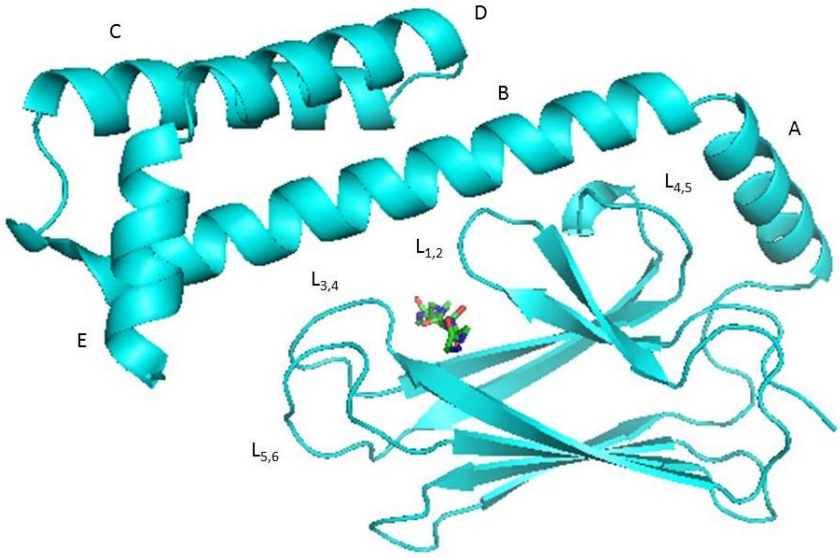

Figure 1. Models of DnaK NBD (A) and SBD (B) based on X-ray diffraction. NBD is shown with four subdomains labeled (PDB code 1DKG). SBD is shown in complex with seven-residue peptide substrate (sticks) with helices and loops labeled (PDB code 1DKX). Images generated in PyMOL.

Intramolecular communication between the NBD and SBD is crucial for chaperone function. With ATP bound by the NBD, the SBD has low affinity for client proteins.

Hydrolysis of ATP results in a global conformational change that locks the substrate into the substrate binding pocket. The intrinsic rate of ATP hydrolysis by Hsp70 chaperones is very low, varying between 3×10^{-4} and 1.6×10^{-2} (moles ATP)/(moles Hsp70 · s). ATP hydolysis is accelerated 2-10-fold in the presence of peptide substrates and >1000-fold by the addition of client protein plus the co-chaperone DnaJ of the Hsp40 family. DnaJ begins the chaperone cycle by binding to a client peptide and bringing it to DnaK (Figure 2). The J domain of DnaJ interacts with DnaK and substrate is loaded into the peptide binding cavity. These events lower the activation energy for the hydrolysis of ATP, but the precise mechanism of ATP hydrolysis stimulation by DnaJ and substrate is not known (Mayer and Bukau, 2005).

The next step in the chaperone cycle is removal of nucleotide in preparation for rebinding of ATP and release of substrate. The intrinsic ADP dissociation rate for DnaK is very slow, between 4×10^{-3} and 3.5×10^{-2} s^{-1}. The nucleotide exchange factor GrpE accelerates nucleotide release by several orders of magnitude by opening the nucleotide binding cleft and inducing rotation of NBD subdomain IIB by 14° (Harrison et al., 2007). The GrpE homodimer interacts with DnaK's NBD via the C-terminal half of two long α-helical coils and a globular "headpiece" domain. The N-terminal half of GrpE's α-helical coils interact with DnaK's interdomain linker and regulate nucleotide exchange (Moro et al., 2007).

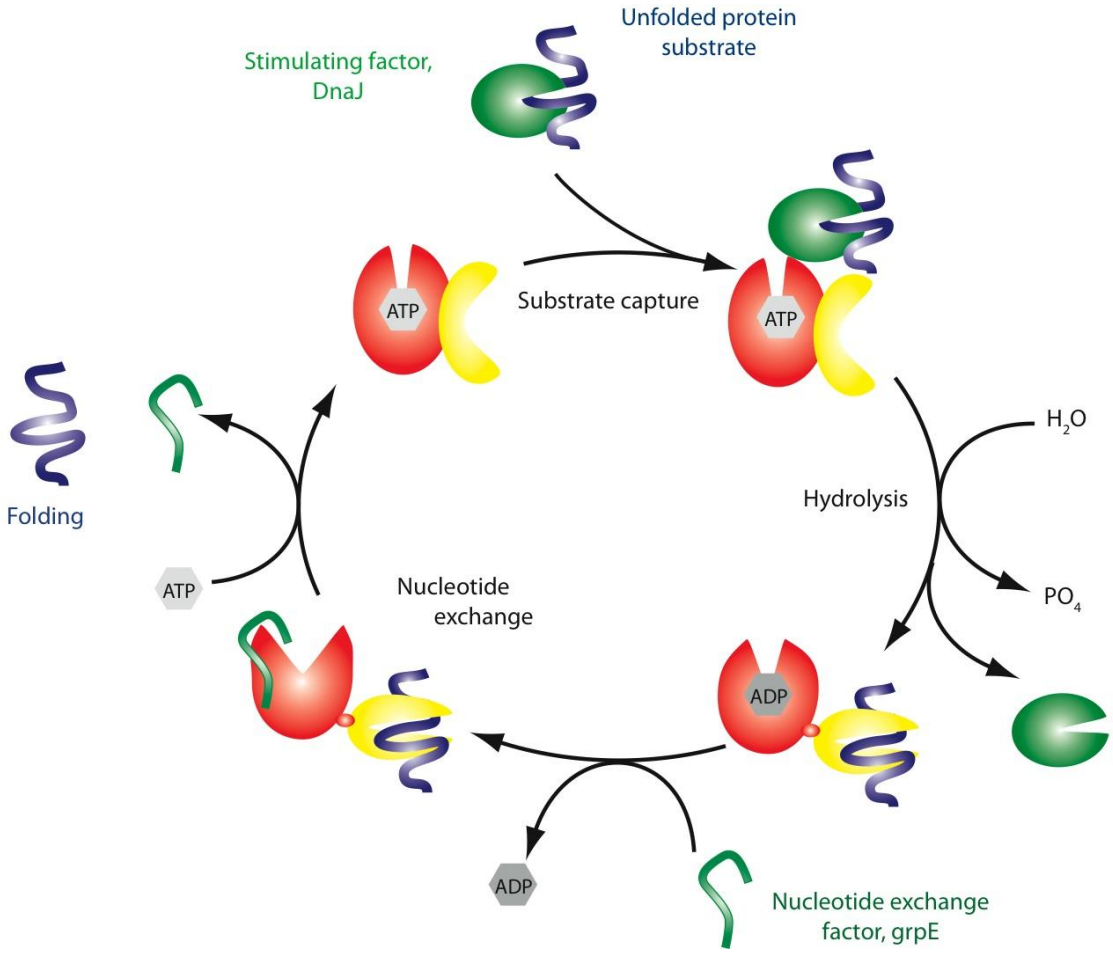

Figure 2. DnaK chaperone cycle (from S. Wilbanks and B. Carlisle). Co-chaperone DnaJ loads an unfolded polypeptide into the SBD of ATP-bound DnaK, stimulating ATP hydrolysis and closing of the substrate binding lid. Nucleotide exchange factor GrpE then removes nucleotide from the NBD. GrpE and substrate are released upon ATP rebinding.

The mechanism of interdomain communication in Hsp70s is an exciting field of ongoing investigation. While it is widely accepted that nucleotide or substrate binding induces global conformational changes, there is disagreement over the nature of such changes. Broadly speaking, studies on Hsp70 allostery are divided into two camps: one providing evidence for compaction of Hsp70 in the nucleotide-free and ADP-bound forms compared to the ATP-bound state, and one asserting the NBD and SBD are largely disjoined in the ADP-bound conformation and only upon ATP binding does formation of a significant interface between the NBD and SBD occur. In support of the former model, a SAXS study of DnaK showed an increase in radius of gyration (R_g) upon addition of ATP (Shi et al., 1996). However, full length DnaK is vulnerable to dimerization, which would artificially inflate the R_g above the true monomer value. Second, an X-ray crystal structure of bovine Hsc70 in the nucleotide-free state showed the groove between lobes IA and IIA on the NBD and helix A in

the SBD ("lid") form an interface proposed to facilitate interdomain communication, while the interdomain linker is exposed to solvent (Jiang et al., 2005). However, two mutations at the proposed interdomain interface were required to generate diffracting crystals. Moreover, removing the helical lid of the SBD does not disable allosteric interdomain communication in DnaK (Pellecchia et al., 2000), a finding difficult to reconcile with the lid forming a key element of the interdomain interface. Finally, an NMR model of *T. thermophilus* DnaK with the C-terminus deleted and two mutations in the peptide binding cleft showed a different NBD-SBD interface that was rigidified in the ADP-bound form compared to the ATP-bound conformation (Revington et al., 2005).

The majority of studies on Hsp70 demonstrate, and a consensus is now being reached, that the NBD and SBD are actually disjoined in the ADP-bound form and closely interacting in the ATP-bound form. First, ATP binding to a C-terminally truncated version of Hsc70 less prone to aggregation than full-length decreases the radius of gyration compared to the ADP-bound and nucleotide-free states (Wilbanks et al., 1995). Second, addition of ATP results in quenching and blueshift in the fluorescence of DnaK's only endogenous tryptophan residue, as well as protection of the interdomain linker from proteolysis, compared to nucleotide-free and ADP-bound forms of DnaK (Buchberger et al., 1995), suggesting burial of the linker in an overall more compact conformation. Third, multiple NMR studies have shown no stable interaction between the NBD and SBD is formed in nucleotide-free or ADP-bound DnaK, as the sum of individual NBD and SBD spectra equals that of two-domain DnaK with no significant changes. ATP binding to two-domain DnaK, however, induces global chemical shifts relative to the isolated NBD and SBD, indicating substantial interdomain interaction in the ATP-bound state (Swain et al., 2006; Bertelsen et al., 2009; Swain et al., 2007). Fourth, a crystal structure of ADP-bound DnaK from *Geobacillus kaustophilus* showed the NBD and SBD disjoined from each other, although it was not clear whether the DnaK dimers formed in the crystal were valid models for monomeric chaperone (Chang et al., 2008).

Research in the past few years has pointed to the conserved interdomain linker as central to the mechanism of Hsp70 allosteric communication. The C-terminal half of the linker segment between NBD and SBD is the best conserved element in Hsp70s of archaea, eubacteria, and eukaryotes (Karlin and Brocchieri, 1998). Mutation of DnaK linker domain residues VLLL (389-392) to AAAA or VDDL destroys interdomain communication, as bound substrates are not released upon ATP binding and ATP hydrolysis is not stimulated by DnaJ plus substrate binding (Laufen et al., 1999). Amide hydrogen exchange shows that ATP binding stabilizes the NBD and destabilizes the SBD, and that the linker is solvent-exposed in

the absence of nucleotide and completely buried in the presence of ATP (Rist et al., 2006). An isolated DnaK NBD construct including the conserved hydrophobic VLLL linker segment (residues 1-392) has 13-fold greater ATPase activity than DnaK(1-388), leading to the conclusion that the linker acts as a switch to stimulate ATPase activity. Circular dichroism thermal stability studies and electrospray ionization mass spectrometry of DnaK(1-392) and DnaK(1-388) indicate that the linker induces a closed conformation of the ATPase domain. In addition, ATP binding by DnaK(1-392) causes large chemical shift changes in linker leucine residues. NMR data indicate that the linker segment docks to a hydrophobic cleft between subdomains IA and IIA of the NBD, interacting with L177 and I373. In the SBD, ATP binding destabilizes the substrate binding pocket but stabilizes other regions, presumably due to interface formation with the NBD. Titration of substrate into the ATP-bound form of DnaK returns NMR resonances to those characteristic of the individual domains, leading Swain et al. to propose that substrate binding loosens interdomain contacts and allows the linker to dock on the NBD, stimulating ATP hydrolysis (Swain et al., 2007). Further evidence for linker docking comes from the crystal structure of Hsp70 homolog Hsp110 from yeast, which shows the hydrophobic NBD-SBD linker buried in the hydrophobic groove between NBD subdomains IA and IIA (Liu and Hendrickson, 2007).

A complete NMR solution conformation of full length DnaK in the ADP-bound form combined with previous research allowed Bertelsen et al. to arrive at the current description of DnaK interdomain communication. The NMR model depicted ADP-bound DnaK in a domain disjoining conformation. The linker region between the domains was determined to be a dynamic random coil, but an average organization was defined that positions the SBD near subdomain IA of the NBD. Bertelsen et al. propose that with ADP and substrate bound, the SBD and linker sample the surface of subdomains IA and IIA of the NBD. Upon ATP binding the groove between IA and IIA opens, permitting docking of the linker in the groove and interaction of loops L2,3 and L5,6 with subdomain IA, leading to a change in substrate binding affinity (Pellecchia et al., 2000, Bertelsen et al., 2009).

Study of protein dynamics by intramolecular FRET

Intramolecular Förster resonance energy transfer (FRET) is a common method for investigating protein conformational changes. FRET is the transfer of energy via a nonradiative dipole-dipole interaction from an excited donor fluorophore to an acceptor fluorophore approximately 10 to 100 Å away. Because the efficiency of energy transfer varies with the inverse sixth power of fluorophore separation distance, FRET is a sensitive "molecular ruler" for calculating the distance between fluorophores (Stryer and Haugland,

1967). FRET has been used extensively in biology to track intermolecular interactions as well as intramolecular dynamics of proteins and protein-nucleic acid complexes. In particular, single molecule FRET (smFRET) has been used to probe questions about DNA replication, recombination, transcription, translation, RNA folding, and dynamics of proteins ranging from ion channels to molecular motors (Roy et al., 2008). Single molecule studies provide information on the heterogeneity of a sample and allow one to detect subpopulations that may exist but are hidden by ensemble averaging (Mapa et al., 2010).

The efficiency of energy transfer E is given as

$$E = 1 - F_{DA}/F_D \qquad \text{[Equation 1]}$$

where F_{DA} and F_D are the donor fluorescence intensities in the presence and absence of acceptor, respectively. Transfer efficiency can be converted to distance by

$$E = (1 + (R/R_0)^6)^{-1} \qquad \text{[Equation 2]}$$

where R is the fluorophore separation distance and R_0 is the Förster radius at which E=0.5 (Figure 3). The Förster radius depends on the spectral overlap of the donor emission spectrum and the acceptor absorption spectrum as well as the relative orientation of the donor emission dipole moment and the acceptor absorption dipole moment according to the equation

$$R_0 = \{[9Q_0(\ln 10)\kappa^2 J]/[128\pi^5 n^4 N_A]\}^{1/6} \qquad \text{[Equation 3]}$$

where Q_0 is the fluorescence quantum yield of the donor in absence of the acceptor, κ^2 is the dipole orientation factor, *n* is the refractive index of the medium, N_A is Avogadro's number, and J is the spectral overlap integral given as

$$J = \int f_D(\lambda)\varepsilon_A(\lambda)\,\lambda^4\,d\lambda \qquad \text{[Equation 4]}$$

where f_D is the normalized donor emission spectrum and ε_A is the molar acceptor extinction coefficient. κ^2 ranges from 0 to 4 and equals 2/3 for randomly oriented donors and acceptors, i.e. fluorophores free to rotate about their point of attachment. $\kappa^2 = 2/3$ is often assumed and is usually acceptable even with modest restriction of rotation. Nonetheless, uncertainties in κ^2 as well as size of the fluorophores are leading causes of error in distance calculations based on FRET (Haugland, 2005).

A)

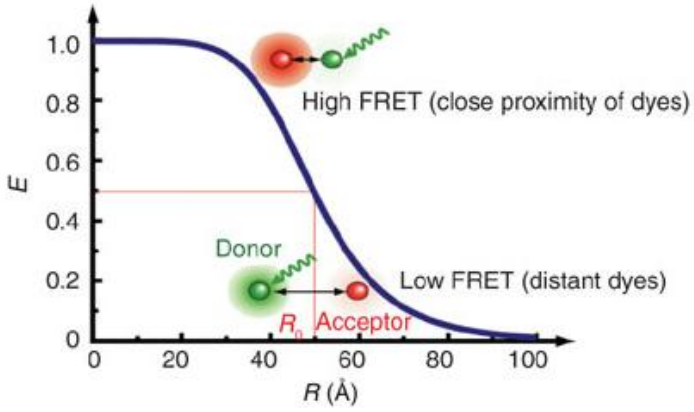

B)

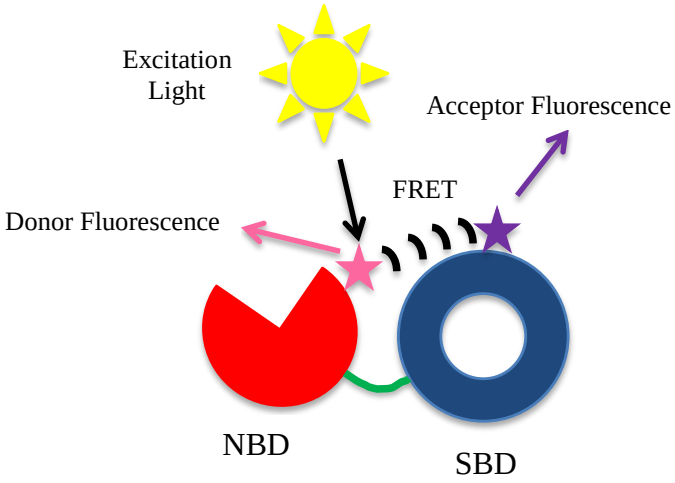

Figure 3. A) FRET efficiency E as a function of inter-dye distance (R) for R_0=50 Å (Roy et al., 2008). B) Schematic of intramolecular FRET with DnaK. The donor fluorophore (pink star) is conjugated to a cysteine in the NBD, and the acceptor fluorophore (purple star) is conjugated to a cysteine in the SBD. Either donor or acceptor fluorescence can be used to calculate E.

Several strategies exist for site-specific fluorescent labeling of proteins. Incorporation of fluorescent moieties into proteins genetically allows one to obtain a homogenous sample composed completely of the desired labeled species. For example, a protein may be tagged with cyan and yellow fluorescent proteins at each terminus (Pedersen et al., 2008). Another approach less likely to disrupt protein structure and function and more amenable to precise distance measurements is to incorporate an unnatural fluorescent amino acid into a protein using a nonsense codon and an orthogonal tRNA/aminoacyl-tRNA synthetase pair (Summerer et al., 2006), although this method may result in low protein yield.

Proteins can also be chemically labeled with small exogenous synthetic fluorophores, which typically do not interfere with protein activity and permit high resolution distance measurements by FRET. For instance, hydrizide dyes will bind to unnatural amino acids containing ketone-groups, although this strategy gives poor fluorescent labeling yield (Roy et al., 2008). Other strategies include binding tris-NTA/fluorophore conjugates to histidine-tagged proteins (Strunk et al., 2009) and using luminescent nanocrystals (quantum dots) that are less vulnerable to photobleaching than organic fluorophores (Galvez et al., 2008).

The low frequency of cysteine residues in most proteins combined with thiol-specific chemistry make cysteine conjugation the most common fluorescent labeling technique for proteins. Because maleimides react exclusively with cysteine thiol groups at pH < 8.0 ("Thiol-Reactive Probes," 2006), maleimide-dye conjugates are typically used for this strategy. For smFRET, it is usually acceptable to make a two-cysteine variant of a protein, label simultaneously with both donor and acceptor maleimides to produce a mixture of homo-labeled and the desired hetero-labeled species, and then determine if individual molecules are hetero-labeled by their fluorescence signature (Nettels et al., 2009). To increase yield of hetero-labeled protein, one may label first with the donor fluorophore, purify the singly labeled species by anion exchange chromatography, and then label with the acceptor fluorophore (Allen et al., 2008).

Goal of this thesis: Fluorescent double-labeling of DnaK and study of conformational changes by intramolecular FRET

DnaK is especially amenable to thiol-specific fluorescent labeling strategies because it has just one endogenous cysteine at position 15. C15 can be mutated to serine and cysteines introduced at various positions on the surface of the SBD with minimal effect on chaperone function (Smock and Gierasch, unpublished observations; Short and Wilbanks, unpublished observations). In the past, the Wilbanks lab had performed FRET experiments with DnaK using the protein's sole tryptophan at position 102 in the NBD as the donor fluorophore and 5-({2-[(iodoacetyl)amino]ethyl}amino)naphthalene-1-sulfonic acid (IAEDANS) conjugated to a single cysteine at one of several sites in the SBD as the acceptor. Dr. Wilbanks used steady state fluorescence and donor fluorescence lifetimes to calculate the distance between W102 and the various cysteines in the absence and presence of ATP. Consistent with DnaK models from SAXS, NMR, and homology to yeast Hsp110, the distance between W102 and the SBD cysteines decreased upon addition of ATP. For example, the distance between R517C and W102 decreased from 27 to 23 Å and the distance between A413C and W102 decreased from 30 to 24 Å with ATP compared to no nucleotide.

The FRET method used previously has a number of limitations, however, which can be surmounted by double-labeling DnaK with two exogenous fluorophores. First, single molecule FRET (smFRET) is not possible with the tryptophan-IAEDANS technique because of the low quantum yield of tryptophan. In contrast, DnaK labeled with two bright exogenous fluorophores would permit smFRET studies that could lead to detection of intermediate conformations and measurement of conformation lifetimes. Second, the variety of distance measurements in the tryptophan-IAEDANS method is limited to those originating at W102, whereas a much wider variety of distances could be measured by double-labeling. Third, the tryptophan-IAEDANS technique prohibits FRET measurements in the presence of substrate peptides and co-chaperones, which are likely to have significant effects on DnaK's conformational states, because of the additional tryptophan residues. A double-labeled DnaK reagent would not only allow investigation of the influence of substrates and co-chaperones, but could further facilitate study of DnaK dynamics inside a crowded cell challenged with heat shock, oxidative stress, mutant protein synthesis, or inducers of apoptosis. Fourth, the tryptophan and IAEDANS emission spectra overlap with absorbance and fluorescence spectra of some Hsp70 inhibitors of interest (see Results). In contrast, a double-labeled DnaK can be labeled with two Alexa Fluor dyes that absorb and emit energy at longer wavelengths than most Hsp70 activity modulators. Thus, the aims of this thesis are to overcome the limitations of the tryptophan-IAEDANS method by labeling DnaK with two exogenous fluorophores, and to perform preliminary experiments demonstrating that double-labeled DnaK can be used to detect the protein's conformational changes.

To achieve the goal of double labeling DnaK, we first measured the reactivity to fluorescent maleimides of cysteines introduced at a variety of positions throughout DnaK. We also characterized the spectral properties of single-labeled DnaK. Then we removed DnaK's endogenous cysteine and introduced two new cysteines, one at position 136 in the NBD and one at position 423 in the SBD, which react at different rates to Alexa Fluor maleimides. We've taken advantage of the different labeling kinetics to increase yield of hetero-labeled protein in a two-step labeling reaction. In bulk solution the fluorescently labeled protein reports DnaK's nucleotide-dependent conformational change with a 16% decrease in donor fluorescence in the ATP versus nucleotide-free state. We will show preliminary results on the application of the labeled protein to analysis of Hsp70 activity modulators.

Chapter 2

Materials and Methods

Materials

Organisms

Escherichia coli, strain DH5α. Used for cloning and plasmid synthesis. Genotype *E. coli B F –ϕ80lacZΔM15 Δ(lacZYA-argF) U169 endA1 recA1 hsdR17 (r_k^-,m_k^+) supE44 thi-1 gyrA96 relA1 phoA.*

E. coli, strain BB1553. Used for expression of recombinant DnaK from pMSK plasmid derivatives. Heat shock sensitive, *Δdnak* derivative of MC4100. Genotype F' *araD139 Δ(argF-lac) U169 rpsL150 relA1 deoC1 ptsF25 rpsR flbB5310 ΔdnaK::cat sidB10* (Bukau and Walker, 1990).

Plasmids

All plasmids are derivatives of pMSK, used for isopropyl β-D-1-thiogalactopyranoside (IPTG)-inducible expression of wild-type (WT) DnaK. pMSK was created by subcloning the wild-type DnaK gene from plasmid JZ515 (C. Georgopoulos; Department of Biochemistry; University of Utah School of Medicine; Salt Lake City, UT 84132; USA) using the 5' XbaI and 3' HindIII sites into the bacterial expression vector pMS119-EH using the same sites (Montgomery et al., 1999). Before the structural gene there are about 40 bp of 5' untranslated sequence between the XbaI site and the start codon, which includes the ribosomal binding site. There are also ~560 bp of 3' untranslated sequence after the stop codon and before the HindIII site. The XbaI-HindIII fragment is 2,514 base pairs (bp), and the total size of the pMSK plasmid is 6,481 bp. pMSK contains an ampicillin resistance cassette (see Appendix for map). The following were created by site-directed mutagenesis of pMSK:

pMSK [S423C/C15S], derivative of pMSK. Used for expression of DnaK S423C/C15S (prepared by D. Pippig, former student of Dr. Sigurd Wilbanks).

pMSK [T136C/C15S], derivative of pMSK. Used for expression of DnaK T136C/C15S (prepared by R. Budhidarmo), former student of Dr. Sigurd Wilbanks).

pMSK [R517C/C15S], derivative of pMSK. Used for expression of DnaK R517C/C15S (prepared by D. Pippig).

Enzymes

Pfu polymerase and buffer (Stratagene[2])

Proteinase K (BDH Laboratory Supplies)

Restriction enzymes XbaI and BglII and Buffer H (Roche)

T4 DNA ligase and buffer (Roche)

[2] See page 25 for addresses of all suppliers.

DNA primers

All DNA oligomers were synthesized by Invitrogen.

pMS119-EH forward (fwd): $^{5'}$CAGGAAACAGAATTCGAGCTCGG$^{3'}$

55 bp upstream of DnaK coding region, in multiple cloning site, of pMSK plasmids

T136C-fwd: $^{5'}$GGTGAACCGGTATGTGAAGCTGTTATCACC$^{3'}$

T136C-reverse (rev): $^{5'}$CGGTACGGTGATAACAGCTTCACATACCGG$^{3'}$

Overlapping primers for introducing T136C mutation, mutant codon underlined

DnaK 1623-1606: $^{5'}$ATGGTCGCCCTGGTTGCG$^{3'}$

Reverse primer in DnaK gene

DnaK 1021-1002: $^{5'}$CAACGAGGATAACGTCGTCG$^{3'}$

Reverse primer for DNA sequencing

Chemicals and reagents

1 kilobase (kb) DNA ladder (Invitrogen)

2-(N-morpholino)ethanesulfonic acid (MES) (AppliChem)

30% acrylamide/bis solution 37.5:1 (2.6% C) (Bio-Rad)

4-(2-hydroxyethyl)-1-piperazineethanesulfonic acid (HEPES) (AppliChem)

Adenosine diphosphate (ADP) (Sigma product number A2754)

Adenosine triphosphate (ATP) (Sigma product number A2383)

Agarose (AppliChem)

Ammonium persulfate (APS) (BioRad)

Ampicillin (amp) (USB Corporation)

Bromophenol blue (Peking's Reagent)

Chloramphenicol (chlor) (USB Corporation)

Coomassie Brilliant Blue R-250 (BDH Laboratory Supplies)

N-Cyclohexyl-2-aminoethanesulfonic acid (CHES) (Sigma)

Deoxyribonucleotide triphosphates (dNTPs) (Roche)

Disodium hydrogen phosphate (AppliChem)

Dithiothreitol (DTT) (Roche)

Ethylenediaminetetraacetic acid (EDTA) (AppliChem)

Immobilized TCEP disulfide reducing gel (Thermo Fisher Scientific)

Isopropyl β-D-1-thiogalactopyranoside (IPTG) (AppliChem)

β-mercaptoethanol (BME) (Sigma)

Phenylmethanesulfonylfluoride (PMSF) (Sigma)

Piperazine-N,N′-bis(2-ethanesulfonic acid) (PIPES) (Sigma)

QiaPrep Spin Miniprep Kit (Qiagen)

Qiaquick PCR Purification Kit (Qiagen)

Reduced glutathione (GSH) (Sigma)

Sodium dodecyl sulfate polyacrylamide gel electrophoresis (SDS-PAGE) standards, low range (BioRad)

Sodium dihydrogen phosphate (Scharlau)

Sodium dodecyl sulfate (SDS) (BDH Laboratory Supplies)

Tetramethylethylenediamine (TEMED) (Riedel-de Häen)

Tris (AppliChem)

Tris(2-carboxyethyl)phosphine (TCEP) (Invitrogen)

Triton X-100 (Sigma)

D-Tryptophan (Sigma)

Tween 20 (Sigma)

Fluorescent dyes

All purchased from Molecular Probes, Invitrogen.

5-({2-[(iodoacetyl)amino]ethyl}amino)naphthalene-1-sulfonic acid (IAEDANS)

(7-diethylamino-3-(4'-maleimidylphenyl)-4-methylcoumarin) (CPM)

Alexa Fluor 488 C_5 maleimide (AF488)

Alexa Fluor 555 C_2 maleimide (AF555)

Alexa Fluor 594 C_5 maleimide (AF594)

Hsp70 activity modulators

All drugs were originally a gift from J. Gestwicki (Gestwicki Lab; Life Sciences Institute; 210 Washtenaw Avenue; Ann Arbor, MI 48109-2216; USA). See Chang et al., 2008. Myricetin and methylene blue were later purchased from Sigma.

115-7c

116-9e

SW02

CE12

Myricetin (MY) (Sigma)

Methylene blue (MB) (Sigma)

Chromatography resins

Adenosine 5'-triphosphate-agarose; C-8 linkage with nine-atom spacer (Sigma product number A2767) used in 1.1 cm diameter, 10 cm long Ace glass column

DEAE sepharose fast flow (Amersham Biosciences) used in 2.5 cm diameter, 25 cm long Ace glass column

Phenyl sepharose 6 fast flow (low sub) (GE Healthcare) used in Econo-column (Bio-Rad)

Consumables

DispoEquilibrium Biodialyser 10 kilodalton (kDa) molecular weight cutoff (MWCO) (The Nest Group)

Nunc 96 MicroWell plates, black, polystyrene, flat bottom (Thermo Fisher Scientific)

PD-10 desalting columns (GE Healthcare)

NAP-5 desalting columns (GE Healthcare)

SnakeSkin pleated dialysis tubing, 10 kDa MWCO (Thermo Fisher Scientific)

Ultrafree-MC Centrifugal Filter Devices, Durapore polyvinylidene fluoride (PVDF) membrane, 0.22 μm (Millipore)

Vivaspin 20 ultrafiltration devices, 10 and 30 kDa MWCO (GE Healthcare)

Equipment

ÄKTAprime purification system (GE Healthcare)

Biologic HR Workstation, Biologic HR Controller, and Model 2128 Fraction Collector (BioRad)

Cary 50 Bio UV-visible spectrophotometer (Varian)

Cary Eclipse fluorescence spectrophotometer (Varian)

Circular dichroism DCM-10 spectrophotometer (Olis)

HiLoad 26/60 Superdex 200 column (Pharmacia Biotech)

HiPrep 26/10 desalting column (Amersham Biosciences)

Mini-Protean 3 Cell polyacrylamide gel running apparatus (BioRad)

Mini-Sub Cell GT agarose gel running apparatus (BioRad)

Molecular Imager FX (BioRad)

Mono Q 4.6/100PE anion exchange column (GE Healthcare)

Phenyl sepharose HP 1 mL column (Pharmacia Biotech)

Polarstar Optima fluorescence spectrophotometer (BMG Labtech)

Reacti-Vials, 1 mL (Thermo Fisher Scientific)

T-Professional basic gradient thermocycler (Biometra)

Solutions

Growth media

Lysogeny broth (LB) media: 1% weight/volume (w/v) bacto-tryptone, 0.5% w/v yeast extract, 1% w/v NaCl. For agar plates 1.5% w/v bacto-agar was added. Amp (50 μg/mL) and chlor (25 μg/mL) added where appropriate.

PCR-based mutagenesis

Pfu Buffer (10X): 200 mM Tris-HCl pH 8.8, 100 mM KCl, 100 mM $(NH_4)_2SO_4$, 20 mM $MgSO_4$, 1% Triton X-100, 1 mg/mL nuclease-free bovine serum albumin (BSA)

Ligation Buffer (10X): 660 mM Tris-HCl pH 7.5, 50 mM $MgCl_2$, 10 mM DTT, 10 mM ATP

DnaK purification (all buffers filtered through 0.2 micron filter and degased)

Lysis Buffer and Anion Exchange Low Salt Buffer: 20 mM Tris-HCl pH 6.9, 50 mM NaCl, 100 μM EDTA, 100 μM PMSF (added immediately before use)

Anion Exchange High Salt Buffer: 20 mM Tris-HCl pH 6.9, 1.0 M NaCl, 100 μM EDTA, 100 μM PMSF (added immediately before use)

EDTA Dialysis Buffer: 20 mM Tris-HCl pH 6.9, 150 mM KCl, 4 mM EDTA

ATP-agarose Low Salt Buffer: 20 mM Tris-HCl pH 6.9, 25 mM KCl, 3 mM $MgCl_2$

ATP-agarose High Salt Buffer: 20 mM Tris-HCl pH 6.9, 1.0 M KCl, 3 mM $MgCl_2$

ATP-agarose Elution Buffer: 20 mM Tris-HCl pH 6.9, 25 mM KCl, 3 mM $MgCl_2$, 3 mM ATP

Gel Filtration Buffer: 20 mM HEPES pH 7.6, 100 mM KCl, 5 mM $MgCl_2$

Fluorescent labeling (All buffers were argon-purged before use.)

Fluorescent Labeling (FL) Buffer: 50 mM Tris-HCl pH 7.4, 100 mM KCl, 0.5 mM EDTA, 1 mM $MgCl_2$. pH variations (50 mM buffer): 5.5 (MES), 6.0 (MES), 6.5 (MES), 7.0 (PIPES), 7.0 (sodium phosphate), 7.5 (Tris-HCl), 8.0 (Tris-HCl), 8.5 (Tris-HCl), 9.0 (CHES). 9.5 (CHES), 10.0 (CHES). Adjunct variations: 10% volume/volume (v/v) glycerol, 10% v/v dimethyl sulfoxide (DMSO), 1% w/v SDS, 1% v/v Triton X-100, 1% v/v Tween, 1 mM D-tryptophan.

MonoQ Start Buffer: 20 mM Tris-HCl pH 6.9

MonoQ Elution Buffer: 20 mM Tris-HCl pH 6.9, 1.0 M NaCl

pH variations (20 mM buffer): 5.0 (potassium acetate), 6.0 (MES), 7.5 (Tris-HCl)

Phenyl Sepharose Start Buffer: 50 mM sodium phosphate pH 7.0, 1.0 M ammonium sulfate

Phenyl Sepharose Elution Buffer: 50 mM sodium phosphate pH 7.0

pH variations (50 mM buffer): 9.0 (CHES)

Agarose gel electrophoresis and polyacrylamide gel electrophoresis (PAGE)

50X TAE: 2M Tris, 5.71% v/v glacial acetic acid, 50 mM EDTA, pH 8.0

6X DNA Loading Dye: 0.25% w/v bromophenol blue 0.25% w/v xylene cyanol, 40% w/v sucrose

SDS-PAGE resolving gel: 0.375 M Tris-HCl pH 8.8, 0.1% w/v SDS, 10 or 12% acrylamide, 0.5% w/v APS, 0.05% v/v TEMED

SDS-PAGE stacking gel: 0.125 M Tris-HCl pH 6.8, 0.1% w/v SDS, 5% acrylamide, 0.75% w/v APS, 0.125% v/v TEMED

10X SDS-PAGE Electrophoresis Buffer: 250 mM Tris, 1.92 M glycine, 1% w/v SDS, pH~8.3

5X SDS Sample Loading Buffer: 60 mM Tris-HCl pH 6.8, 25% v/v glycerol, 2% w/v SDS, 14.4 mM β-mercaptoethanol, 0.1% w/v bromophenol blue

Coomassie Gel Stain: 25% v/v isopropanol, 10% v/v glacial acetic acid, 0.05% w/v Coomassie Blue R-250

Coomassie Gel Destain: 5% v/v isopropanol, 7% v/v glacial acetic acid, 4% v/v glycerol

SAXS

SAXS Buffer: 20 mM Tris-HCl pH 7.6, 100 mM KCl, 5 mM $MgCl_2$, 5 mM DTT.

Addresses of Suppliers

AppliChem
Global Science & Technology Ltd.
PO Box 101253
North Shore Mail Centre, Auckland 0745
New Zealand
www.applichem.com

BDH Laboratory Supplies
VWR International
Global Export Services
3850 North Wilke Road
Suite 300
Arlington Heights, IL 60004
USA
www.vwr.com

Bio-Rad
Bio-Rad Laboratories (New Zealand) Pty. Ltd.
PO Box 300-571
Albany, Auckland
New Zealand
www.bio-rad.com

Biometra
Biometra GmbH
Rudolf-Wissell-Str. 30
D-37079 Goettingen
Germany
www.biometra.de

BMG Labtech
BMG Labtech Pty. Ltd.
2/24 Carbine Way
Mornington,Victoria 3931
Australia
www.bmglabtech.com

GE Healthcare
Level 1, 8 Tangihua Street
Auckland 1010
New Zealand
www.gelifesciences.com

Invitrogen
Invitrogen New Zealand Ltd.
18-24 Botha Road
Penrose, Auckland 1006
New Zealand
www.invitrogen.com

Millipore
Millipore Australia Pty. Ltd.
9A Byfield Street
North Ryde, New South Wales 2113
Australia
www.millipore.com

Olis
130 Conway Drive
Suites A, B & C
Bogart, GA 30622
USA
www.olisweb.com

Peking's Reagent
Peking Reagent Factory
Peking, China

Pharmacia Biotech (owned by GE Healthcare)
Level 1, 8 Tangihua Street
Auckland 1010
New Zealand
www.gelifesciences.com

Qiagen
Bio-Strategy Ltd.
22A William Pickering Drive
Albany, Auckland
New Zealand
www.qiagen.com

Riedel-de Häen
Honeywell Riedel-de Häen
Seelze, Germany
www.riedeldehaen.com

Roche
Roche Diagnostics New Zealand Ltd.
PO Box 62-089
15 Rakino Way
Mt. Wellington, Auckland
New Zealand
www.roche.com

Scharlau
Scharlab S.L. (Chemical Plant)
Ctra. de Polinyà a Sentmenat, Km. 8,2
08181 Sentmenat, Barcelona
Spain
www.scharlau.com

Sigma
Sigma-Aldrich Pty. Ltd.
PO Box 970
Castle Hill, New South Wales 1765
Australia

Stratagene
Agilent Technologies, Inc.
Life Sciences and Chemical Analysis Group
5301 Stevens Creek Boulevard
Santa Clara, CA 95051-7201
USA
www.agilent.com

The Nest Group
The Nest Group, Inc.
45 Valley Road
Southborough, MA 01772-1323
USA
www.nestgrp.com

Thermo Fisher Scientific
Biolab Ltd.
244 Bush Road
Albany, Auckland
New Zealand
www.thermofisher.com

USB Corporation (distributed by GE Healthcare)
Level 1, 8 Tangihua Street
Auckland 1010
New Zealand
www.gelifesciences.com

Varian
Varian Australia Head Office
679 Springvale Road
Mulgrave, Victoria 3170
Australia
www.varianinc.com

Methods

Protein purification

Transformation of BB1553

Approximately 100 ng of a pMSK derivative was mixed gently with 100 μL of ultra-competent *E. coli* strain BB1553 prepared by the Inoue method (Inoue et al., 1990) and held on ice for 30 min. Cells were heat-shocked at 37°C for 45 seconds then held on ice for 2 min. 1 mL of LB medium was added and cells shaken at 28°C for 45 min. Cells were spun down in a microcentrifuge, all but 50 μL supernatant was removed, and the cell pellet was resuspended in the remaining medium and plated onto LB plates with 25 μg/mL chlor and 50 μg/mL amp. Plates were incubated at 28°C overnight. Transformants were grown in LB with 25 μg/mL chlor and 50 μg/mL amp at 28°C.

Cell culture and lysis

To make a glycerol stock of BB1553 harboring a pMSK derivative, 0.5 mL of culture at OD_{600} = 0.8 was mixed with 0.5 mL 50% glycerol, vortexed, allowed to equilibrate for 20 min, snap frozen in liquid nitrogen, and stored at -80°C. To test protein expression, a 3 mL culture grown at 28°C was induced with 400 μM IPTG when the optical density at 600 nm (OD_{600}) reached 0.6, then grown for at least four more hours. A culture volume equal to 0.2 mL/(measured OD_{600}) was centrifuged and the pellet was resuspended in 40 μL of 5X SDS Sample Loading Buffer and boiled for 10 min. 10 μL was run on a 10% polyacrylamide gel.

For DnaK purification, 2 × 25 mL LB (25 μg/mL chlor and 50 μg/mL amp) in 125 mL flasks were inoculated 1:100 with BB1553 containing a pMSK derivative and grown overnight at 28°C. Samples from these cultures were diluted 1:100 in 4 × 400 mL LB + chlor + amp in 2 L flasks for large scale growth at 28°C. When OD_{600} reached 0.6, IPTG was added to 400 μM. After overnight growth, cells were spun down at 6000 relative centrifugal force (rcf) for 10 min. Half of the pellet was stored at -20°C for later purification and half was resuspended in approximately 100 mL of Lysis Buffer such that a 1/40 dilution of the cell slurry gave an OD_{600} of ≤ 1.0. A Dounce homogenizer was used to remove cell clumps. The cell slurry was transferred to a steel beaker secured in an ice water bath. A Branson Sonifier

with intensity 9 and duty cycle 50% was used to lyse the cells in 4-min periods (typically two or three) until a tenfold reduction in OD_{600} was achieved. Cell debris were removed by spinning at 20,000 rcf for 30 min.

Column care

All chromatography columns were stored in either 20% ethanol or 1 mM Na_3N. Before and after applying running buffers, all columns were rinsed with MilliQ water. Columns were attached to the fast protein liquid chromatography (FPLC) equipment drop to drop to avoid the introduction of air bubbles onto the column.

Diethylaminoethyl cellulose (DEAE) column

The DEAE column was equilibrated with one column volume (CV) Anion Exchange Low Salt Buffer, one CV Anion Exchange High Salt Buffer, and one CV low salt buffer. Clarified cell lysate was applied to the column at 3 mL/min. All eluate was collected in 5 mL fractions. The column was rinsed with 100 mL low salt buffer and protein eluted with a 480 mL gradient (3 CV) from 0 to 60% high salt buffer. The column was cleaned with a 150 mL gradient (1 CV) from 60 to 100% high salt buffer, followed by 30 mL 100% high salt buffer, a 30 mL gradient from 100 to 0% high salt, and 250 mL of low salt buffer.

Fractions containing large amounts of DnaK, as shown by a prominent 70 kDa band on an SDS-PAGE gel, were pooled and dialyzed overnight against 2 × 2 L of EDTA Dialysis Buffer.

ATP agarose column

Dialyzed protein was brought to 10 mM $MgCl_2$ to facilitate binding to ATP-agarose and centrifuged at 20,000 rcf for 15 min. The supernatant was loaded onto the ATP-agarose column equilibrated in ATP Agarose Low Salt Buffer at 2 mL/min. The column was washed with 12 mL ATP Agarose High Salt Buffer and 12 mL low salt buffer. DnaK was eluted with 40 mL of ATP Elution Buffer, followed by low salt buffer, while collecting 2.0 mL fractions. Fractions containing large amounts of relatively pure DnaK as determined by SDS-PAGE were pooled.

Gel filtration column

HiLoad 26/60 Superdex 200 column was equilibrated with 400 mL of Gel Filtration Buffer. Pooled fractions were concentrated in Vivaspin 10 or 30 kDa MWCO spin filters to just under 5 mL and loaded onto the column at 3 mL/min by direct injection. All eluate was collected from 80 to 360 mL post-injection in 5 mL fractions. Fractions with high yield and

purity were concentrated in 10 or 30 kDa MWCO spin filters to approximately 12 mg/mL, determined by absorbance at 280 nm with the filtrate as a blank using ε_{280} for DnaK of 24.2 mM^{-1} cm^{-1}.[3] Protein was snap frozen in liquid nitrogen and stored at -80°C.

CPM labeling

Purified protein was incubated either with immobilized TCEP disulfide reducing gel according to the manufacturer's instructions or with free TCEP for 15 min at room temperature and subsequently run through a PD-10 desalting column to remove TCEP. Protein concentration was determined by Bradford Assay in microtiter plates using 2, 5, 10, 15, and 20 μL of protein with 200 μL of Bradford reagent. The absorbance at 560 nm of each reaction was read using a microplate reader. The slope of the trendline was taken to be a linear function of protein concentration, and wild-type DnaK denatured in 8M acid urea with concentration determined by tryptophan absorbance (ε_{280} = 20.9 mM^{-1} cm^{-1})[3] was used as standard. The DnaK mutant proteins were diluted to 1 μM unless otherwise noted and 200 μL were added in triplicate to a black microtiter plate. The Polarstar Optima fluorescence spectrophotometer was used to track the reaction with a 390 nm excitation filter and 460 nm emission filter and photomultiplier tube (PMT) gain set to 80% of saturation for a well containing CPM fully reacted with either GSH or BME. Fluorescence measurements were taken at 0.4-second intervals with 10 flashes/interval over about 70 seconds. At approximately 3 seconds a mechanical pump injected 5 μL of 2 μM CPM in dimethyl sulfoxide (DMSO) to give a final CPM concentration of 50 nM, and then the plate was shaken for 1 second. The initial rate of reaction was taken as the mean slope of the fluorescence trace from 5-20 seconds. Some progress curves were fit in Kaleidagraph to pseudo first-order kinetics according to the equation

$$\text{Fluorescence} = \alpha \times (1 - e^{-kt}) \qquad \text{[Equation 5]}$$

where α is a constant, k is the reaction rate constant, and t is time. Some experiments were performed with 700 μL of 1 μM protein in a semi-microcuvette on a Cary Spectrophotometer, in which case 7 μL of 5 μM CPM in DMSO was added to start the reaction.

For CPM time courses run with proteinase K digestion in 96-well plate format, proteinase K from a 0.11 mg/mL stock was added to DnaK diluted in FL Buffer pH 7.4 already reduced with immobilized TCEP. A constant total volume of 3.8 μL composed of

[3] Estimates of the extinction coefficient at 280 nm of DnaK vary considerably from 15.9 mM^{-1} cm^{-1} (ExPASy) to 27.0 mM^{-1} cm^{-1} (Palleros et al., 1993). The 20.9 mM^{-1} cm^{-1} value for denatured DnaK was determined by amino acid analysis and chosen as midway between several estimates determined using different methods, and the 24.2 mM^{-1} cm^{-1} value for native DnaK was calculated using denatured DnaK as a standard.

proteinase K stock and buffer was added to reactions with varying final proteinase K concentrations. The plate was incubated at room temperature for 1.5 hours before beginning CPM time courses.

For CPM time courses run with SDS, a 2% w/v SDS solution in FL Buffer pH 7.4 (with NaCl substituted for KCl) was used to create 1 μM DnaK solutions with a range of SDS concentrations.

Fluorescence labeling kinetics by fluorescence anisotropy

DnaK stocks were reduced with immobilized TCEP according to the manufacturer's instructions. After reduction, a Bradford assay was performed to determine the protein concentration in each DnaK stock as above. For fluorescent labeling kinetics measured by fluorescence anisotropy, 50 μL of 10 μM DnaK was mixed with 50 μL of 10 μM Alexa Fluor dye, both in FL Buffer, in one well of a 96-well plate and immediately inserted into the Polarstar spectrophotometer with fluorescence anisotropy reader head attached and appropriate filters installed (Table 1). The gain for both emission channels was set each day on the well with the highest concentration of free fluorophore for a target milli-polarization (mP) of 35. Fluorescence at both emission channels was measured in 5 second intervals with 50 flashes/interval. Optima software was used to calculate polarization and anisotropy changes over time.

Table 1. Filter sets used in the Polarstar Optima fluorescence spectrophotometer for fluorescence polarization and steady-state fluorescence measurements.

Fluorophore	**Excitation Filter**	**Emission Filter**
Tryptophan	295-10 (BMG0440)	350-10 (BMG0035)
IADEANS	N/A	490-10 (BMG0130)
CPM	Ex390 (BMG9925)	Em460 (BMG0134)
AF488	490-10 (BMG0130)	Em520-P (BMG0202) (x2)*
AF555	550-10 (BMG0122)	Em590 (BMG0240A)
		Em590 (BMG0303A)*
AF594	590BP10 (BMG0835A)	620BP10 (BMG0731A)

*Matching emission filters used in fluorescence polarization experiments.

SDS-PAGE-based fluorescent labeling kinetics

All fluorescent labeling protocols were carried out in a dark room illuminated by dim yellow light. When possible, the reaction vessel was sheltered by an aluminum foil-covered beaker to further protect dyes from photodamage. DnaK stocks were reduced with immobilized TCEP and concentration determined by Bradford as above. DnaK was then diluted to 1 μM in 600 μL of argon-purged FL Buffer in a 1 mL glass reaction vial with spin vane and screw cap with rubber septum. A 50 μL aliquot was removed from the reaction at time 0 and pseudo-quenched with 50 μL of 1 mM GSH. 6 μL of 1 mM Alexa Fluor dye stock in DMSO was added, bringing the reaction to 10 μM in Alexa Fluor dye. At time points of 15 s, 30 s, 45 s, 60 s, 2 min, 3 min, 4 min, 5 min, 10 min, and 1 h, 50 μL aliquots were removed from the reaction and quenched by vortexing with 50 μL of 1 mM GSH. For time courses with limited proteolysis, ADP was added to each time point to 1 mM and incubated for 10 min, followed by addition of 0.5 mg of proteinase K and incubation for exactly 5 min. Protein was then precipitated with 16 μL of 100% TCA and placed on ice for 20 min. Samples were centrifuged for 10 min at 4°C at 13,000 rcf, the pellet was rinsed with 100 μL acetone, and then centrifuged again for 20 min at 4°C at 13,000 rcf. The pellet was dried on the benchtop, resuspended in 10 μL of 5X SDS-PAGE Sample Loading Buffer, and run on a 10% polyacrylamide gel. The gel was scanned for fluorescence using a Molecular Imager FX scanner with a 523 nm excitation laser and 555 nm long pass emission filter, PMT voltage set to medium sample intensity, and 100 micrometer resolution. Quantity One analysis software in volumes mode was used to determine intensity of fluorescent protein bands. The gel was then stained with Coomassie Blue and densitometry performed in Quantity One to determine total protein in each band. The extent of a labeling reaction at each time point was calculated as (intensity of fluorescence counts)/(intensity of Coomassie) and graphed over time. Reaction rate constants were determined by fitting the time course to the following equation in Kaleidagraph:

$$\text{Fluorescence/Coomassie} = \alpha \times (1 - e^{-kt}) \qquad \text{[Equation 6]}$$

where α is a constant, k is the reaction rate constant, and t is time.

PCR-based mutagenesis and creation of pMSK [T136C/S423C/C15S]

All PCR reactions were set up by mixing concentrated stocks of the reagents shown in Table 2. PCR was performed in a T-Professional basic gradient thermocycler.

Table 2. A) List of reagents used in PCR reactions for introduction of the T136C mutation into pMSK [S423C/C15S]. All reactions contained 50 µL total. B) Thermocycling for PCR reactions.

A)

Reagent	**Reaction 1**	**Reaction 2**	**Reaction 3**
Pfu Buffer (10X stock)	1X	1X	1X
dNTPs (100 mM stock)	2 mM	2 mM	2 mM
pMS119EH-fwd primer (10 µM stock)	500 nM	--	500 nM
T136C rev primer (10 µM stock)	500 nM	--	--
T136C fwd primer (10 µM stock)	--	500 nM	--
DnaK 1623-1606 rev primer (10 µM stock)	--	500 nM	500 nM
Template (~50 ng/µl stock)	50 ng of pMSK [S423C/C15S]	50 ng of pMSK [S423C/C15S]	Gel stab of desired product bands from reactions 1 and 2
Pfu polymerase (2.5 units/µl)	2.5 units	2.5 units	2.5 units

B)

Segment	**Number of Cycles**	**Temperature (°C)**	**Time (min:s)**
1	1	95	0:45
2	28	95	0:45
		60	0:45
		72	2:30 (Reactions 1 & 2) 4:00 (Reaction 3)
3	1	72	10:00

PCR Reaction 3 was purified from enzyme and salts using the Qiaquick PCR Purification Kit. Then the PCR product was digested with 0.5 µL (5 units) each of BglII and

XbaI in 1X Buffer H (Roche) in a 25 μL total reaction for 1 hour at 37°C. Approximately 1 μg of pMSK S423C/C15S was also digested with BglII and XbaI under the same conditions. Both digests were run on a 1% agarose gel that was stained in the dark in a 0.01% ethidium bromide solution and visualized with UV light. Bands corresponding to the cut plasmid (~5 kb) and mutagenized insert (~1.6 kb) were cut out with a razor blade and DNA purified by the freeze and squeeze method (Tautz and Renz, 1983): the gel slice was put in a 0.2 micron spin filter, held at -80°C for 20 min, centrifuged at 13,000 rcf for 10 min, and the filter was rinsed with 10 μL of 3.0 M sodium acetate and centrifuged again for 5 min. The filtrate was recovered, 2.5 volumes of 95% ethanol added, and DNA held at -20°C for 30 min. DNA was pelleted by centrifuging for 15 min at 4°C and supernatant removed. The pellet was washed with 70% ethanol, allowed to dry at room temperature, and resuspended in 10 mM Tris-HCl pH 8.5. The concentration of gel-purified cut plasmid and insert was determined by absorbance at 260 nm using a Nanodrop spectrophotometer. Insert and plasmid were ligated together with a 3:1 insert:plasmid molar ratio with 1 unit T4 DNA ligase in 15 μL of Ligation Buffer, incubated at 16°C overnight. 5 μL of the ligation reaction was used to transform 100 μL DH5α competent cells prepared by the Inoue method (Inoue et al., 1990). The DNA-cell mixture was held on ice for 30 min, heat-shocked at 42 °C for 45 s, and recovered on ice for 2 min. 1 mL of LB medium was added and cells shaken at 37°C for 1 hour. 50 μL of cells were plated on LB plates with 50 μg/mL amp (dilute inoculum), then the remaining cells were spun down in a microcentrifuge, all but 50 μL supernatant was removed, and the cell pellet was resuspended in the remaining medium and plated (concentrated inoculum). Plates were incubated at 37°C overnight. Transformants were grown in LB plus 50 μg/mL amp and plasmid DNA purified using the QiaPrep Spin Miniprep Kit. Plasmid DNA was sequenced at the Allan Wilson Centre at Massey University using the pMS119EH fwd and DnaK 1021-1002 rev primers.

Fluorescent double labeling of DnaK

Care was taken to protect all fluorescent dyes from photodamage by covering reaction vessels in aluminum foil and working in a dark room with illumination from a dim yellow light.

Two pot labeling

DnaK stocks were reduced with either immobilized TCEP or free TCEP, which was subsequently removed using a PD-10 or NAP-5 desalting column, and protein concentration

determined by Bradford assay. 14.5 mL of 1 μM DnaK (1 mg) in FL Buffer pH 8.5 was added to a reaction vessel with stir bar. 145 μL of 1 mM fluorescent dye stock in DMSO was added and the reaction allowed to progress for 60 s before quenching with 290 μL of 50 mM GSH. The reaction was concentrated to approximately 5 mL using Vivapsin 30 kDa MWCO spin filters and injected onto a HiPrep 26/10 desalting column (pre-equilibrated with 5 CV of FL Buffer pH 8.5) to remove excess free dye at a flow rate of 10 mL/min with 2 mL fractions throughout the run. Fractions deemed pure of free dye, eluting at approximately 12-16 mL, were pooled for chromatography to isolate singly labeled species. For the MonoQ column, sample was loaded by direct injection, the column was washed with 15 mL of MonoQ Start Buffer, protein was eluted with a 25 mL gradient from 0 to 50% MonoQ Elution Buffer, the column washed with 8.5 mL of 100% elution buffer, and the column re-equilibrated with 15 mL of start buffer. Flow rate was 2.0 mL/min and 0.5 mL fractions were collected during the elution and washing steps. For phenyl sepharose chromatography, sample was loaded onto the Phenyl Sepharose 1 mL HP column by direct injection, the column was washed with 8 mL of Phenyl Sepharose Start Buffer, protein eluted with a 15 mL gradient from 0 to 100% Phenyl Sepharose Elution Buffer, and column re-equilibrated with 8 mL start buffer. The flow rate was 1.0 mL/min and 0.5 mL fractions were collected during elution and re-equilibration steps. Variations on the above procedures are discussed in results. Fractions deemed to contain DnaK mostly single-labeled at T136C were pooled and buffer exchanged back into FL Buffer pH 8.5 using the HiPrep desalting column. The singly labeled protein was Ar-purged and reduced with 10 μM free TCEP, and then the second fluorescent dye was added to 10 μM. The reaction was allowed to proceed for 2 hours at room temperature, then moved to 4°C overnight, and finally quenched with 1 mM GSH. Excess free dye was removed again on the HiPrep desalting column run in FL Buffer pH 8.5. The Cary fluorescence spectrophotometer was used to obtain fluorescence spectra of doubly labeled protein in the presence of nucleotides and after proteinase K digestion.

One pot labeling

Concentration of DnaK T136C/S423C/C15S was determined by diluting in 8M acid urea and measuring absorbance at 280 nm. DnaK was then diluted to 1 μM in FL Buffer pH 8.5 + 10% glycerol. Free TCEP was added to 10 μM and incubated with DnaK for 15 min, but not removed by desalting. The first fluorescent dye was added to 1 μM and the labeling reaction allowed to proceed for 30 min before addition of the second fluorescent dye to 10

μM. After 2 hours the reaction was quenched with 1 mM GSH, excess free dye removed on the HiPrep desalting column, and fluorescence spectra taken as above.

IAEDANS labeling

DnaK R517C/C15S was prepared for labeling by exchanging into FL Buffer in Vivaspin 30 kDa MWCO filters (three tenfold dilutions) and re-concentrated to approximately 10 mg/mL. 50 mM IAEDANS was made up in dimethylformamide (DMF). Protein solution was placed in a Reacti-Vial with rubber/Teflon seal and spin vane and purged with argon. Free TCEP was added to 0.5 mM and the solution stirred for 30 min. IAEDANS was added to bring the dye concentration to approximately 290 μM or twice the protein concentration. Three additional 2 × additions of dye were made 30 min apart. After all IAEDANS additions were made, GSH was added to a concentration of 120 mM to quench the labeling reaction. Labeled protein was exchanged back into Gel Filtration Buffer using Vivaspin 30 kDa MWCO filters.

Modeling programs

Swiss PdbViewer and PyMOL were used to view X-ray diffraction-based models of the DnaK NBD and SBD (PDB accession 1DKX and 1DKG) and NMR-based models of full length DnaK (PDB accession 2KHO) as well as create figures. The "access" command in Swiss PdbViewer was used to calculate the relative solvent accessibility of a given introduced cysteine residue (C) with 100% accessibility considered as C in an extended conformation in the pentapeptide GGCGG.

Limited proteolysis of DnaK with Hsp70 activity modulators

Limited proteolysis was carried out in 50 μL of FL Buffer pH 7.5 containing 1 μM DnaK R517C/C15S, 1 mM nucleotide, 0.5 mM DTT, and 100 μM Hsp70 activity modulator. The reaction was begun by adding 0.5 μL of a 1 mg/mL proteinase K stock stored at 4°C for months at a time in 50 mM Tris-HCl pH 8.0, 1 mM $CaCl_2$. After 5 min at room temperature, the reaction was quenched with 16 μL 100% trichloroacetic acid (TCA) and protein precipitated on ice for 20 min. The reaction was centrifuged at 13,000 rcf for 10 min at 4°C, the pellet rinsed with 100 μL acetone, and the sample centrifuged again for 20 min. The pellet was allowed to dry on the benchtop, resuspended in 10 μL 5X SDS-PAGE Sample Loading Buffer, and run on a 12% polyacrylamide gel.

FRET analysis of Hsp70 activity modulators

IAEDANS-labeled DnaK at 6 μM in Gel Filtration Buffer was added to a 96-well plate at 100 μL per well. Hsp70 activity modulators were added in duplicate to final concentrations of 100 μM, 50 μM, 25 μM, 12.5 μM, and 6.125 μM using 100X stocks in DMSO. A second plate was identical except ATP was added to 1 mM after addition of activity modulator using a 100X ATP stock. Fluorescence spectra were taken in the Polarstar spectrophotometer using the appropriate filter sets shown in Table 1.

AF555/AF594 double labeled DnaK at ~0.2 μM in FL Buffer pH 8.5 + 10% glycerol was aliquoted at 792 μL per sample and where appropriate mixed with 0.8 μL of 10 mM ADP stock to bring to 10 μM ADP. Then either 0.8 μL of DMSO vehicle was added or 50 mM MB stock was added to bring to 50 μM MB and allowed to equilibrate for 30 min. A fluorescence emission spectrum was taken upon excitation at 520 nm, then 8 μL of 100 mM ATP stock was added to the cuvette. After 45 min the fluorescence emission spectrum was taken again.

SAXS

SAXS data were collected on Beamline 4-2 of the Stanford Synchrotron Research Laboratory with the assistance of Hiro Tsuruta. The X-ray wavelength was 1.1271 Å. Data were collected in the angular range $0.001 < s < 0.0252$ with the detector 2.5 m from the sample, where scattering vector $s = 4\pi\sin\theta/\lambda$ where θ is the scattering angle and λ is the wavelength of X-rays. A Rayonix MX225-HE detector was used to collect data in two opposite 90º wedges around the primary beam. Protein samples were prepared at 1 mg/mL in SAXS Buffer with varying mixtures of nucleotides and Hsp70 activity modulators at saturating concentrations in 0.1% DMSO if applicable. All protein samples were filtered (0.22 μm) before data collection. Sixteen individual scattering curves of 3 seconds each were collected for each sample. If excessive variation was observed between individual curves an additional sample was prepared. After exclusion of curves differing by more than 10% from the initial curve, all remaining curves for each sample were averaged and the scattering curve from buffer alone (collected immediately before or after each sample) was subtracted. Data were processed using the ATSAS software package (Konarev et al., 2006). Radii of gyration were calculated from Guinier plots made in the Primus program.

Chapter 3

Results

CPM as a tool to assess cysteine reactivity

We chose cysteine residues as targets for fluorescent labeling due to the unique reactivity of cysteines to fluorophores containing maleimide and iodoacetic acid functional groups as well as the fact that DnaK has just one endogenous cysteine. We hypothesized that site-specific labeling of DnaK could be accomplished by finding two surface-exposed sites on the protein that reacted to fluorophores with a greater than threefold difference in rate. We planned to create a DnaK variant for FRET studies that would contain cysteines at both the fast-reacting and slow-reacting positions. Then we would label the double-cysteine variant first in a short labeling reaction with one fluorophore, after which the majority of fast-reacting sites but few slow-reacting sites would be labeled, followed by a long labeling reaction with a second fluorophore to label the slow-reacting site to completion.

To identify fast-reacting and slow-reacting sites, we measured the reactivity of a library of single-cysteine DnaK variants to the maleimide 7-diethylamino-3-(4'-maleimidylphenyl)-4-methylcoumarin (CPM) (Figure 4). CPM is initially non-fluorescent and fluoresces only upon binding to a thiol, permitting detection of the conjugation reaction in real-time as fluorescence increases. We hypothesized that relative reactivity of various cysteines to CPM would be predictive of relative reactivity to other fluorescent maleimides, in particular the Alexa Fluor dyes we wished to use as FRET fluorophores.

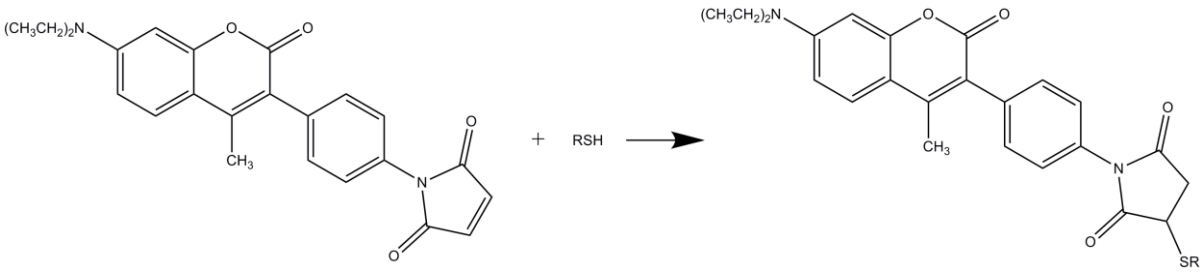

Non-fluorescent Fluorescent

Figure 4. CPM-thiol reaction. The thiol is added across the carbon-carbon double bond of the maleimide to yield a thioether.

We first wished to ensure that CPM-thiol conjugation is a well-behaved bimolecular reaction for single-cysteine DnaK variants. For initial analysis of cysteine reactivity, reaction rates were approximated by the mean slope of a progress curve during the first fifteen seconds after adding CPM. We found that the reaction rate increased linearly with increasing DnaK concentration as well as increasing CPM concentration, verifying that the fluorescence measured was a result of a reaction between protein and CPM and not oxygen or chemicals in the reaction buffer (Figure 5). Nevertheless, when closely examining CPM progress curves

we noticed a fast initial rate of reaction as well as a slow secondary rate of reaction (probably due to reaction of CPM with oxygen) that did not fit well to a single pseudo-first order rate.

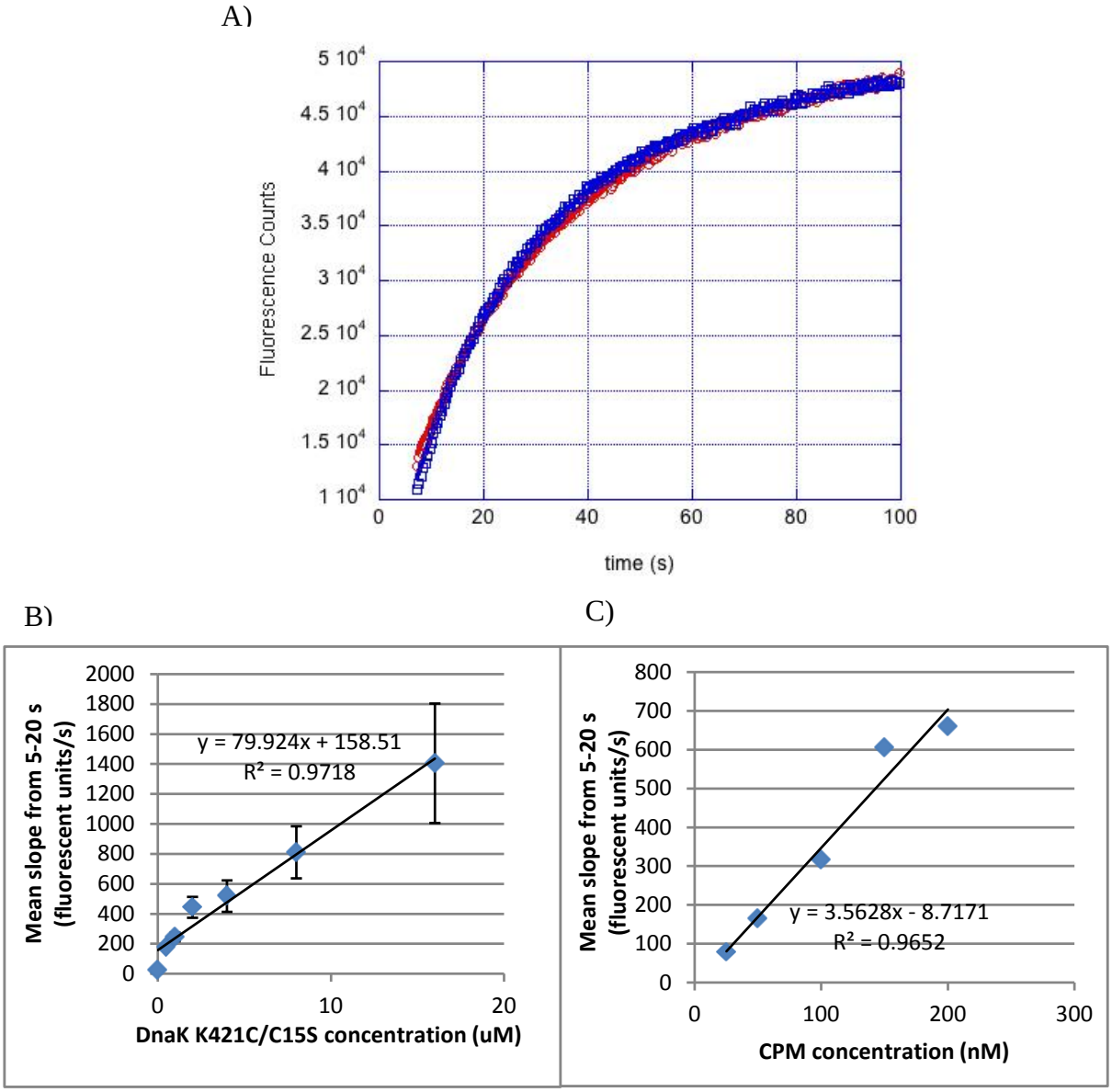

Figure 5. A) Sample progress curves (duplicates) for reaction of 50 nM CPM with 1 μM DnaK T136C/C15S. CPM reaction rate is linearly dependent on concentration of single-cysteine DnaK K421C/C15S (B) and CPM (C). Data points and error bars in (B) represent average and standard deviation, respectively, of three reactions. Linear fits calculated in Excel.

The reactivity to 50 nM CPM varies greater than tenfold across a range of seven single-cysteine DnaK variants at 1 μM concentration [Although K498C and A480C technically contain two cysteines, the endogenous C15 is buried in the NBD and reacts

minimally to CPM (data not shown)]. The background rate of reaction of 50 nM CPM with no protein present is 24 ± 4 fluorescent units/s, presumably due to reaction with dissolved oxygen in the buffer. The C15S variant of DnaK with no cysteines reacts to CPM at an initial rate of 51 ± 5 fluorescent units/s, which may be due to reaction with oxygen plus slow reaction with lysine residues. In the experiment shown in Figure 6, the slowest single-cysteine variant was S423C/C15S in the SBD (50 ± 20 fluorescent units/s) and the fastest single-cysteine variant was T136C/C15S in the NBD (540 ± 70 fluorescent units/s).

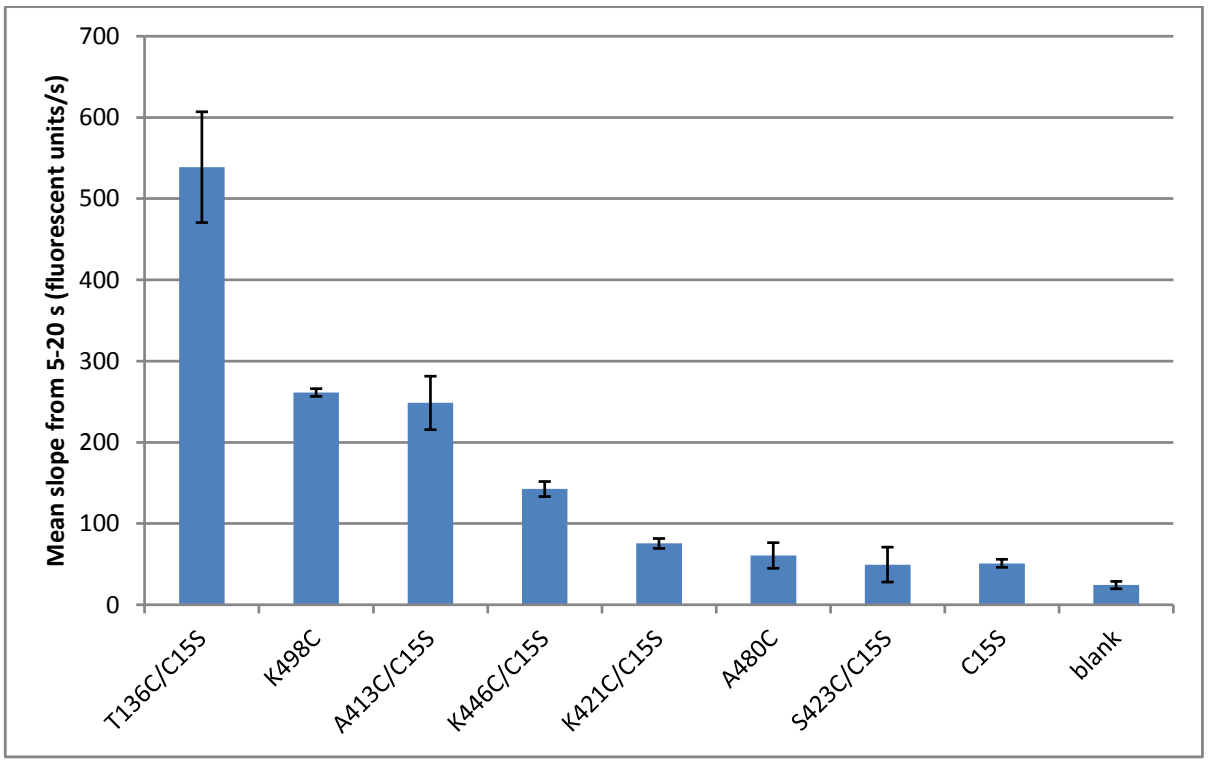

Figure 6. Reactivity of DnaK variants to CPM, as assessed by the mean slope of progress curves during the first fifteen seconds after addition of CPM. Labeling reactions were carried out in 96-well plate format with 1 μM DnaK and 50 nM CPM. Error bars represent standard deviation of three reactions.

We hypothesized that the variability in CPM reactivity among single-cysteine DnaK variants may reflect different accessibility to solvent for different cysteines. As a first step in testing this hypothesis we used Swiss Pdb Viewer to calculate the percent accessibility of the cysteine residues based on X-ray diffraction models of the NBD and SBD. The "access" command gives the relative accessibility of a residue X compared to a 100% reference value being computed in an extended conformation of the pentapeptide GGXGG (Schwede and Guex). The "access" algorithm accurately predicts CPM reactivity for some cysteines but not for others (Table 3). For example, S504C has a very high percent accessibility of 51% as well

as a fast CPM reaction rate of 880 fluorescent units/s. However, T136C has a relatively small percent accessibility (22%) but a large CPM reaction rate (540 fluorescent units/s).

Next we looked for a correlation between CPM reaction rates and the rate of amide hydrogen exchange for the peptide segment containing each cysteine. Rates of hydrogen exchange reflect solvent accessibility of protein regions (Rist et al., 2006). Rist et al. divided DnaK peptide segments into four bins based on percent deuteration after ten minutes in D_2O (0-25%, 25-50%, 50-75%, 75-100%). Again, CPM reaction rates reflect percent deuteration for some cysteines but not others; moreover, percent deuteration does not correlate well with accessibility calculated by Swiss Pdb Viewer. The Rist peptide segments were rather long, up to 26 amino acids, so percent deuteration of a segment may not accurately reflect solvent accessibility of one cysteine within the segment.

Finally, we manually inspected X-ray diffraction models of the NBD and SBD to see if there is a correlation between the electrostatic potential surrounding a cysteine and CPM reactivity. The majority of cysteines are found in negative or neutral regions; only S504C occupies a positively charged region. S504C also has a very high reactivity to CPM, so it is possible that nearby positive charges stabilize the nucleophilic thiolate anion.

Table 3. Summary of accessibility data and CPM labeling rates (from Figure 6) for mutant cysteine residues in DnaK. Percent accessibility was calculated using the Swiss PdbViewer "access" command for cysteines after virtually mutating them in the DnaK X-ray crystal structure. Percent deuteration refers to the proportion of amide hydrogens exchanged for deuterium in peptide segments in which a given wild-type residue is included (Rist et al., 2006). For electrostatic potential, the electrostatic potential surface was calculated for DnaK in PyMOL and the color reflecting degree of charge immediately surrounding each mutant cysteine was assessed by eye; --: negative, -: slightly negative, 0: neutral, +: slightly positive, ++: positive. Neighboring amino acids are those within 5 angstroms of the mutant residue, calculated from crystal structures loaded in PyMOL. The CPM reactivity rates of the last three mutants were measured in a separate experiment and so are not directly comparable with those above.

Mutant residue	**CPM Reactivity (fluorescent units/s)**	**Percent Accessibility of Cysteine**	**Percent Deuteration of Peptide Segment After 10 min**	**Electrostatic Potential of Surrounding Surface**	**Neighboring Amino Acids**
T136C	539	22	0-25	-	E94, D132, R135, F137
K498C	261	32	50-75	-	F457, S487, E496, E497, I499
A413C	249	29	50-75	0	S398, L399, T410, I412
K446C	143	8	0-25	--	R445, D526, F529, D530
K421C	76	29	50-75	-	H422, S423, T475, D477
A480C	61	48	0-25	--	I418, P419, D481, G482, D479
S423C	49	26	50-75	0	K421, E473, T475, D477, S487
S504C	879	51	50-75	+	K502, A503, S505, G506
A449C	552	47	0-25	0	G406, R447, A448, D450, N451
E430C	267	21	50-75	-	A429, D431, N432, Q433, R467, H544

To test experimentally if reactivity of a cysteine to CPM reflects solvent accessibility of the cysteine, we investigated the effect of proteinase K digestion on CPM reaction rate for three single-cysteine DnaK variants. Proteinase K is a broad spectrum serine protease with preference for peptide bonds adjacent to the carboxyl group of aliphatic and aromatic amino acids (Ebeling et al., 1974). Digestion with proteinase K should destroy tertiary structures limiting solvent accessibility at certain sites, leading to a fast CPM reaction rate for all single-cysteine variants. Incubation of DnaK with 0.1% w/w proteinase K for six hours at 37 degrees C leads to complete digestion of DnaK as shown by the lack of protein bands on an SDS-PAGE gel (data not shown). For K446C/C15S, CPM reactivity increases from 260 ± 10 fluorescent units/s with no proteinase K present to 340 ± 50 fluorescent units/s with 0.01% proteinase K before decreasing again for higher proteinase K concentrations. Surprisingly, for K421C/C15S there is no trend in CPM reactivity with increasing proteinase K concentration, and for T136C/C15S there is a dramatic decrease in CPM reactivity from 1930 ± 90 fluorescent units/s with no proteinase K to 240 ± 10 fluorescent units/s with 3% proteinase K (Figure 7A). It may be that proteinase K inhibits the CPM-cysteine reaction in some fashion. It is also possible that cysteine oxidation occurs during incubation of DnaK with proteinase K.

We next tried to maximize the CPM labeling rate by denaturing DnaK with SDS. At intermediate concentrations of SDS (0.003%-0.03%), CPM rates become larger and highly variable, however SDS concentrations above 0.3% decrease CPM reaction rates to a fraction of the rate with no SDS present (22 ± 14 fluorescent units/s at 2% SDS compared to 889 ± 140 fluorescent units/s at 0% SDS for T136C/C15S) (Figure 7B). To determine if the increase in reaction rate at intermediate SDS concentrations is due to unfolding of DnaK, we used circular dichroism, a technique based on the difference in absorption of left-handed and right-handed circularly polarized light by chiral molecules. α-helix and β-sheet secondary structures and random coils each have unique CD spectra, and at 222 nm α-helices and β-sheets give a large negative CD signal while random coils give a CD signal of approximately zero. Thus, increases in the CD signal from a negative value upon addition of SDS would indicate denaturation of DnaK. With 3 μM DnaK and 0.1% SDS, a concentration higher than that at which we saw an increase in CPM reactivity, the CD at 222 nm is -25.5 millidegrees compared to -29.5 millidegrees with no SDS (data not shown). This corresponds to a less than 15% change in CD signal in the presence of 0.1% SDS, leading us to conclude that at SDS concentrations between 0.003% and 0.03% where we see large and highly variable CPM rates, there is minimal denaturation of DnaK.

A)

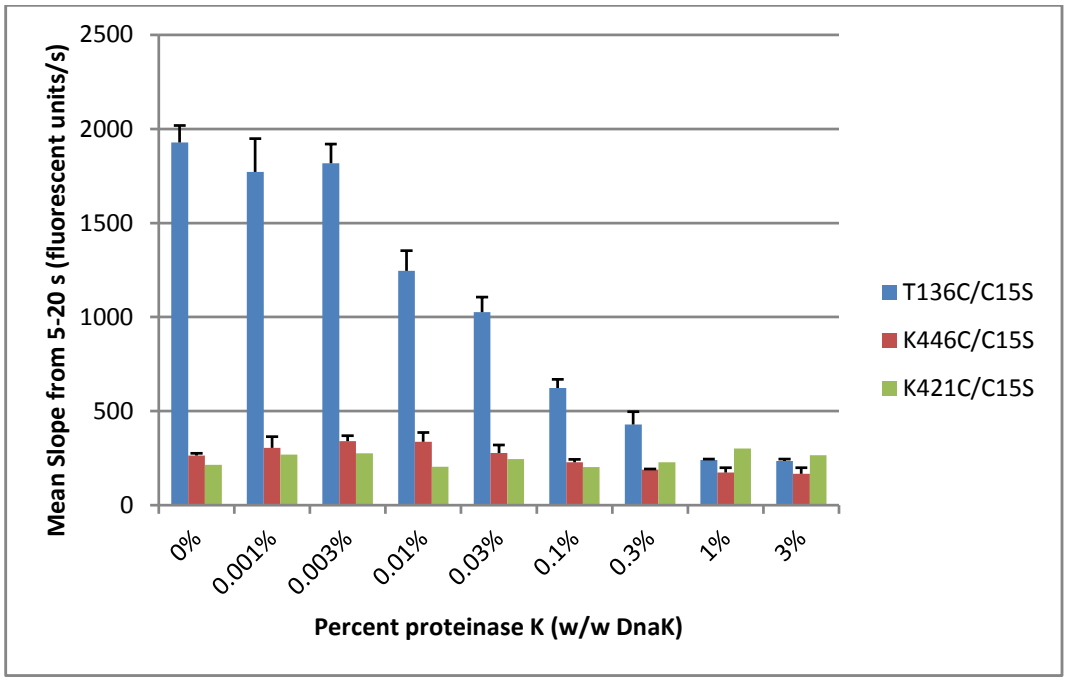

B)

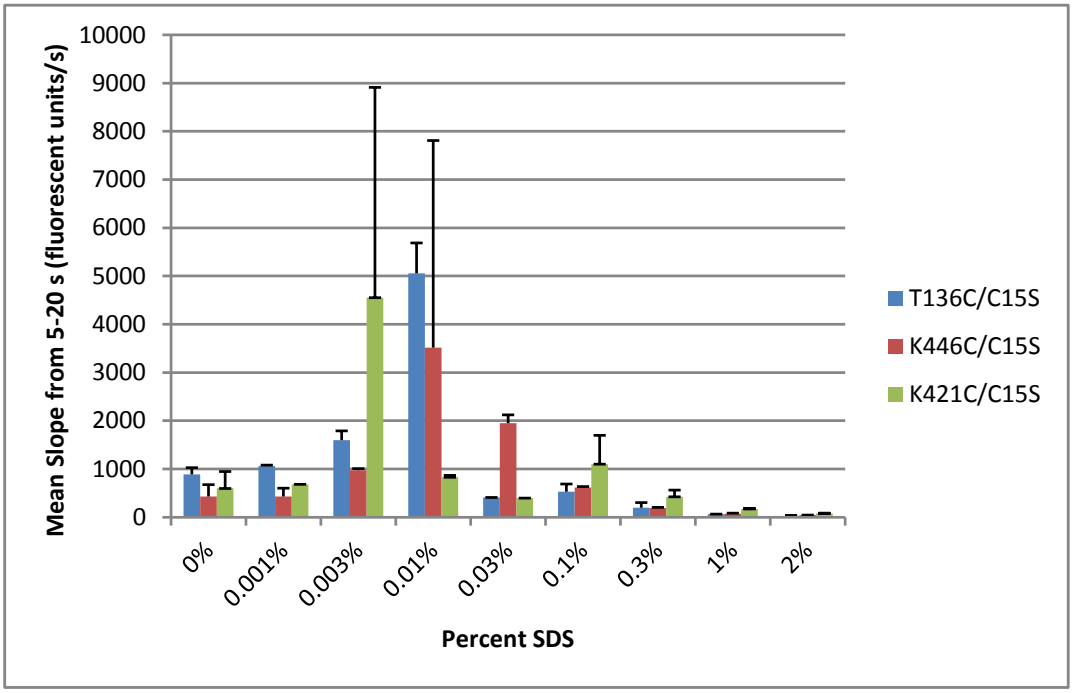

Figure 7. Effect of proteinase K (A) and SDS (B) on CPM reaction rate for three single-cysteine DnaK variants. Data and error bars represent average and standard deviation of duplicates.

Since we desired to have the FRET donor and acceptor in different domains, it was convenient that the fast-reacting cysteine T136C is in the NBD and the slow-reacting cysteine

S423C is in the SBD. We chose to further characterize these locations and possibly augment their difference in reactivity by performing CPM labeling under a range of pH conditions, as it is likely that the rate-limiting step in the cysteine-CPM reaction is deprotonation of the thiol. We carried out reactions of CPM to DnaK T136C/C15S and S423C/C15S at pH ranging from 5.5 to 10 and fit the progress curves to pseudo first-order rates in Kaleidagraph. Between pH 5.5 and 6.5 the rate is extremely slow for both T136C and S423C. The rates climb steeply between pH 7 and 8 and are relatively constant between pH 8 and 9. Above pH 9 the rates increase again rapidly, probably due to deprotonation of lysines. The greatest difference in rates between T136C and S423C occurs at pH 8.5, when the rate constant for T136C is $0.12 \pm 0.02\ s^{-1}$ and for S423C is $0.043 \pm 0.003\ s^{-1}$ (Figure 8).

If the rate limiting step in the CPM-thiol reaction is indeed deprotonation of the cysteine thiol, then the rate should be directly proportional to the concentration of thiolate anion

$$r = \alpha \times [S^-] \qquad \text{[Equation 7]}$$

where α is a constant. According to the definition of the acid dissociation constant (K_a),

$$K_a = ([H^+][S^-])/[HS] \qquad \text{[Equation 8]}$$

Let $\beta = [HS] + [S^-]$, a constant. Then $[HS] = \beta - [S^-]$ and equation 8 can be rearranged to

$$[S^-] = \beta \times \{K_a/([H^+] + K_a)\} \qquad \text{[Equation 9]}$$

or

$$[S^-] = \beta \times \{K_a/(10^{-pH} + K_a)\} \qquad \text{[Equation 10]}$$

Plugging into Equation 7 and letting $\gamma = \alpha \times \beta$ we have

$$r = \gamma \times [K_a/(10^{-pH} + K_a)] \qquad \text{[Equation 11]}$$

We fit the pH dependence of the CPM reaction below pH 9 to equation 11 and found the pK_a values for T136C and S423C to be 7.8 and 7.6, respectively. The plateau in reactivity for both sites between pH 8 and 9 suggests the cysteines are fully ionized in these pH conditions where we see the largest difference in reactivity between the sites. Thus, the nearly threefold difference in reaction rate between T136C and S423C at pH 8.5 is not due to significantly different pK_a's. Rather, the rate difference must be due to other electrostatic or steric factor(s).

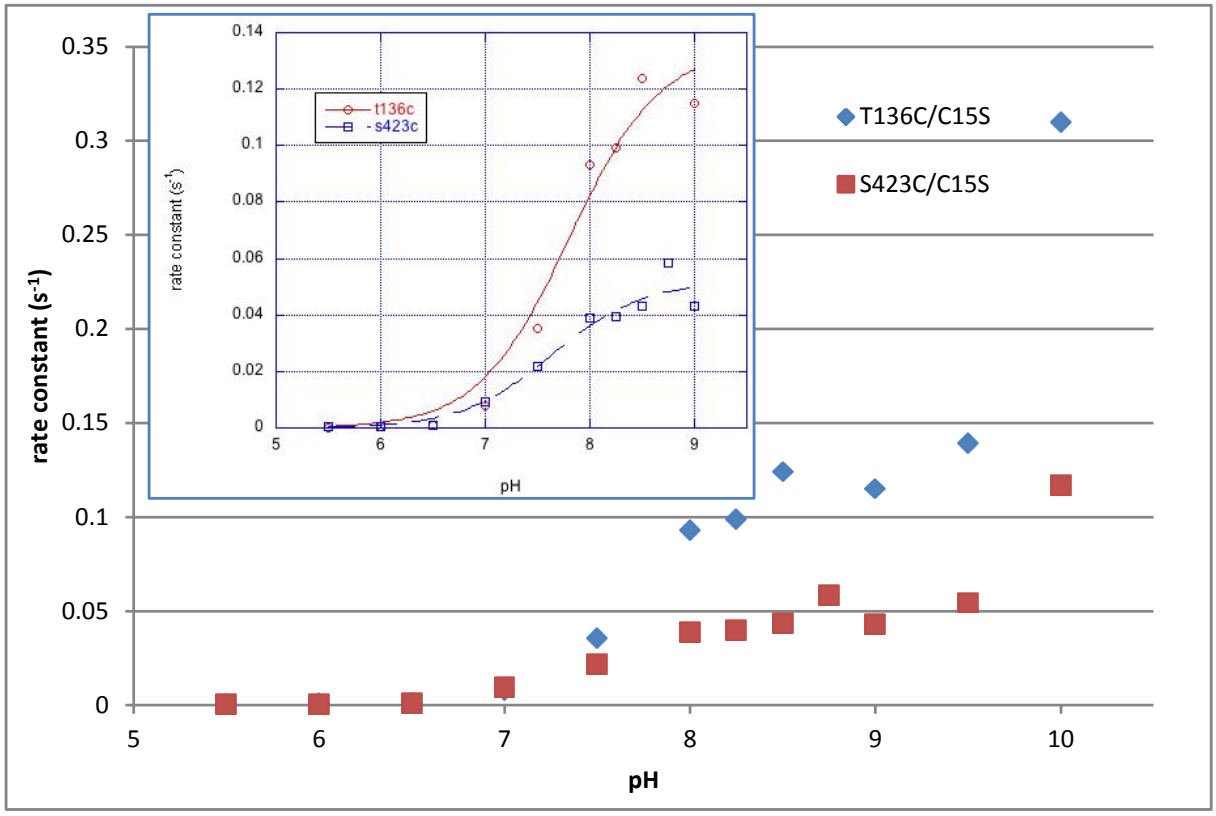

Figure 8. pH dependence of DnaK-CPM reaction. Inset shows region of the curves that can be fit to a single deprotonation event with pK_a of T136C = 7.8 (R^2 = 0.973) and pK_a of S423C = 7.6 (R^2 = 0.959).

Characterization of Alexa Fluor dyes

Our results demonstrated that at pH 8.5, the CPM reactivity of T136C in the NBD and S423C in the SBD differ by approximately threefold. Although useful for assessing maleimide reactivity, CPM is not especially suitable as a FRET fluorophore due to its low quantum yield and lack of a combatible partner fluorophore. For FRET fluorophores we planned to use Alexa Fluor maleimides, which are bright enough for single molecule studies, photostable, fluoresce over a wide pH range, and have good water solubility (Haugland, 2005). As a first step in characterizing the fluorescence properties of the Alexa dyes, we measured the fluorescence of a twofold serial dilution of Alexa Fluor 488 and Alexa Fluor 555 in water. Figure 9 shows the fluorescence of each dilution on a log-log scale. At concentrations down to approximately 10 nM, fluorescence goes linearly with dye concentation, whereas below 10 nM nonlinear effects begin to be observed as the sensitivity limit of the Polarstar fluorescence spectrometer is reached (increasing the voltage across the photomultiplier tube may permit even higher sensitivity). Since we will be working with

fluorescently labeled proteins at concentrations in the hundreds of nanomolar to low micromolar, the sensitivity of the Polarstar is sufficient.

A)

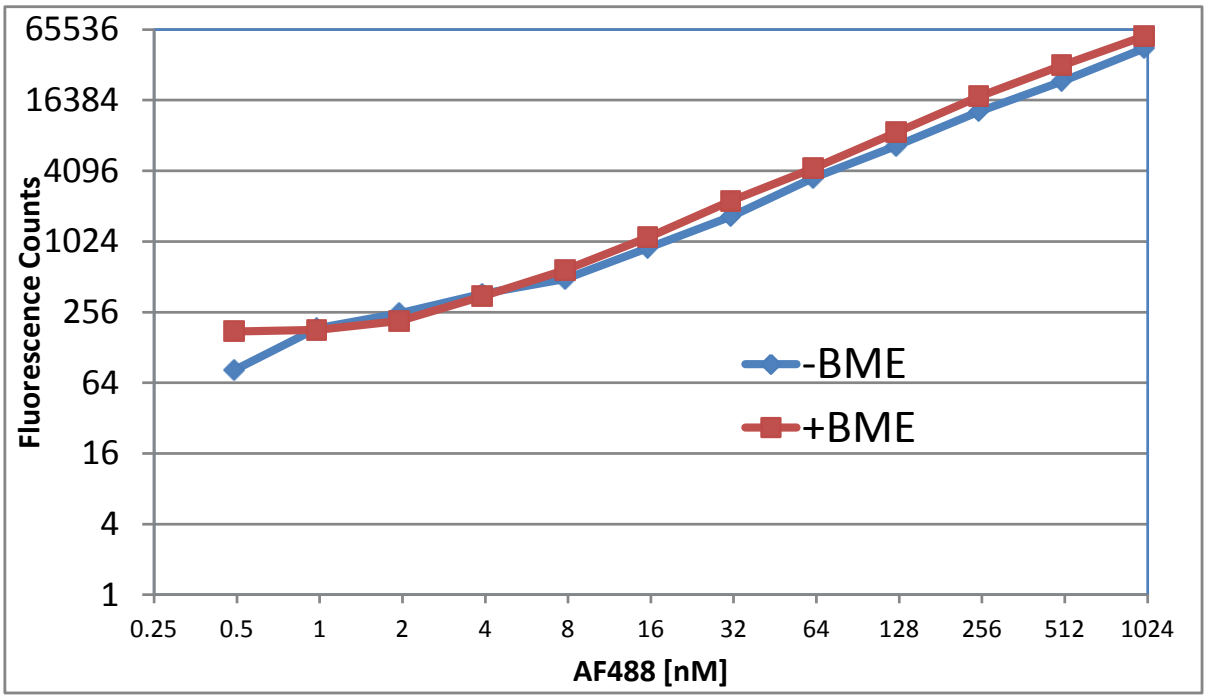

B)

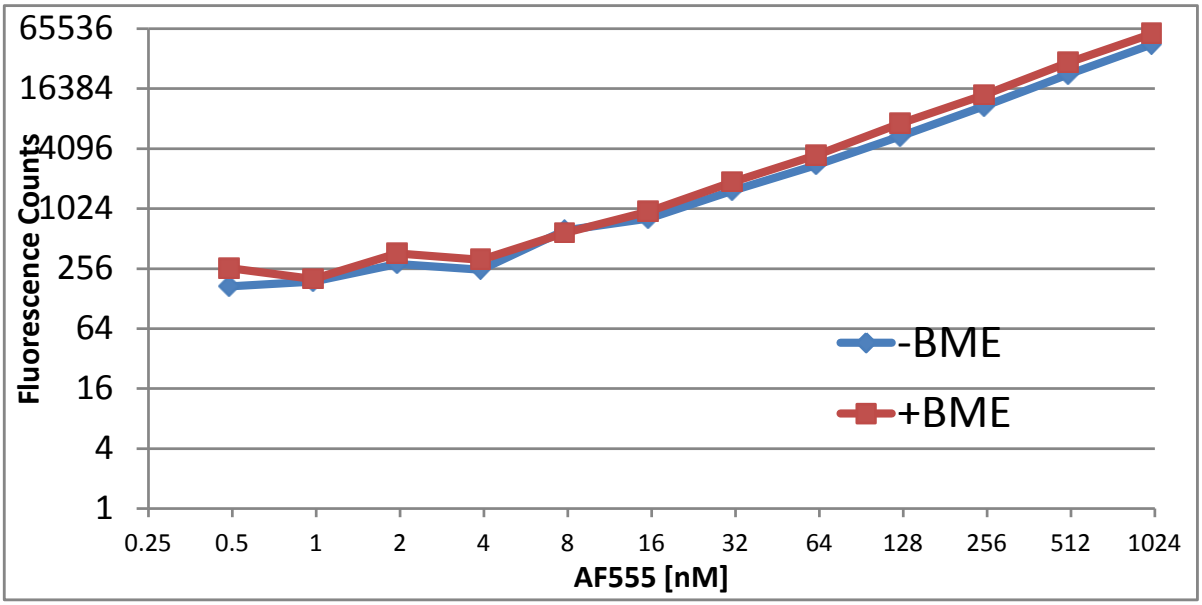

Figure 9. Serial dilution series of Alexa Fluor maleimides 488 and 555 in water. Fivefold excess of β-mercaptoethanol (BME) was added to one set of dilutions as a low molecular weight thiol to react with the maleimide.

As a second step in characterization of the Alexa Fluor maleimides, we determined their quantum yield both free in solution and bound to DnaK single-cysteine variants

T136C/C15S and S423C/C15S. Since we did not have reference fluorophores with known quantum yields at the required excitation wavelengths, we will report "quantum yield" as (fluorescence counts)/(absorbance units) (in fact, fluorescence counts/absorbance units is directly proportional to quantum yield). The quantum yield of both AF488 and AF594 is concentration independent below 1 μM and is approximately 530 (fluorescence counts)/(absorbance units) for AF488 and approximately 2500 (fluorescence counts)/(absorbance units) for AF594. Above 1 μM the fluorescence yield decreases for both dyes, probably because the fluorescence emitted by some dye molecules is absorbed by surrounding dye molecules before it is detected by the photomultiplier tube (Figure 10). Next we measured the quantum yield of AF488 and AF594 when bound to T136C/C15S and S423C/C15S at [DnaK-dye] ≈ 200 nM. Interestingly, the quantum yield of AF488 decreased by about 25% when bound to both T136C and S423C, but the quantum yield of AF594 increased by 7% when bound to T136C and S423C (Table 4). This suggests that there are no position-specific effects on the quantum yield of DnaK-bound AF488 and AF594.

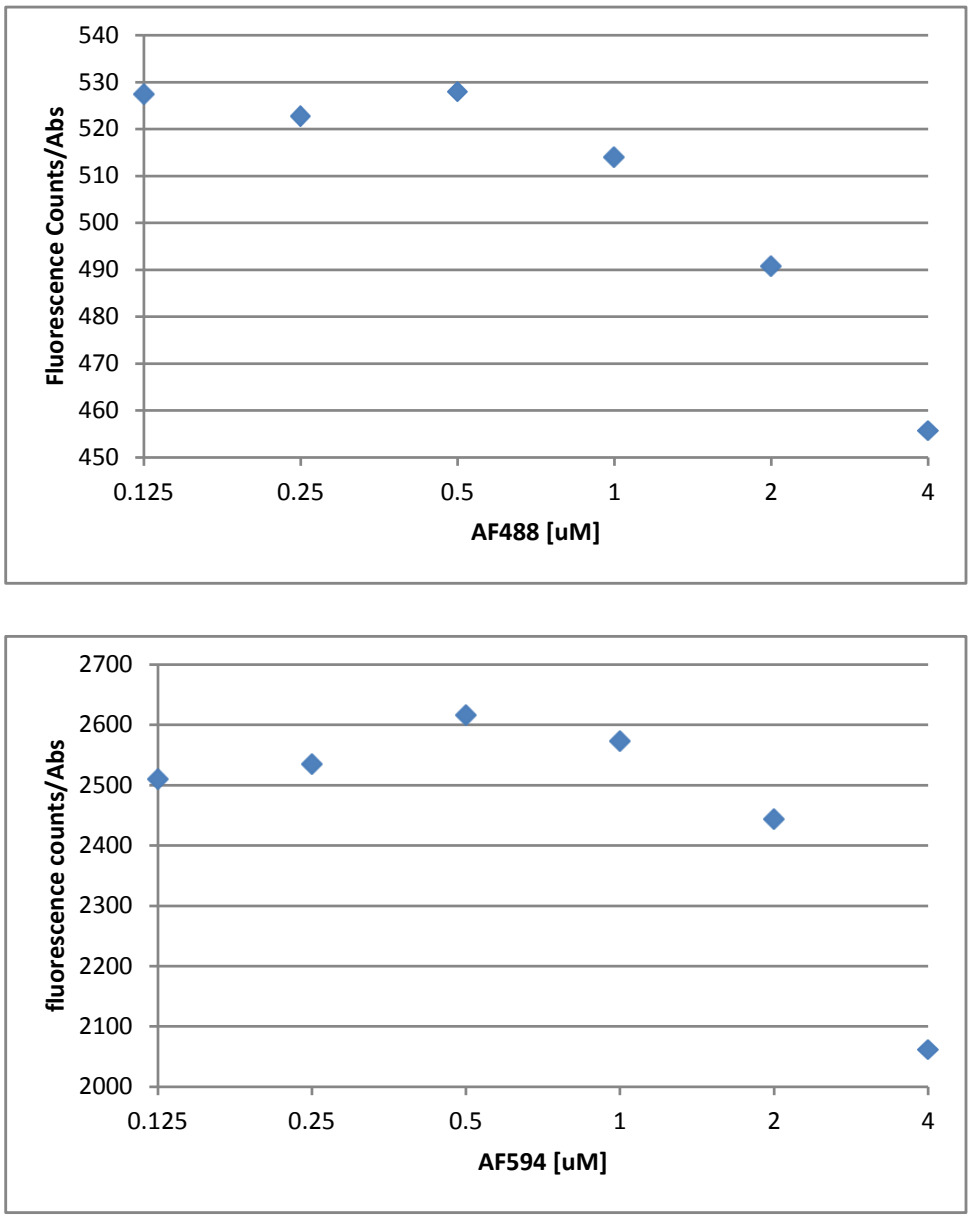

Figure 10. Fluorescence quantum yield of AF488 and AF594 in Fluorescent Labeling Buffer pH 8.5 + 10% glycerol reacted with 100-fold excess GSH.

Table 4. Fluorescence quantum yield of AF488 and AF594 bound to DnaK T136C/C15S and S423C/C15S in Fluorescent Labeling Buffer + 10% glycerol. All values expressed in (fluorescence counts)/(absorbance units).

	AF488-bound	**AF594-bound**
DnaK T136C/C15S	394	2700
DnaK S423C/C15S	413	2711

Reactivity of Alexa Fluor maleimides to T136C and S423C

We next wished to characterize the reactivity of the Alexa Fluor maleimides and ensure that the relative reaction rates at T136C and S423C to Alexa dyes reflected those to CPM. We first attempted to monitor the dye-thiol conjugation reaction via fluorescence anisotropy, a technique based on the fact that a fluorophore excited with plane polarized light will emit polarized light in the same plane if the fluorophore remains stationary throughout the excited state. If the fluorophore rotates or tumbles during the excited state, fluorescence will be emitted in a different plane. In general, a small organic fluorophore in solution will have rotational correlation time faster than its fluorescence lifetime, so an ensemble of small fluorophores in solution will emit fluorescence in every orientation at random as each fluorophore rotates in a different direction, i.e. fluorescence is depolarized. If the fluorophore is bound to a large protein, however, the rotational correlation time will be relatively slower, leading to preservation of polarization in fluorescence emitted. Thus, the progress of a fluorophore-protein conjugation reaction can be assessed by monitoring changes in fluorescence polarization over time. Polarization P is defined as

$$P = (I_v - I_h) / (I_v + I_h) \qquad \text{[Equation 12]}$$

and the related parameter anisotropy r is defined as

$$r = (I_v - I_h) / (I_v + 2I_h) \qquad \text{[Equation 13]}$$

where I_v is the intensity of vertically polarized emission light and I_h is the intensity of horizontally polarized emission light, and excitation light is vertically polarized. Polarization P ranges from – 0.33 to + 0.5 and anisotropy r ranges from – 0.25 to + 0.4 (Haugland, 2005). Figure 11 depicts the fluorescence anisotropy technique in schematic form.

We hypothesized that conjugation of Alexa Fluor dye to DnaK would cause an increase in fluorescence anisotropy that would allow us to track the reaction in real time. The reaction of AF555 with DnaK T136C/C15S causes an increase in anisotropy from

approximately 30 anisotropy milli-units (mu) to 60 mu over about ten minutes. Surprisingly, the reaction of AF555 with DnaK S423C/C15S begins at about 67 mu and over a similar time course the fluorescence anisotropy decreases slightly to 60 mu. The reaction of DnaK S504C/C15S to AF555 also produced the expected increase in anisotropy during conjugation, whereas every other variant tested (K421C/C15S, K498C, and WT) gave slightly decreasing curves. For the reactions producing increasing anisotropy curves, the fluorescence intensity of both polarized emission channels increased and vertically polarized emission light increased more than horizontally polarized emission light. For reactions producing slightly decreasing anisotropy curves, both emission channels decreased slowly (Figure 12). Similar anisotropy curves were obtained in reactions of DnaK variants with AF488.

Interestingly, another experiment showed that the fluorescence anisotropy of free AF488 is approximately 22 mu whereas the fluorescence anisotropy of purified DnaK T136C/C15S and S423C/C15S labeled with AF488 is about 120 mu (Table 5). This suggests that unreacted free dye present during the conjugation reaction may interfere with fluorescence polarization, possibly by absorbing polarized fluorescence and re-emitting it scrambled. We concluded that fluorescence polarization was not a useful method for tracking the DnaK-Alexa dye reaction.

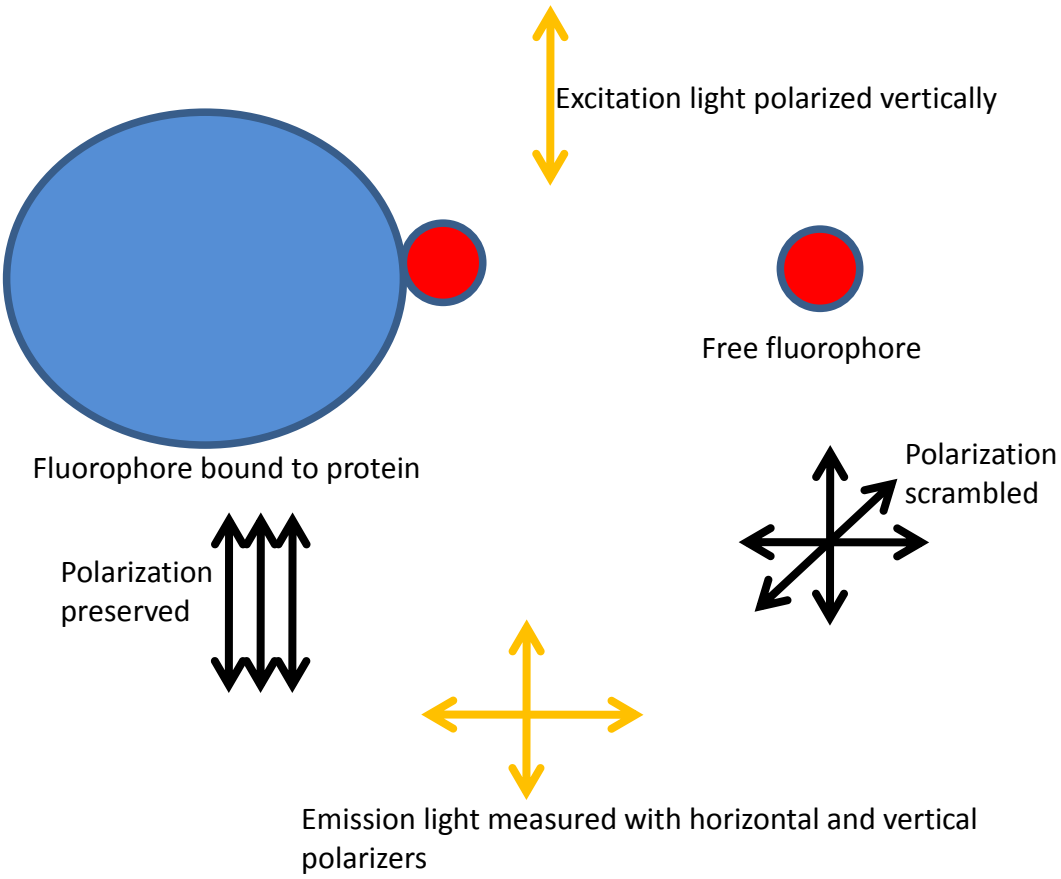

Figure 11. Schematic of fluorescence anisotropy. The sample is excited with vertically polarized light. Rotational diffusion of free fluorophore is much faster than the fluorescence lifetime, leading to emission of fluorescence at random in all orientations. Rotational diffusion of fluorophore bound to a large protein is slow compared to the fluorescence lifetime, leading to preservation of polarization. Emission light is detected through vertical and horizontal polarizers.

A)

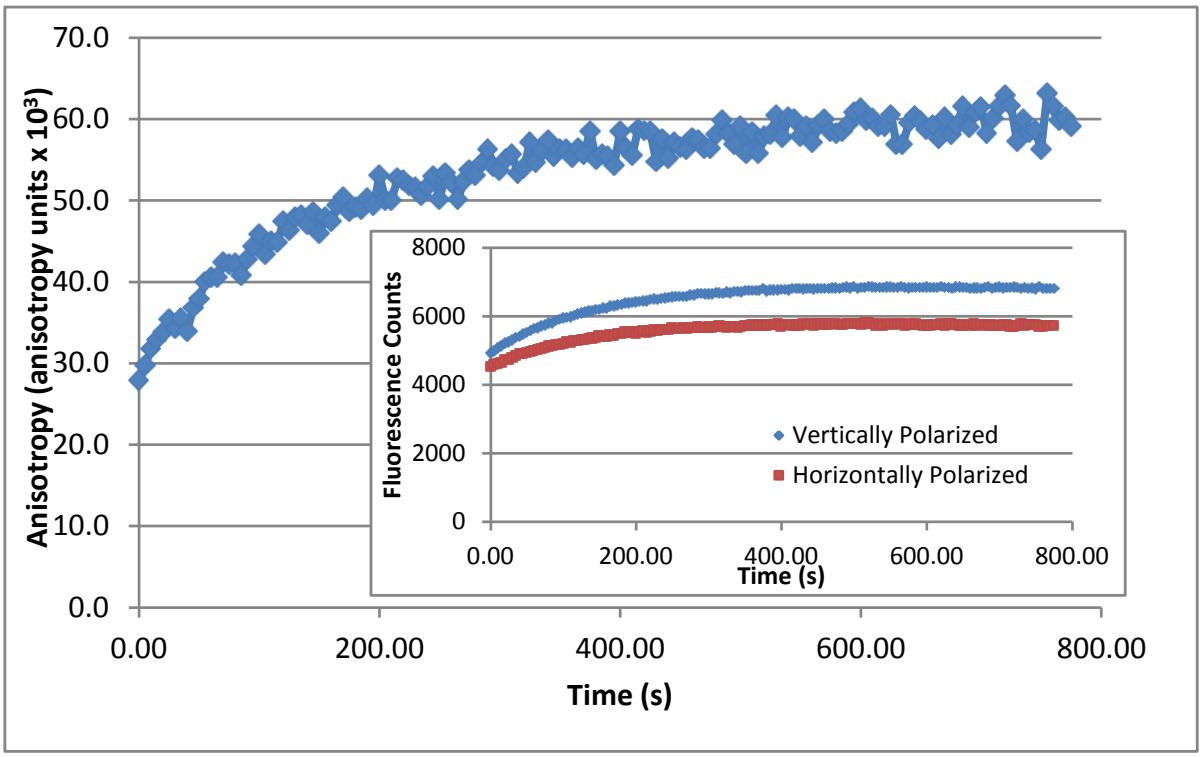

B)

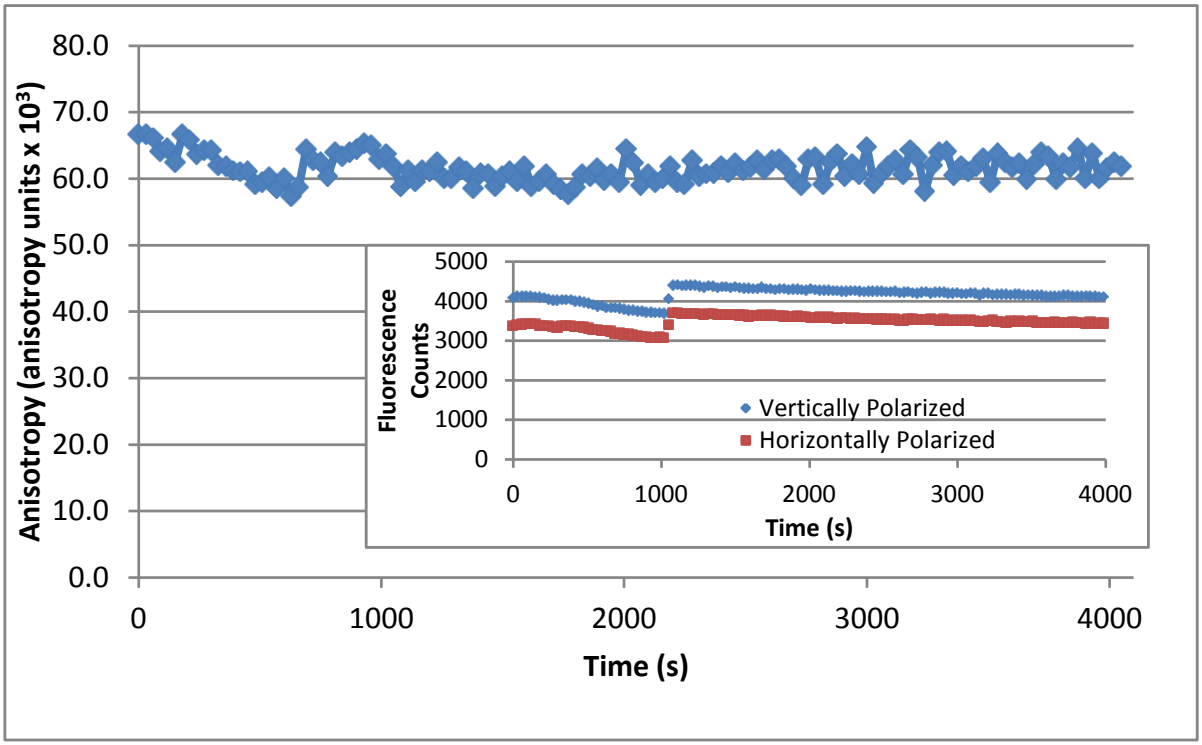

Figure 12. Reaction of Alexa Fluor 555 with DnaK T136C/C15S (A) and S423C/C15S (B) at pH 7.4 tracked by fluorescence anisotropy. Dye-protein conjugation produces an increase in anisotropy for the T136C/C15S reaction, but an unexpected small decrease in anisotropy for the S423C/C15S reaction. Insets show the intensity of fluorescence detected at the vertically polarized and horizontally polarized emission channels.

Table 5. Fluorescence anisotropy of AF488 reacted with 100-fold excess GSH ("free") or bound to DnaK T136C/C15S and S423C/C15S. Protein-bound samples are approximately 0.2 μM. All samples in FL Buffer pH 8.5 + 10% glycerol.

AF488	Anisotropy (mu)
Free 0.125 μM	22.5
Free 0.25 μM	21.6
Free 0.5 μM	21.8
Free 1 μM	21.7
Free 2 μM	20.9
Free 4 μM	21.2
Bound to T136C/C15S	119.5
Bound to S423C/C15S	120.4

Due to the suspicious results from fluorescence anisotropy time courses for some DnaK variants, we moved from real-time monitoring of the conjugation reaction to quenching time points with 100-fold excess GSH. We ran protein from each time point on an SDS-PAGE gel and used a fluorescence gel scanner in combination with densitometry software to quantify the intensity of the fluorescent protein band at each time point. The fluorescence intensity was normalized to the intensity of the Coomassie-stained protein band as assessed using the same software. Figure 13 shows the fluorescence labeling time courses of AF555 with DnaK T136C/C15S and S423C/C15S. We chose to run three labeling reactions for each DnaK variant at pH 8.0, 8.5, and 9.0, as the greatest difference in reaction rates for CPM at T136C and S423C occurred within this pH range. For both DnaK variants the reaction proceeds faster at higher pH values. We fit the progress curves to pseudo-first order kinetics in Kaleidagraph and found the greatest difference in reaction rates (≈ twentyfold) occurs at pH 8.5, where the rate for T136C/C15S is $0.029 \pm 0.001\ s^{-1}$ and the rate for S423C/C15S is $0.00141 \pm 0.00005\ s^{-1}$.

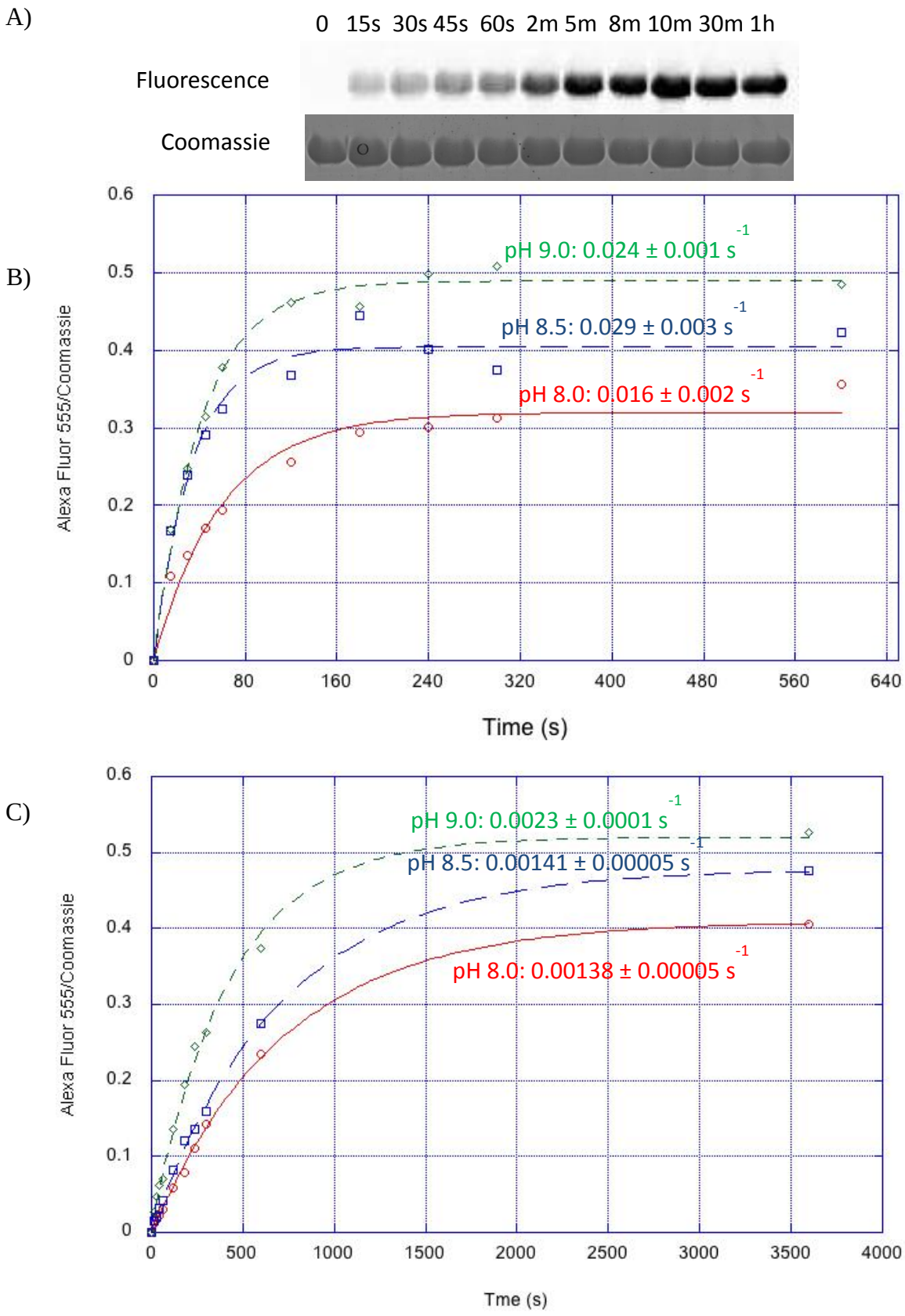

Figure 13. A) Sample DnaK-Alexa dye reaction visualized on SDS-PAGE gel, in this case with T136C/C15S and AF555. For each time point, the extent of the reaction was determined by dividing the volume of fluorescence counts in the DnaK band by the intensity of Coomassie staining of the band. B) and C) DnaK-AF555 reaction progress curves followed using the gel-based method at three different pH values for T136C/C15S (B) and S423C/C15S (C). Rate constants with errors are given as calculated in Kaleidagraph.

Creation of pMSK [T136C/S423C/C15S] and purification of DnaK T136C/S423C/C15S

The above experiments demonstrated that the reactivity of T136C to two different fluorescent maleimides is greater than the reactivity of S423C. In the case of CPM, there is a threefold difference in reaction rate constants between the cysteines at pH 8.5, and for Alexa Fluor 555 there is a twentyfold difference in rate constants. Since T136C is located in the NBD and S423C is located in the SBD, positions 136 and 423 are convenient sites for conjugating fluorophores which could be used to detect interdomain distance changes via FRET. The Bertelsen et al. NMR model of full length DnaK with ADP bound predicts the α carbons of T136 and S423 to be approximately 39 Å apart (Figure 14). The Alexa Fluor dye pair with the best matched Förster radius for such a distance is the AF555-AF594 pair, for which R_0 = 47 Å. Assuming the NMR model is accurate and there are no changes in Förster radius upon conjugation of the fluorophores to DnaK, the FRET efficiency in the ADP-bound state would be 75%. In the ATP-bound form the NBD and SBD should hypothetically become closer and increase FRET beyond 75%. Another FRET pair the Wilbanks lab has immediately available is the AF488-AF594 pair, for which R_0 = 60 Å. If this dye pair is used, FRET efficiency in the ADP-bound state would theoretically be 93%. Thus, T136C and S423C are not ideal positions for fluorescent labeling with the Alexa Fluor dyes because DnaK's conformational change would result in a modest change in FRET. Nevertheless, the large difference in reactivity to maleimides at the two sites led us to proceed with production of a DnaK T136C/S423C/C15S variant.

We employed a PCR-based strategy to introduce the T136C mutation into the gene encoding DnaK S423C/C15S on the pMSK [S423C/C15S] plasmid (Figure 15). We began by amplifying two neighboring regions of the DnaK gene using mutant PCR primers. In one reaction, the forward primer contained an ACT→TGT codon change producing a T→C amino acid substitution at position 136 (T136C fwd), and the reverse primer was template-strand bases 1623-1606 of the DnaK gene (DnaK 1623-1606). In the second reaction, the forward primer was 55 bp upstream of the beginning of the DnaK coding sequence (pMS119EH-fwd) and the reverse primer contained a region complementary to the T136C codon change (T136C rev). Nanogram quantities of both PCR products were removed from an agarose gel and mixed in a secondary PCR reaction with pMS119EH-fwd and DnaK 1623-1606 primers only. The secondary PCR product, an approximately 1.6 kb fragment containing the T136C mutation, and pMSK [S423C/C15S] were cut with BglII and XbaI restriction enzymes and ligated together, producing pMSK [T136C/S423C/C15S]. This plasmid was transformed into BB1553 cells for protein expression.

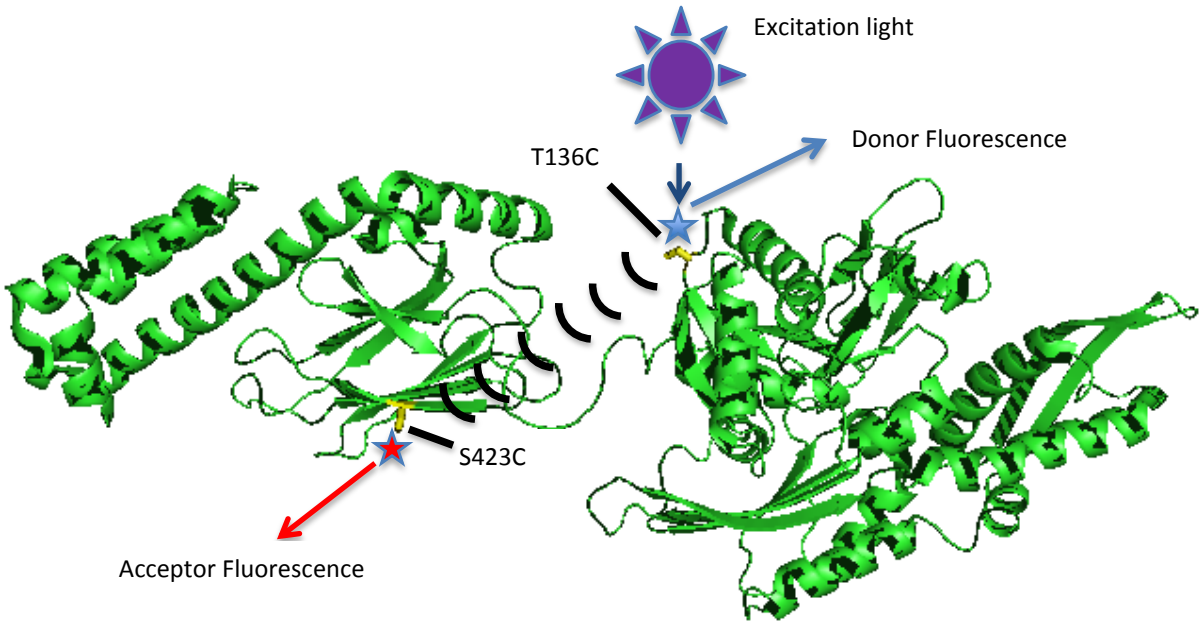

Figure 14. Location of T136C, the donor fluorophore conjugation site, and S423C, the acceptor fluorophore conjugation site, in DnaK. Image generated in PyMOL from PDB file 2KHO (Bertelsen et al., 2009).

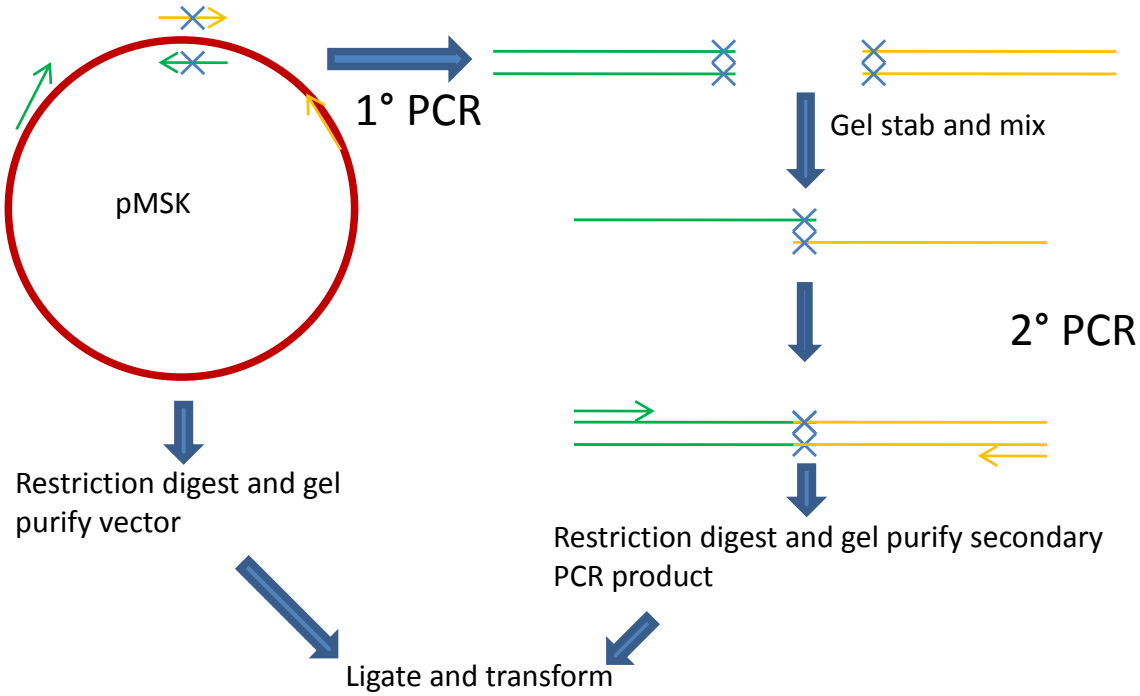

Figure 15. PCR-based mutagenesis to create pMSK [T136C/S423C/C15S].

The Wilbanks lab has developed an efficient purification protocol using three chromatography steps for DnaK, which we employed to purify DnaK T136C/S423C/C15S. The protocol consists of a crude anion exchange step, an ATP affinity step, and polishing with gel filtration. DnaK T136C/S423C/C15S behaved similarly to other DnaK variants during purification (Figure 16). Yield was approximately 60 mg.

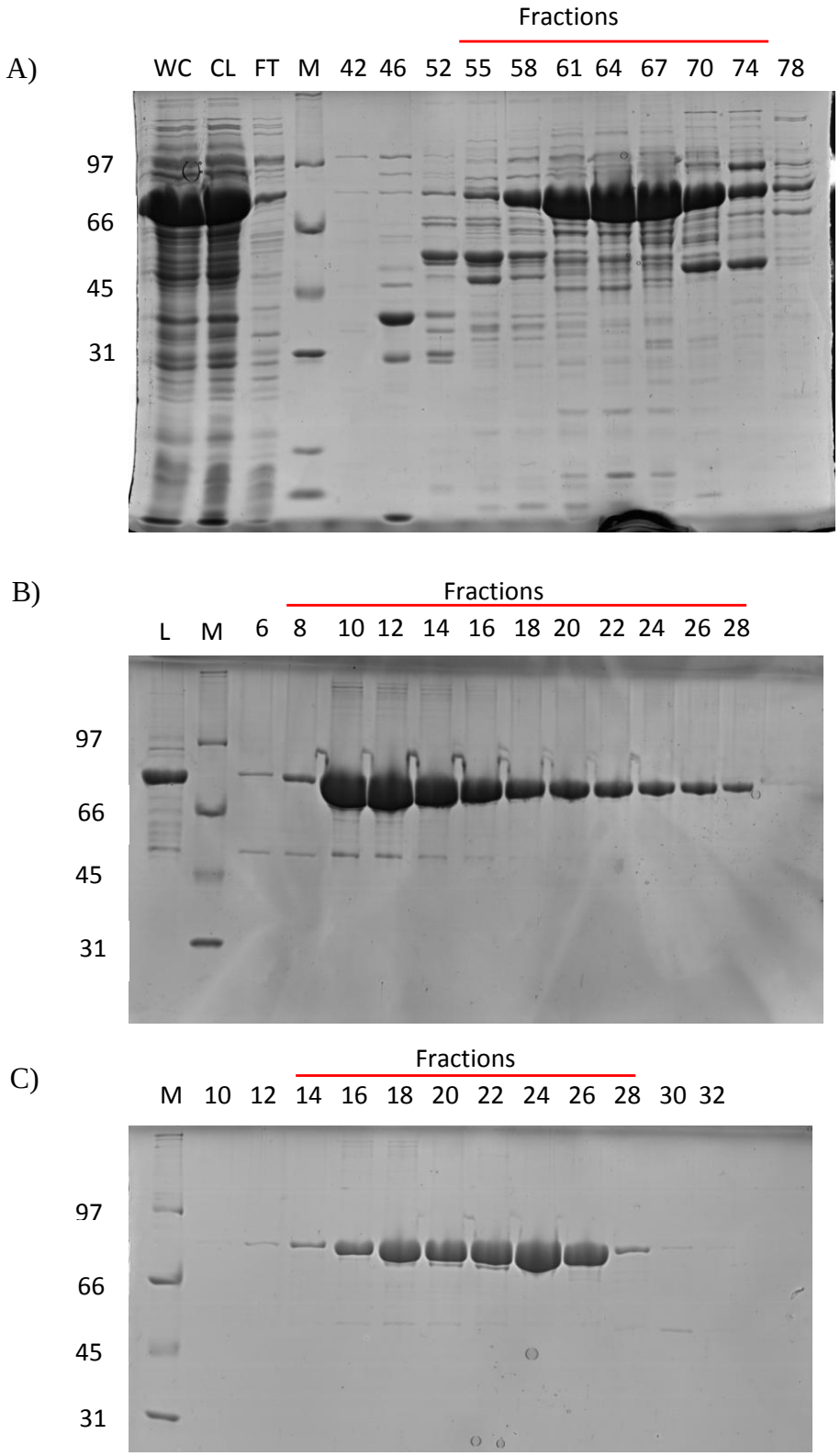

Figure 16. SDS-PAGE protein gels showing purification of DnaK T136C/S423C/C15S in three chromatographic steps. Numbers shown on left of each gel give molecular weight of marker bands in kilodaltons. A) DEAE anion exchange column fractions. Whole cell lysate (WC), centrifuged clarified lysate (CL), and column flow-through (FT) samples were also loaded onto gel. B) ATP-agarose column fractions. A sample from column load (L) after dialyzing DEAE fractions containing DnaK is also shown. C) Gel filtration column fractions. M=Marker. Red lines indicate fractions pooled.

As a first step in assessing the ATPase and chaperone activity of DnaK T136C/S423C/C15S, we asked whether this new DnaK variant is capable of undergoing a nucleotide-dependent conformational change, as determined by limited proteolysis. In the presence of ATP, DnaK digested for five minutes with proteinase K runs primarily in one band on an SDS-PAGE gel at about 60 kDa representing a C-terminal truncation, whereas in the presence of ADP digested DnaK runs as three bands corresponding to full length protein at approximately 70 kDa, the NBD at approximately 45 kDa, and the SBD at approximately 25 kDa. DnaK T136C/S423C/C15S shows the same nucleotide-dependent change in limited proteolysis pattern as T136C/C15S and S423C/C15S, suggesting that the two-cysteine variant is actively responding to nucleotide (Figure 17). ATPase activity assays and luciferase refolding assays will need to be performed to verify that T136C/S423C/C15S is functionally equivalent to wild-type DnaK.

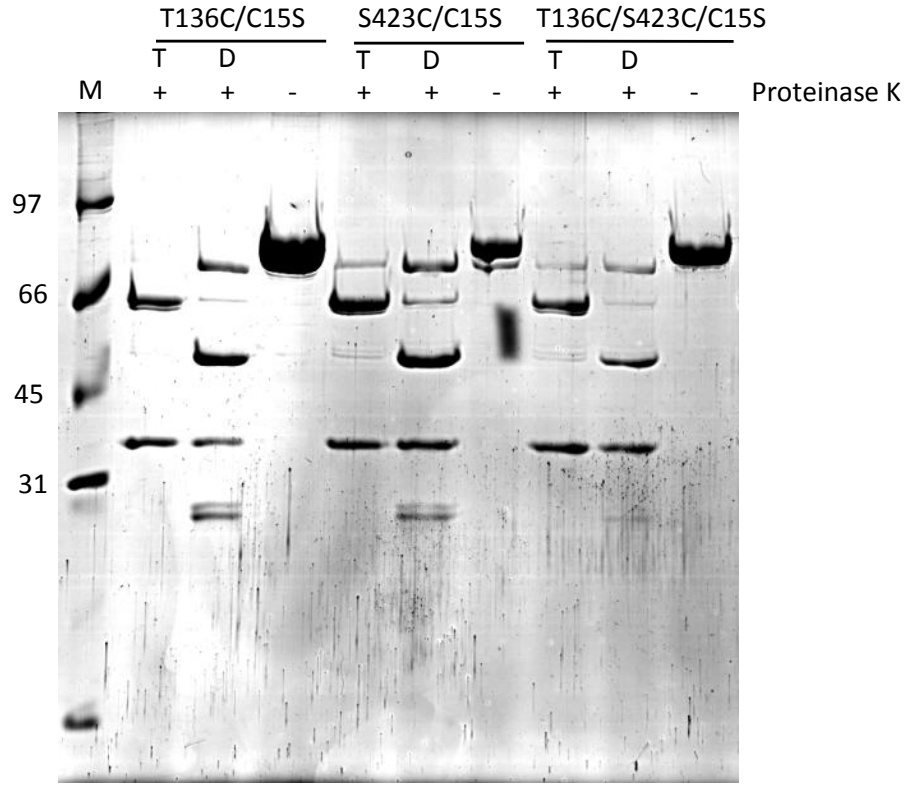

Figure 17. Limited proteolysis of DnaK variants in the presence of 1 mM ATP (T) or 1 mM ADP (D). Undigested samples of each variant are also shown (- proteinase K). Molecular weights in kDa of marker bands are indicated on left.

We wished to verify that the relative reactivities to Alexa Fluor dyes of T136C and S423C in DnaK T136C/S423C/C15S are similar to the reactivities of the cysteines in the individual DnaK single cysteine variants T136C/C15S and S423C/C15S. Limited proteolysis of quenched reaction aliquots in the presence of ADP allowed us to track the fluorescent labeling reactions occurring at T136C in the NBD and S423C in the SBD. The extent of the reaction at a particular time and cysteine was quantified by the fluorescence/Coomassie ratio in each band as done with undigested protein. The increase in ratio over time was graphed in Kaleidagraph and fit to pseudo-first order kinetics with rate constants of $0.048 \pm 0.005\ s^{-1}$ and $0.0035 \pm 0.0006\ s^{-1}$ for AF594 labeling at T136C and S423C, respectively (Figure 18). This thirteen-fold difference in reactivity between T136C and S423C in the double-cysteine DnaK variant agrees with the twentyfold difference in reactivity seen between DnaK single-cysteine variants T136C/C15S and S423C/C15S.

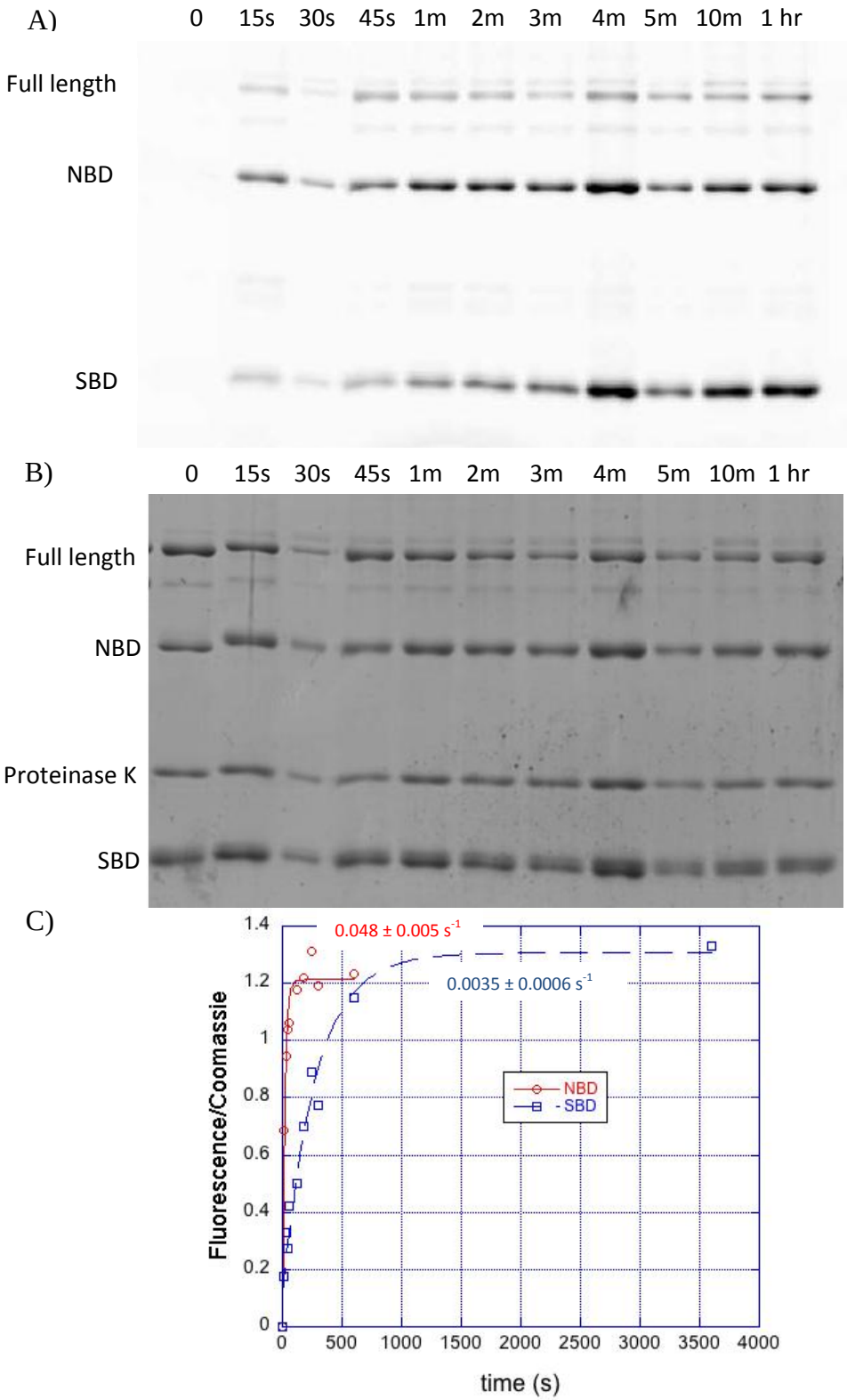

Figure 18. Conjugation of AF594 to T136C and S423C in DnaK T136C/S423C/C15S monitored by limited proteolysis. At the time points shown, aliquots were removed from the labeling reaction, quenched with excess GSH, digested for five minutes with proteinase K, and run on an SDS-PAGE gel. The gel was scanned for fluorescence (A) and then stained with Coomassie (B) to measure total protein in each band. C) Fluorescence/Coomassie was graphed over time for the NBD and SBD and fit to pseudo first order kinetics in Kaleidagraph with reaction rate constants and error shown.

Fluorescent double labeling of DnaK T136C/S423C/C15S: Two pot method

In our first effort at fluorescent double labeling, we ran a short reaction of AF555 donor fluorophore with T136C/S423C/C15S to label most of the fast-reacting T136C, attempted to enrich in singly labeled species by various chromatographic methods, and then labeled to completion at the slow-reacting S423C. We decided to complete all labeling reactions at pH 8.5, where we observed the greatest difference in labeling rates between T136C and S423C for both CPM and the Alexa Fluor maleimides. We also decided to run the first labeling reaction for 60 seconds because results from kinetics studies of single-cysteine and double-cysteine variants indicated that T136C would be 80-90% labeled at this point whereas S423C would be 10-20% labeled.

Although the major product of the first labeling reaction should be protein singly labeled at T136C, small amounts of double-labeled and unlabeled protein would also be present. Since FRET measurements are typically done by measuring donor-side fluorescence, protein doubly labeled with donor would lead to artificially high donor fluorescence in FRET experiments. In an attempt to remove doubly labeled and unlabeled DnaK from the reaction mixture we first tried to run the quenched labeling reaction over the MonoQ anion exchange column. The Alexa Fluor dyes have several charges that may affect the salt concentration at which labeled protein is eluted.

First we labeled DnaK T136C/S423C/C15S with AF555 for 60 s and then ran the quenched reaction on the MonoQ column in Tris pH 7.5, eluting protein with an increasing salt gradient from 0 to 500 mM NaCl. Under these pH conditions, labeled protein eluted in two overlapping equal sized peaks at a salt concentration of approximately 300 mM (Figure 19). Fractions containing DnaK were digested with proteinase K for five minutes and run on an SDS-PAGE gel (Figure 20). In most of the fractions the fluorescence/Coomassie ratio for the NBD band was approximately twice the fluorescence/Coomassie ratio for the SBD band. Fractions containing mostly singly labeled species at a particular position could not be identified. The data are consistent with a mixture of double-labeled, single-labeled, and unlabeled protein eluting together over about seven mL of elution volume. Elution time does not appear to be controlled by the degree or position of labeling; rather, protein conformation, aggregation state, or cysteine oxidation may be responsible for broad, double-peaked elution. On the other hand, limited proteolysis does not allow us to rule out the possibility that similar amounts of DnaK singly labeled at both T136C and S423C run in one peak, while double-labeled DnaK runs in the other. This is unlikely, however, due to the large difference in

labeling rates at the two cysteines. Furthermore, we found that DnaK T136C/S423C/C15S labeled first with either AF555 or AF594 behaves similarly on the MonoQ at pH 7.5.

In an attempt to improve separation, we ran DnaK T136C/S423C/C15S labeled first with AF555 over the MonoQ column at pH 6.9 (Tris), 6.0 (MES), and 5.0 (potassium acetate). At pH 6.9 labeled protein behaved similarly to pH 7.5, with protein eluting in two partially overlapping peaks at about 300 mM NaCl. At pH 6.0 labeled protein eluted in one sharp peak between 100 and 200 mM NaCl. At pH 5.0 no DnaK was detected in any eluate fractions. Since the pK_a of DnaK is close to 5.0, it is likely that protein either precipitated or did not reversibly bind to the MonoQ column under these conditions. Finally, we attempted separation in a HEPES buffer at pH 7.5 with 50 μM tryptophan, an aromatic amino acid that we hoped would engage in ring stacking with the aromatic Alexa fluor dyes and affect the elution time of particular labeled species. In this run we also reduced the slope of the increasing salt gradient by a factor of 3. Rather than improve separation, however, these measures only caused the mixture of labeled species to elute over a greater volume.

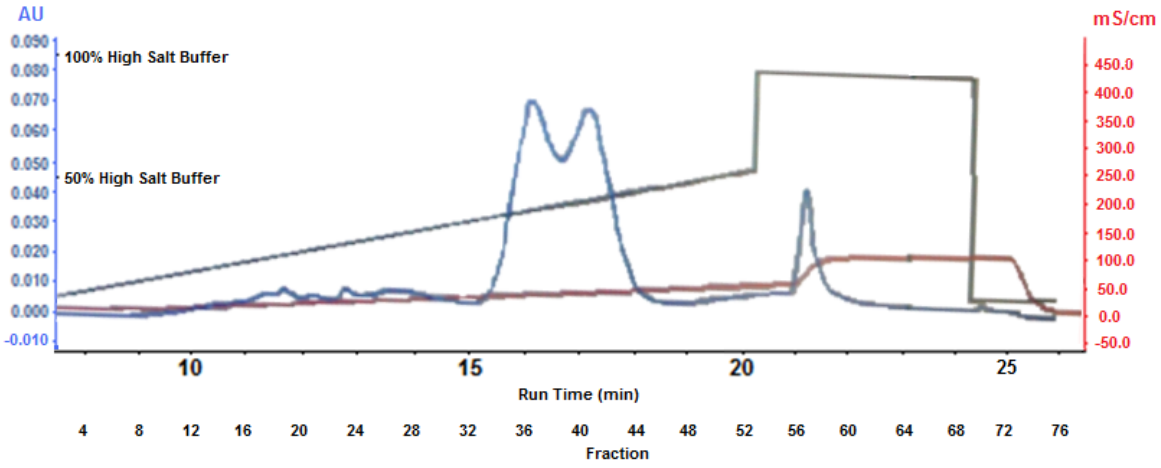

Figure 19. DnaK T136C/S423C/C15S was labeled for 60 s with AF594 loaded on MonoQ anion exchange column at pH 7.5 and eluted with an increasing salt gradient from 0 to 500 mM NaCl. Chromatogram shows UV absorbance (blue), conductivity (red) and percent high salt buffer (black). Protein elutes in two equal sized peaks.

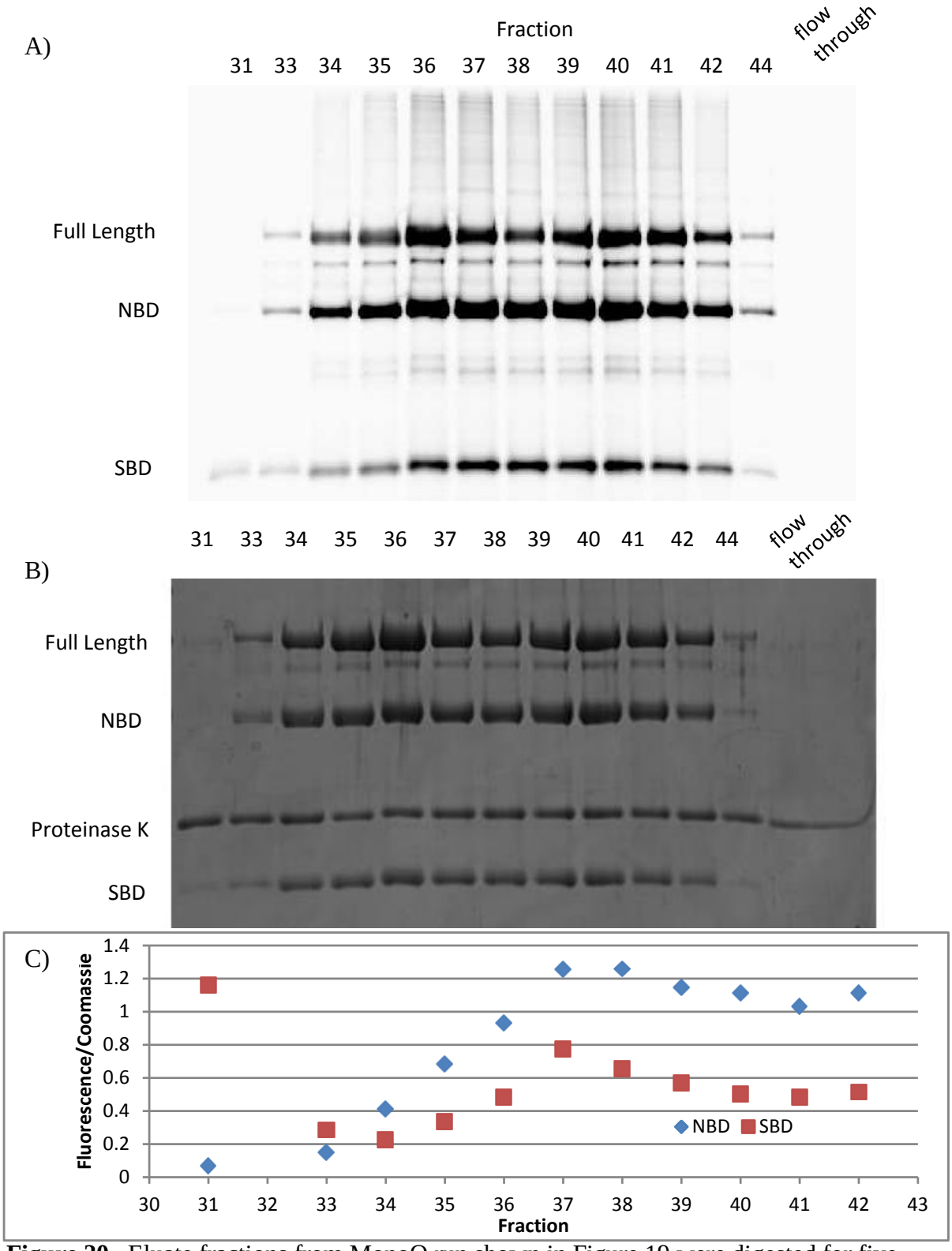

Figure 20. Eluate fractions from MonoQ run shown in Figure 19 were digested for five minutes with proteinase K and run on an SDS-PAGE gel. The gel was scanned for fluorescence (A) and stained with Coomassie (B) to determine total protein in each band. C) With the exception of early fractions containing little protein, the fluorescence/Coomassie ratio for NBD bands is approximately twice that for SBD bands.

Unable to find conditions under which the MonoQ gave satisfactory separation of fluorescently labeled DnaK, we moved to a phenyl sepharose column to separate DnaK T136C/S423C/C15S labeled with AF555 first. A sample of 60 s-labeled DnaK was brought to 1.0 M ammonium sulfate, loaded onto the column, and eluted with a decreasing gradient from 1.0 to 0 M ammonium sulfate. After varying pH and temperature, we obtained the greatest degree of separation of labeled species at pH 9.0, room temperature. Under these conditions a mixture of labeled species elutes in the main peak at about 200 mM ammonium sulfate, but the peak has two higher salt shoulders eluting up to 450 mM ammonium sulfate (Figure 21). The first-eluting shoulders may represent DnaK singly labeled at either T136C in the NBD or S423C in the SBD. Under the main peak appears to be a mixture of single- and double-labeled species.

A)

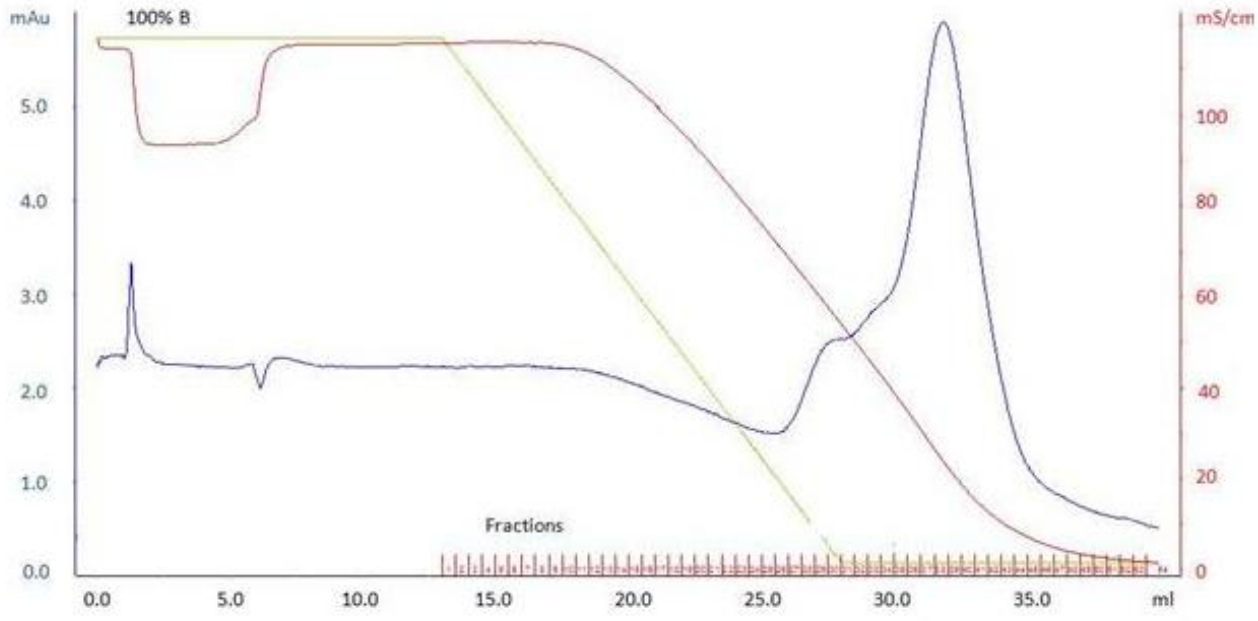

B)

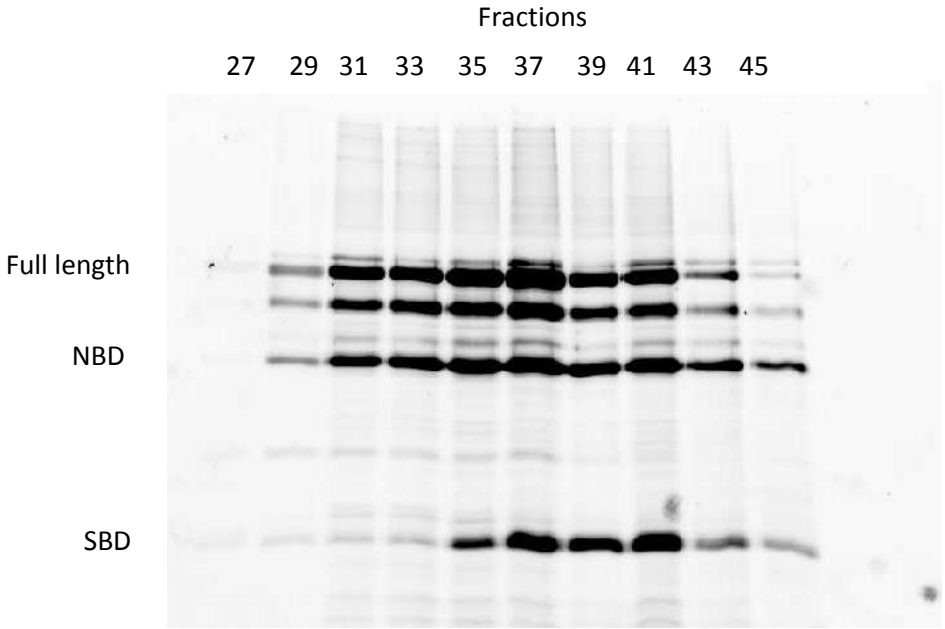

Figure 21. DnaK T136C/S423C/C15S labeled for 60 s with AF555 run on phenyl sepharose column and eluted with a decreasing gradient from 1.0 to 0 M ammonium sulfate. A) Chromatogram showing UV absorbance (blue), conductivity (red), percent start buffer (green), and 0.5 ml fractions over elution volume (ml). Protein species elute in a main peak at approximately 0.2 M ammonium sulfate with two overlapping shoulders extending up to about 0.45 M ammonium sulfate. B) Fractions were subjected to limited proteolysis and run on a 12% SDS-PAGE gel. Gel was scanned for fluorescence and bands corresponding to NBD and SBD identified.

Fractions 29-33 from phenyl sepharose chromatography containing DnaK singly labeled at T136C were pooled and run over a 53-ml HiPrep desalting column to bring protein back into FL buffer. Protein was reduced with TCEP and AF594 added to label S423C to completion. After removal of free dye doubly labeled protein was added to a quartz cuvette and a fluorescence emission spectrum taken upon excitation at 520 nm. The spectrum had two similar sized peaks at 567 nm (589 a.u.) and 612 nm (606 a.u.).

The presence of two peaks does not necessarily indicate FRET from AF555 to AF594 because as shown in Figure 22, AF555 and AF594 can both be excited at 520 nm with emission peaks at approximately 565 nm and 617 nm, respectively. Analysis is further complicated by the fact that the AF555 emission spectrum has a red shoulder that extends into the 617 nm peak. Therefore for a hetero-labeled DnaK, we would expect the emission peak at 617 nm to be the sum of fluorescence from AF555, fluorescence of AF594 due to direct excitation, and fluorescence of AF594 due to FRET. Due to the difficultly in decomposing the 617 nm peak, analysis of FRET for AF555-AF594 hetero-labeled DnaK will focus on AF555 donor fluorescence because 565 nm emission is due almost entirely to AF555. Upon addition of ATP fluorescence emission from AF555 remained identical while fluorescence emission at 617 nm decreased slightly to 587 a.u. (3% decrease) (Figure 23). This result was unexpected because previous experiments with the tryptophan-IAEDANS FRET pair showed a large quenching of tryptophan donor fluorescence upon addition of ATP.

Although we did not see any change in donor fluorescence upon addition of ATP for doubly labeled DnaK in this experiment, it was possible that the Förster radius for the AF555-AF594 dye pair was too large to report an ATP-induced conformational change. That is, with and without ATP, when the NBD and SBD are close and disjoined, respectively, energy transfer from FRET donor to acceptor could have been near 100%. If this was the case, then proteolytic cleavage at the interdomain linker or other sites may cause the NBD and SBD to float apart, leading to a decrease in FRET. To test this hypothesis we added 1 mg proteinase K to the cuvette and took emission spectra every thirty seconds for 10 minutes, expecting to see an increase in AF555 fluorescence. Contrary to expectation, we observed an 8% decrease in fluorescence from AF555 and a 3% decrease in the 617 nm peak after 10 minutes. It may be that interdomain contacts with ATP bound abrogate domain separation even with the cleavage of some peptide bonds. The decrease in emission for both fluorophores could be due to relief from quenching when nearby structures are altered by proteolysis.

In order to ensure that fluorescently labeled protein was present rather than just a mixture of both free AF555 and AF594, we ran a sample on a SDS-PAGE gel (Figure 23C).

We observed a fluorescent band at approximately 70 kDa and weaker bands corresponding to proteolytic fragments of DnaK. After centrifugation of the second labeling reaction with AF594, a pink precipitate formed that we resuspended in 5X SDS Loading Buffer and ran on the gel as well. This precipitate also contained fluorescently labeled DnaK. Unfortunately, fluorescence gel scanning does not permit us to identify the presence of particular fluorophores, but it is possible that doubly labeled DnaK is insoluble in FL Buffer and ended up in the pink precipitate, while the soluble protein is a mixture of singly labeled species only. Another possibility is that doubly labeled DnaK denatures in the FL Buffer, leading to a large separation distance between fluorophores and minimal FRET with and without ATP. This would also explain why we saw no change in FRET with addition of proteinase K. In any case, we concluded that doubly labeled DnaK is unstable in the current labeling conditions.

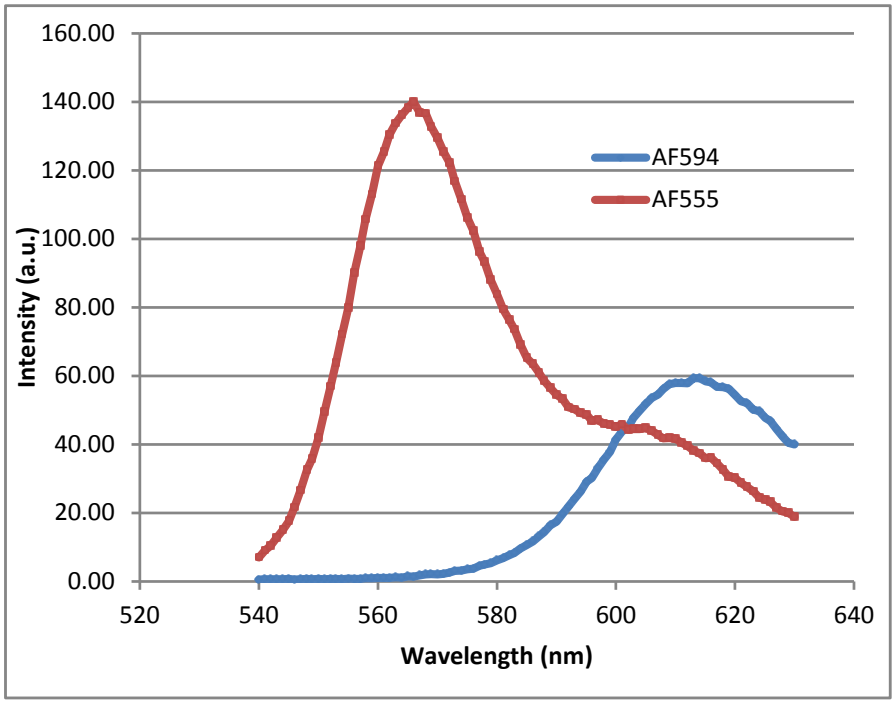

Figure 22. Emission spectra of 1 μM AF555 and AF594 upon excitation at 520 nm.

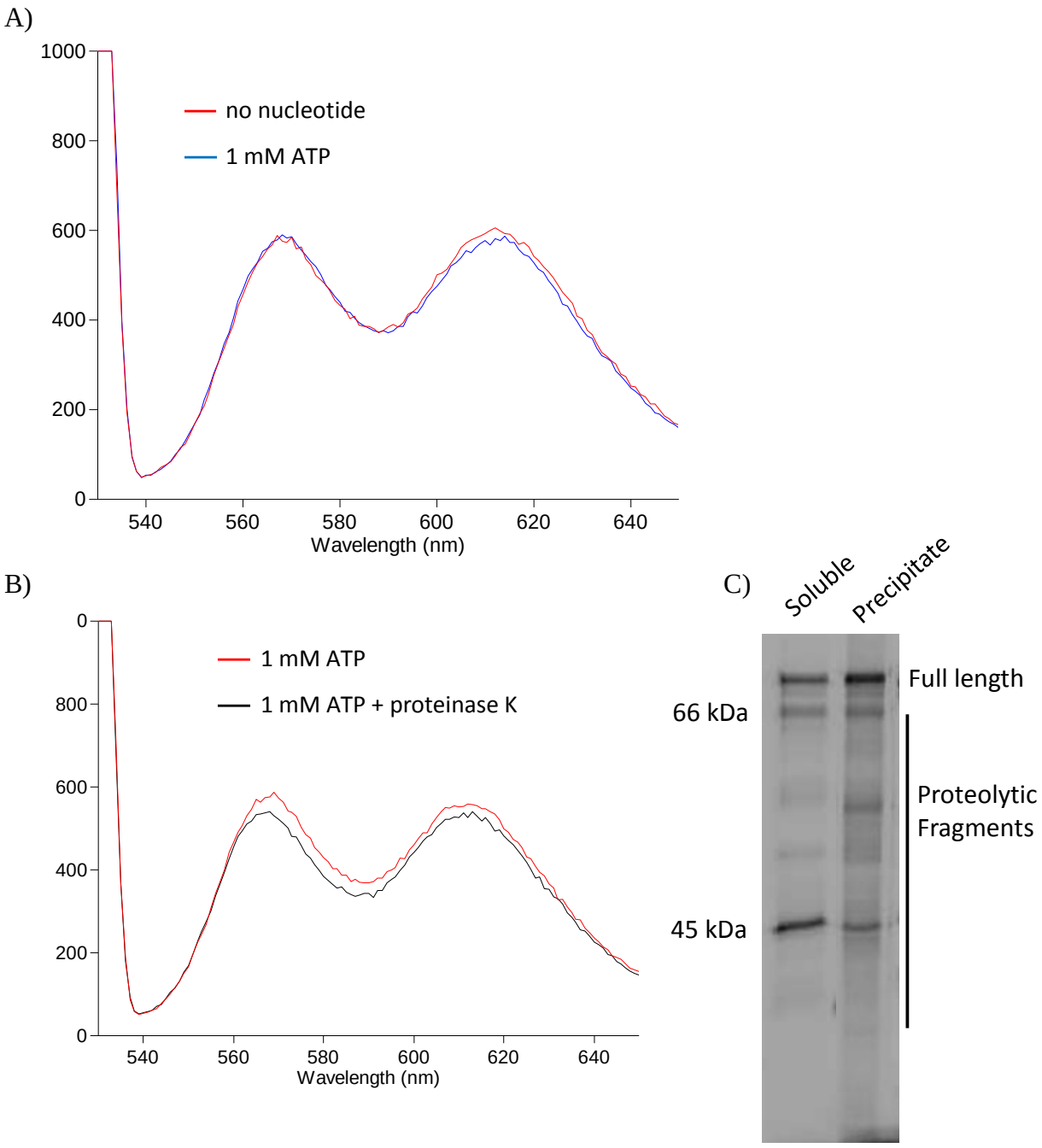

Figure 23. A) Emission spectra of DnaK T136C/S423C/C15S doubly labeled with AF555 and AF594 upon excitation at 520 nm. In this experiment AF555 singly labeled protein was purified using phenyl sepharose chromatography before second labeling with AF594. Spectra were taken with no nucleotide present (red) and with 1 mM ATP (blue). B) Emission spectra as above with 1 mM ATP. Spectra were taken before (red) and ten minutes after (black) addition of 1 mg proteinase K. C) Doubly labeled DnaK run on 12% SDS-PAGE gel and scanned for fluorescence. The pink precipitate formed during the second labeling reaction with AF594 was also resuspended in 5X SDS Loading Buffer and run on the gel.

Screen for conditions under which double labeled DnaK is soluble and active

In order to find conditions under which doubly labeled DnaK is retained in a soluble and native conformation, we screened a variety of buffer conditions. In 1 mL reactions containing 1 μM DnaK T136C/S423C/C15S in a particular buffer we simultaneously added AF555 and AF594 to 1 μM in each dye. The reactions were incubated at room temperature overnight and then centrifuged at 13,000 g for 10 min. In all reactions carried out at pH 6.5, we noticed a pink precipitate formed after centrifugation that contained fluorescently labeled DnaK. Surprisingly, all buffer conditions contained substantial amounts of soluble fluorescently labeled DnaK (Figure 24). To test whether certain reactions contained hetero-labeled DnaK capable of undergoing a conformational shift upon addition of ATP, we added samples from each reaction to a 96-well plate for analysis in the Polarstar spectrophotometer. Since the Polarstar does not have appropriate filters for measuring donor fluorescence only, we hoped to be able to detect a change in fluorescence signature upon addition of ATP using a long pass Em590 filter, through which we would measure all emission in the 617 nm peak from both AF555 and AF594. Percent changes for the various buffer conditions ranged from 2.3 to 9.6 percent and similar buffer conditions gave similar percent changes, suggesting that the degree of change in the 617 nm peak actually represented the condition of labeled DnaK in a particular buffer (Table 6). We tested four conditions, 1% Triton X-100 pH 7.5, 1% Tween pH 7.5, 10% glycerol pH 8.5, and pH 7.5 100 mM KCl, in the Cary spectrophometer where we could directly measure donor fluorescence. Although donor fluorescence decreased significantly for all four conditions tested, for pH 7.5 100 mM KCl the intensity of the 617 nm peak decreased a similar amount, leading us to suspect that fluorescence changes were an artifact of mixing in the ATP stock rather than due to a conformational change. In the 10% glycerol pH 8.5 condition, we observed a 5.8% decrease in donor fluorescence but only a 0.2% decrease in 617 nm peak height after adding ATP, suggesting that the change in donor fluorescence actually reported a conformational change of DnaK. We concluded from the buffer screen that doubly labeled DnaK is susceptible to denaturation or precipitation, especially at lower pH conditions, and that hygroscopic adjuncts may help retain DnaK in a soluble and active state. We chose to perform all future labeling experiments with the Alexa dyes in FL Buffer pH 8.5 + 10% glycerol since the FRET signal of labeled DnaK in this condition was responsive to ATP and we best understand labeling kinetics at pH 8.5.

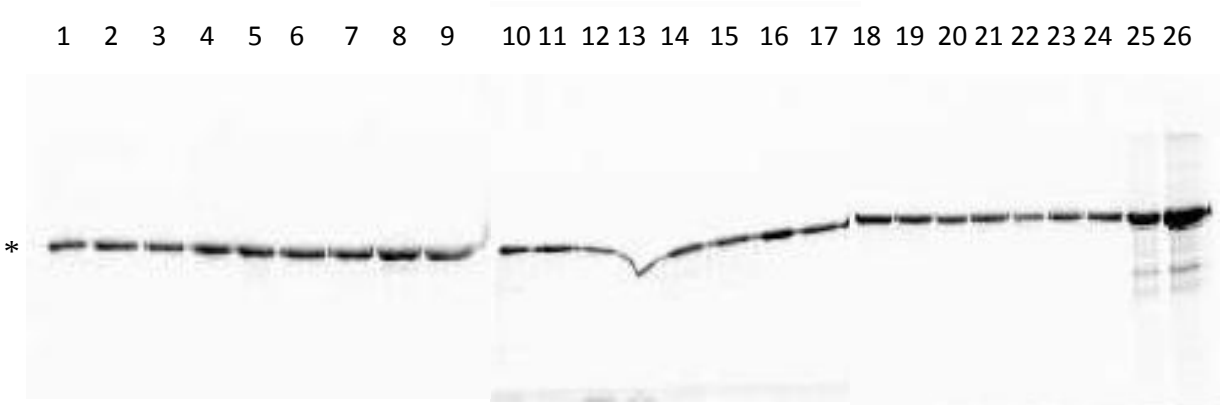

Figure 24. Buffer screen to find optimal conditions for double labeling of DnaK. Samples from 1 mL labeling reactions containing 1 μM DnaK, 1 μM AF555, and 1 μM AF594 were run on 12% SDS-PAGE gels, which were scanned for fluorescence; * indicates full length DnaK. Original FL Buffer contains 50 mM Tris pH 8.5, 100 mM KCl, 0.5 mM EDTA, and 1 mM $MgCl_2$. Screened buffer conditions contain the following modifications: 1) pH 6.5, 10 mM KCl; 2) pH 6.5 100 mM KCl; 3) pH 6.5 200 mM KCl; 4) pH 7.5 10 mM KCl; 5) pH 7.5 100 mM KCl; 6) pH 7.5 200 mM KCl; 7) pH 8.5 10 mM KCl; 8) pH 8.5 100 mM KCl; 9) pH 8.5 200 mM KCl; 10) 10% glycerol pH 7.5; 11) 10% glycerol pH 8.5; 12) 10% DMSO pH 7.5; 13) 10% DMSO pH 8.5; 14) 1% SDS pH 7.5; 15) 1% SDS pH 8.5; 16) 1% Triton X-100 pH 7.5; 17) 1% Triton X-100 pH 8.5; 18) 1% Tween pH 7.5; 19) 1% Tween pH 8.5; 20) 1% tryptophan pH 7.5; 21) 1% tryptophan pH 8.5; 22) 1 mM ATP pH 7.5; 23) 1 mM ATP pH 8.5 24) sodium phosphate pH 7.0. Lanes 25 and 26 contain the precipitates from pH 6.5 100 mM KCl and pH 6.5 200 mM KCl, respectively, resuspended in 5X SDS Loading Buffer.

Table 6. Percent change in 617 nm peak for double-labeled DnaK in all screened buffer conditions upon addition of 1 mM ATP was determined using an Em590 filter in the Polarstar spectrophotometer. For some samples, the change in AF555 donor fluorescence and 617 nm peak height were also measured using the Cary spectrophotometer.

Buffer condition	Percent change in 617 nm peak upon addition of ATP (Polarstar spectrophotometer)	Percent decrease in donor fluorescence upon addition of ATP (Cary spectrophotometer)	Percent decrease in 617 nm peak upon addition of ATP (Cary spectrophotometer)
1% Triton X-100 pH 8.5	9.6		
1% Triton X-100 pH 7.5	9.4	5.9	2.2
10% DMSO pH 7.5	8.6		
10% glycerol, pH 7.5	8.4		
10% glycerol, pH 8.5	7.9	5.8	0.2
1 mM ATP pH 7.5	6.9		
1 mM tryptophan pH 7.5	6.6		
10% DMSO pH 8.5	6.5		
pH 7.5, 200 mM KCl	5.9		
pH 8.5, 100 mM KCl	5.5		
1% Tween pH 8.5	5.4		
1% Tween pH 7.5	5.2	3.9	0.8
1 mM tryptophan pH 8.5	4.9		
1% SDS pH 8.5	4.7		
sodium phosphate pH 7.0	4.7		
pH 8.5, 10 mM KCl	4.5		
pH 7.5, 100 mM KCl	4.3	5.6	4.2
1 mM ATP pH 8.5	4.3		
pH 7.5, 10 mM KCl	4.2		
1% SDS pH 7.5	4.1		
pH 8.5, 200 mM KCl	4.1		
pH 6.5, 10 mM KCl	3.2		
pH 6.5, 200 mM KCl	2.3		
pH 6.5, 100 mM KCl	2.3		

Fluorescent double labeling of DnaK T136C/S423C/C15S: One pot method

We further altered the fluorescent double labeling protocol by eliminating the phenyl sepharose chromatography step after the first labeling reaction with AF555 because we were concerned that ammonium sulfate may contribute to denaturation or precipitation of fluorescently labeled DnaK. Moreover, initial experiments indicated that DnaK does not bind

to phenyl sepharose in the presence of 10% glycerol at 1.0 M ammonium sulfate. In our new protocol, we diluted DnaK T136C/S423C/C15S to 1 μM in FL Buffer pH 8.5 + 10% glycerol, reduced with free TCEP, and added AF555 to 1 μM. After 30 minutes incubation at room temperature, we added AF594 to 10 μM and incubated for a further two hours. We quenched the reaction with excess GSH and removed free dye using the HiPrep desalting column. Using this method, which we call "one pot," doubly labeled DnaK showed a 16% decrease in donor fluorescence upon addition of 1 mM ATP[4] compared to no nucleotide, while the height of the 617 nm peak increased by 6% (Figure 25). It should be noted that nothing was done to remove nucleotide completely from the "no nucleotide" sample, so it may contain a mixture of ATP-bound, ADP-bound, and nucleotide-free DnaK. In contrast, addition of ADP to 1 mM did not lead to a significant change in donor fluorescence beyond the expected dilution effect of adding the 100x ADP stock. In a separately labeled sample of protein, incubation of ADP-bound DnaK with 1 mg proteinase K overnight resulted in a 19% increase in AF555 fluorescence and a 4% decrease in the 617 nm peak, providing further evidence that changes in FRET are reporting changes in fluorophore separation distance.

[4] Because DnaK's K_d values for ATP and ADP are submicromolar, 1 mM ATP or 1 mM ADP are saturating and bring DnaK to an essentially homogeneous ATP-bound or ADP-bound form, respectively.

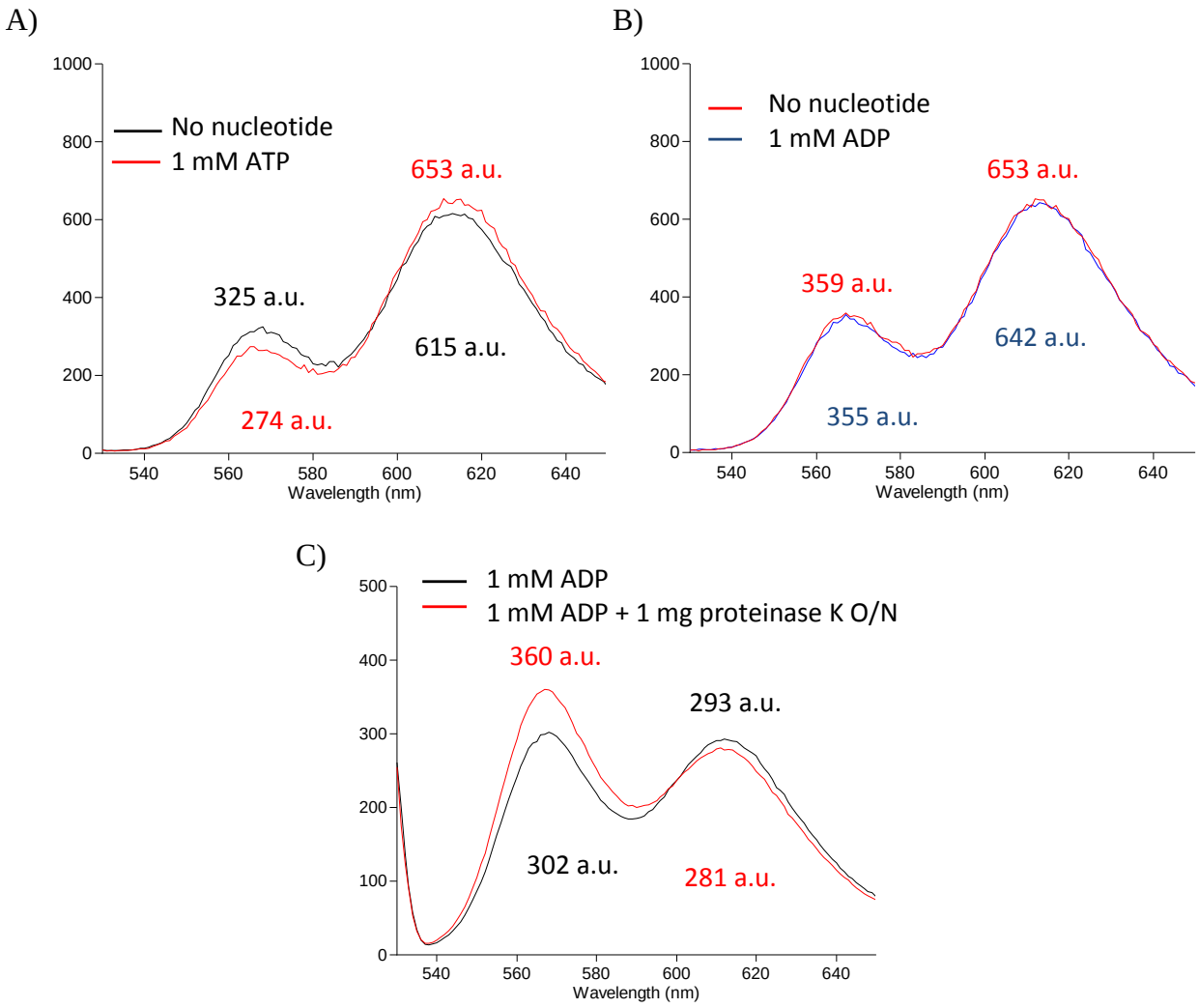

Figure 25. DnaK T136C/S423C/C15S was "one pot" doubly labeled with AF555 and AF594 in FL Buffer pH 8.5 + 10% glycerol. Emission spectra (excitation at 520 nm) were taken with no nucleotide (black) and then with the addition of 1 mM ATP (red) (A) or the addition of 1 mM ADP (B). Note that nothing was done to ensure the "no nucleotide" sample was truly nucleotide free. C) A separately labeled sample had ADP added to 1 mM (blue) and was then incubated overnight with 1 mg proteinase K (red). Peak intensities shown in color of corresponding curve.

While the AF555-AF594 FRET pair reports the nucleotide-dependent conformational shift of DnaK with significant changes in AF555 donor fluorescence, we wanted to see if the AF488-AF594 FRET pair could also be used. Although the predicted Förster distance for the AF488-AF594 pair is 60 Å, suggesting that energy transfer may be close to 100% in the presence of either ATP or ADP, the spectral properties of AF488 are optimal for excitation by the blue argon 488 nm laser used in the University of Otago total internal reflection

microscope. Moreover, AF594 is only minimally excited at 488 nm, so a peak at 617 nm is due almost entirely to FRET rather than direct excitation of AF594. To test whether the AF488-AF594 FRET pair could report DnaK's conformational change, we labeled DnaK T136C/S423C/C15S using the one pot labeling method with AF488 and AF594. This labeled construct showed a 5% decrease in donor fluorescence and a 6% increase in acceptor fluorescence upon addition of ATP (Figure 26). We concluded that the AF488-AF594 dye pair could be used for detection of DnaK's nucleotide-dependent conformational change, although the change in FRET is smaller than that for the AF555-AF594 pair. After a five-hour incubation with proteinase K, AF488 donor fluorescence increases by 37% while acceptor fluorescence decreases almost to background. The large change in FRET upon proteolysis and relatively small change upon addition of nucleotide suggests that the Förster radius for the AF488-AF594 dye pair is not ideally suited for the distance between positions T136C and S423C.

A)

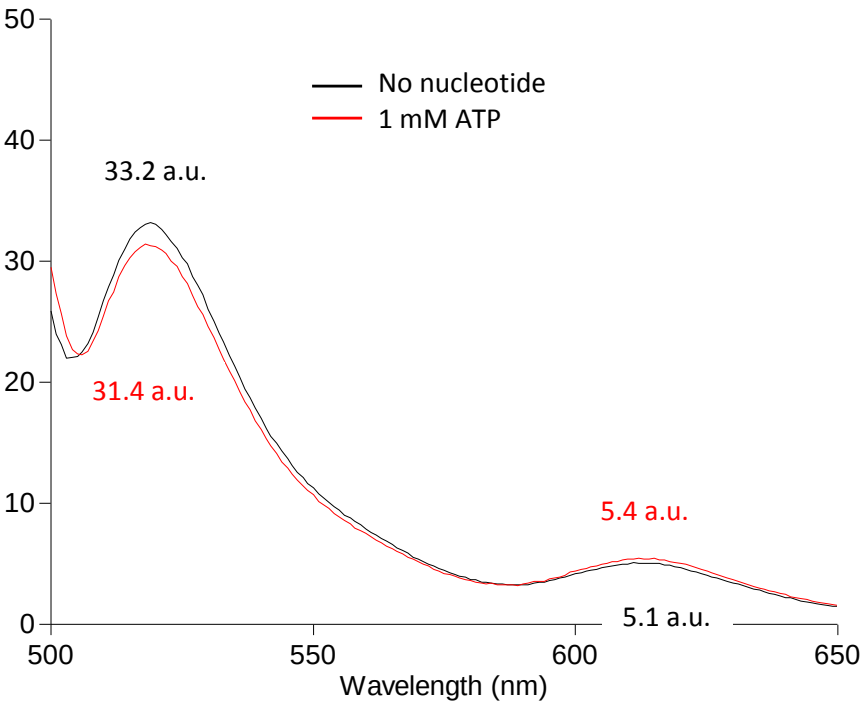

B)

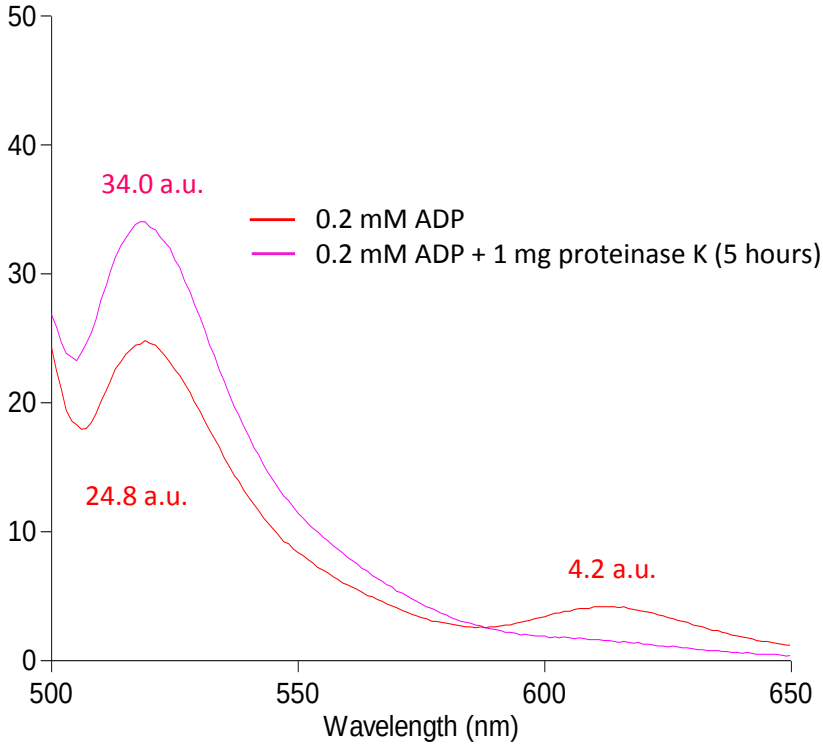

Figure 26. DnaK T136C/S423C/C15S was "one pot" doubly labeled with AF488 and AF594 in FL Buffer pH 8.5 + 10% glycerol. (A) Emission spectra (excitation at 495 nm) were taken with no nucleotide (black) and then with the addition of 1 mM ATP (red). B) Emission spectra for AF488-AF594 labeled protein in the presence of ADP before and after a five-hour incubation at room temperature with proteinase K. Peak intensities shown in color of corresponding curve.

Investigation of Hsp70 ATPase activity modulators

After developing a method for double labeling DnaK, we wished to use the double labeled reagent to probe the biochemical action of Hsp70 activity-modulating compounds (Chang et al., 2008; Wisén and Gestwicki, 2008) and to determine whether the compounds stabilize a particular protein conformation. In preliminary experiments prior to using FRET, however, we employed limited proteolysis of DnaK to ask whether Hsp70 modulators affect conformational changes. With no compounds present, DnaK in 1 mM ADP digested with proteinase K for five minutes runs as three primary bands on an SDS-PAGE gel at approximately 70, 45, and 25 kDa. At both 1 mM and 10 μM ATP, the digest produces two bands at approximately 60 and 45 kDa. We hypothesized that if Hsp70 modulators interfere with DnaK's conformational changes, we might detect variations in the SDS-PAGE banding pattern after limited proteolysis in the presence of either ATP or ADP.

Indeed, when various activity modulators were added to DnaK before the digest at a concentration of 100 μM, the banding patterns changed in different ways for each compound (Figure 27). For SW02, CE12, 116-9e, and MY, the bands with 1 mM ADP were largely unchanged compared to no compound, but in the presence of 1 mM ATP we observed the appearance of the 70 kDa band that was not observed with no compound, suggesting a significant fraction of protein molecules were sampling the ADP-bound form. Surprisingly, the 70 kDa band was not observed in the presence of 10 μM ATP. This counterintuitive result can be explained if there is ADP contamination in the ATP stock and these compounds stabilize the ADP-bound conformation. If this was the case, then there might be enough ADP in the 1 mM ATP digests for the compounds to push the conformational equilibrium toward the ADP-bound state. With 10 μM ATP, the amount of ADP present due to contamination may be too small to facilitate a compound-dependent shift in equilibrium. In the presence of 115-7c, the 1 mM ADP banding pattern again remains unchanged compared to no compound but a 70 kDa band is detected in the 10 μM ATP digest and a fainter band in the 1 mM ATP digest, suggesting that 115-7c also stabilizes the ADP-bound conformation. For MB, an entirely new band is seen just above the proteinase K band for all three digests. This indicates that MB promotes a new peptide cleavage site, which could be due to stabilization of a protein conformation different from both the ATP and ADP-bound states.

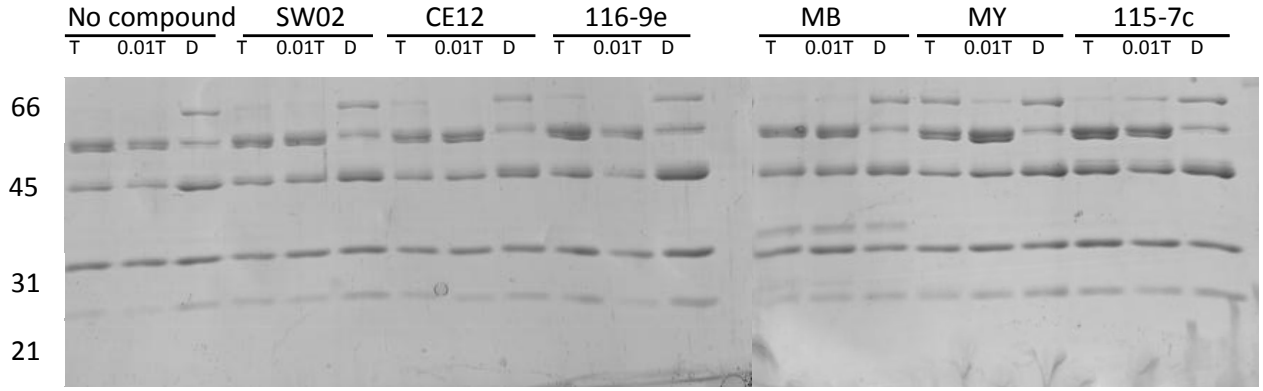

Figure 27. Limited proteolysis of DnaK R517C/C15S in the presence of ATPase activity modulators. Solutions containing 1 μM DnaK, 100 μM activity modulator, and either 1 mM ATP (T), 10 μM ATP (0.01T), or 1 mM ADP (D) were digested for five minutes with 0.5 mg proteinase K and run on a 12% SDS-PAGE gel. Positions of molecular weight markers (kDa) are shown at left. Proteinase K runs just above the 31 kDa marker.

Next we used small angle X-ray scattering (SAXS) to characterize the effects of the Hsp70 activity modulators on the nucleotide-dependent conformational changes of DnaK 1-552ye, a C-terminal truncation less prone to dimerization than full length DnaK. We found that in the presence of either DMSO vehicle or Hsp70 activity modulators, the radius of gyration of DnaK 1-552ye decreases as the ATP/ADP ratio increases. With MY present, however, the radius of gyration at 50, 90, and 100% ATP is less than the radius of gyration in the presence of DMSO vehicle, suggesting that MY may stabilize a tight interaction between the NBD and SBD (Figure 28).

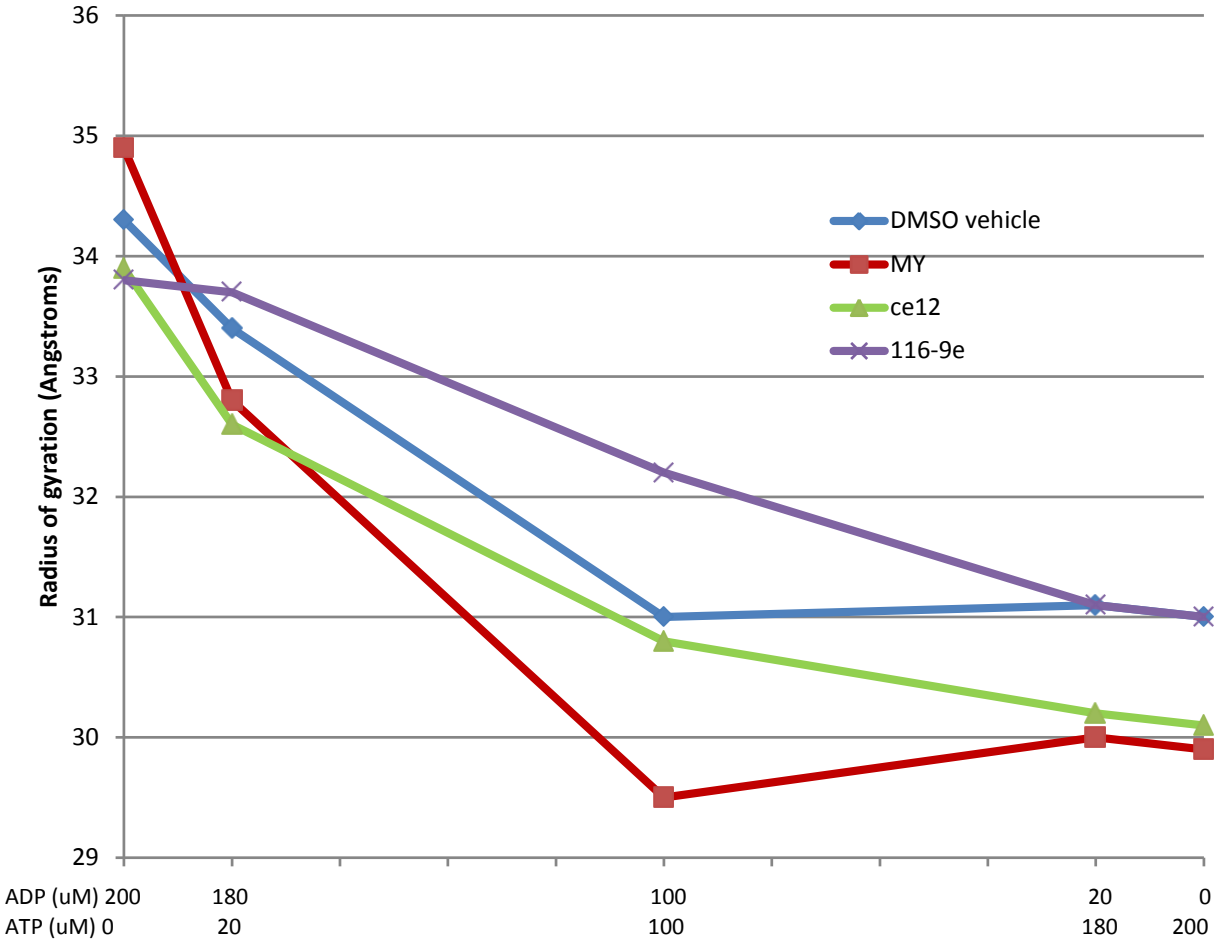

Figure 28. Radii of gyration determined by SAXS for DnaK 1-552ye in the presence of Hsp70 activity modulators MY, ce12, and 116-9e. All compounds are at saturating concentrations in SAXS Buffer + 0.1% DMSO. ATP and ADP concentrations are shown on the X-axis in μM.

Finally, we used FRET to probe the effects of the ATPase activity modulators on DnaK's conformational shift. First we used the singly labeled DnaK R517C/C15S construct, in which DnaK's only endogenous tryptophan residue at postion 102 is the FRET donor and

an IAEDANS fluorophore conjugated to the cysteine introduced at position 517 is the FRET acceptor. For this labeled construct, addition of ATP to 1 mM results in a 35% decrease and slight blueshift in W102 donor fluorescence and a 46% increase in IAEDANS acceptor fluorescence (Figure 29).

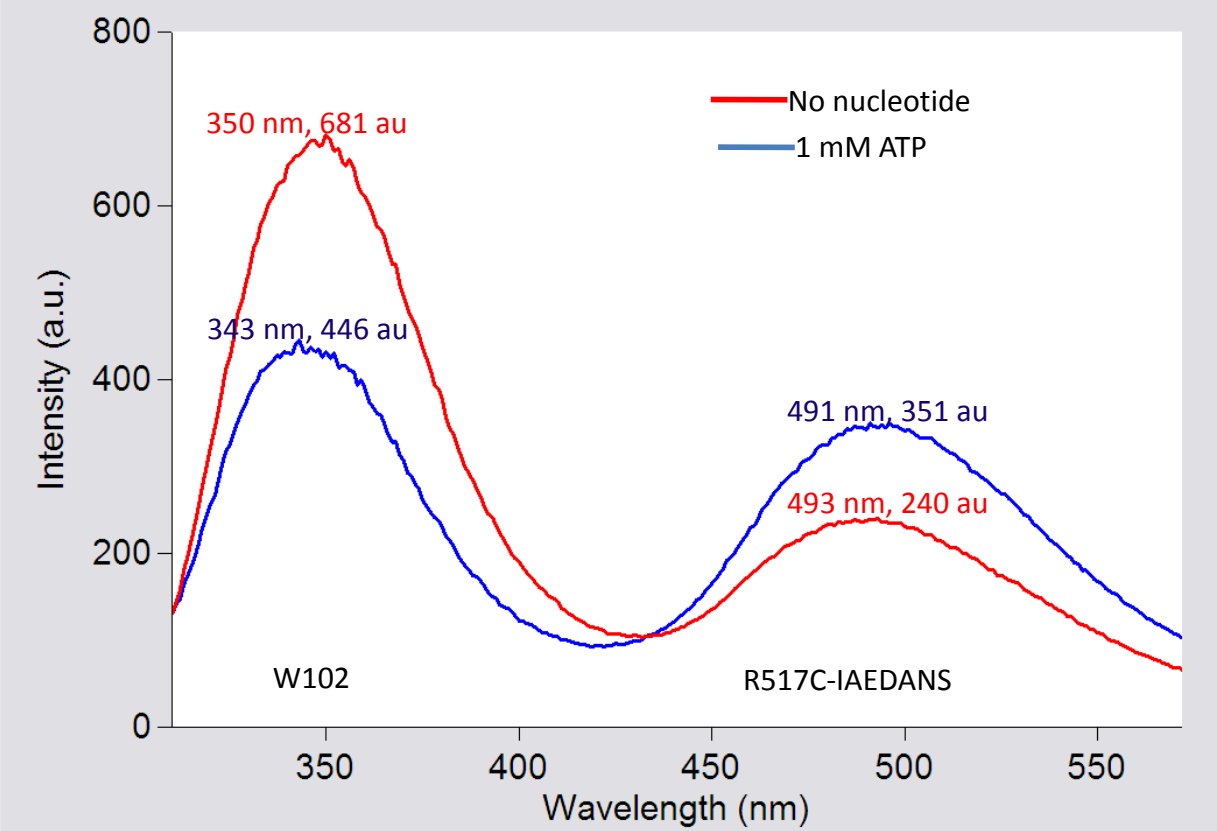

Figure 29. Fluorescence spectra of 6 μM DnaK R517C/C15S labeled with IAEDANS in gel filtration buffer with no nucleotide and in the presence of 1 mM ATP. Peak intensities shown in color of corresponding curve.

We performed FRET experiments with IAEDANS-labeled DnaK and the Hsp70 modulators in 96-well plate format in the Polarstar spectrophotometer. Labeled protein was diluted to 6 μM, mixed with compounds at six concentrations ranging from 1 to 100 μM, and fluorescence spectra taken in the absence and presence of 1 mM ATP. Because most of the compounds absorb light at the tryptophan excitation wavelength, we first analyzed the FRET data by taking the ratio between tryptophan donor fluorescence and IAEDANS acceptor fluorescence, which should be independent of the amount of excitation energy. For some compounds, these ratios change significantly with increasing concentration of drug, but the change with ATP present parallels that with no nucleotide, suggesting that the shift in ratio may actually be due to the spectral properties of the compound itself rather than the

conformation of DnaK. Indeed, most of the compounds also absorb light to varying degrees at 350 and 490 nm, the wavelengths at which fluorescence emission is being measured. To circumvent compound absorbance, we took the ratio of emission at 350 nm -ATP to emission at 350 nm +ATP and the ratio of emission at 490 nm -ATP to emission at 490 nm +ATP. Assuming equal concentrations of compound in the parallel concentration series +/- ATP, these ratios should be independent of a compound's spectral properties. These ratios change only marginally across the concentration series for most of the compounds. The 350 – ATP/350 +ATP ratio increases slightly with increasing compound concentration for all the compounds, suggesting that the compounds may shift DnaK's conformational equilibrium to some extent, but it is impossible to tell in which direction (Figures 30-35).

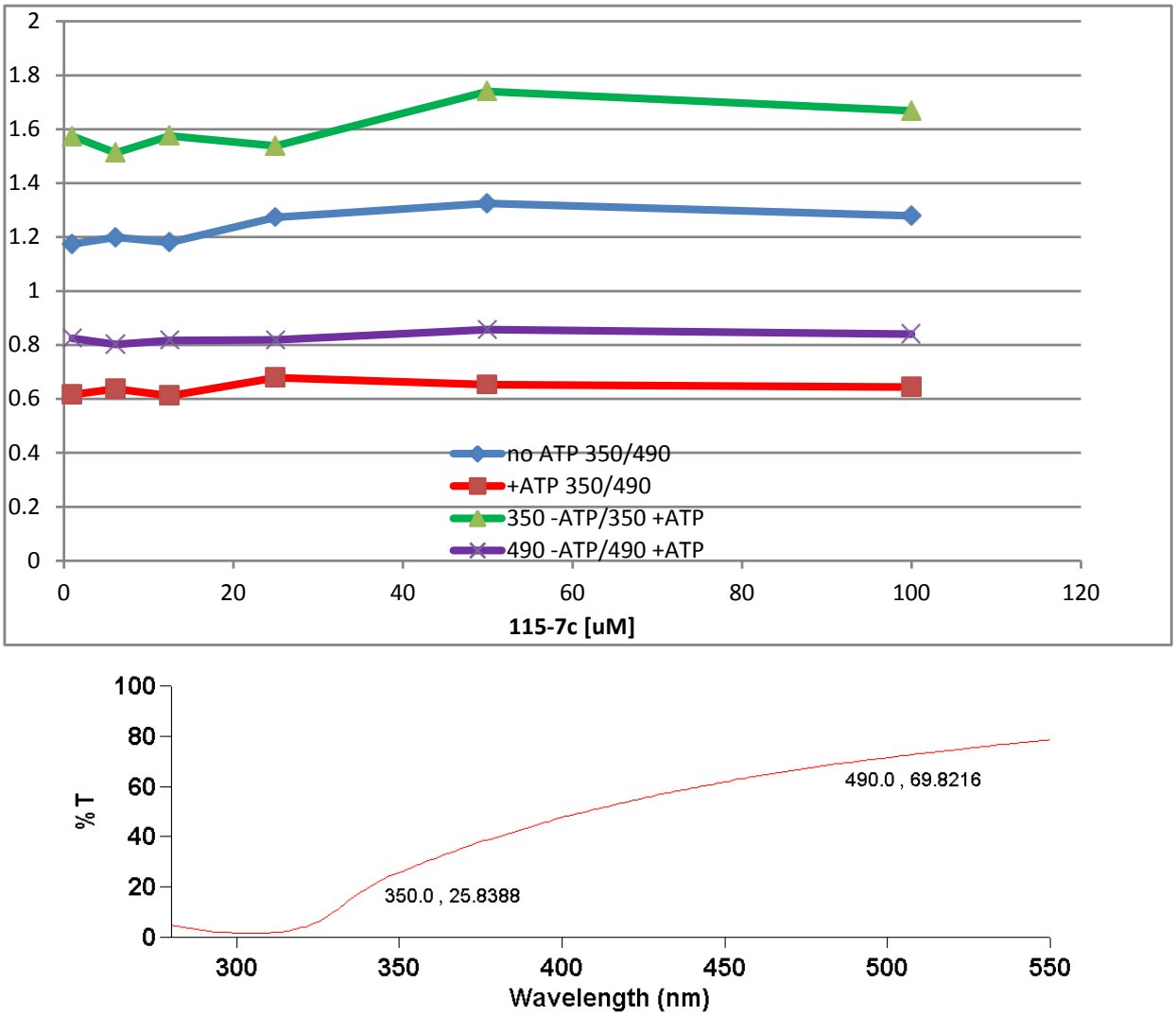

Figure 30. Effect of Hsp70 activity modulator 115-7c on conformational changes of DnaK assessed by FRET between W102 and R517C-IAEDANS. 6 µM IAEDANS-labeled DnaK was mixed with 115-7c at concentrations ranging from 1 to 100 µM in 100 µl samples. One concentration series had no nucleotide added and one series had ATP added to 1 mM. Fluorescence spectra were taken in the Polarstar spectrophotometer with excitation through a 295-10 nm filter and emission through 350-10 nm and 490-10 nm filters. The graphs show the ratio of emission at 350 to emission at 490 without nucleotide, emission at 350 to emission at 490 with 1 mM ATP, emission at 350 without nucleotide to emission at 350 with 1 mM ATP, and emission at 490 without nucleotide to emission at 490 with 1 mM ATP. Absorbance spectra converted into percent transmission are also shown.

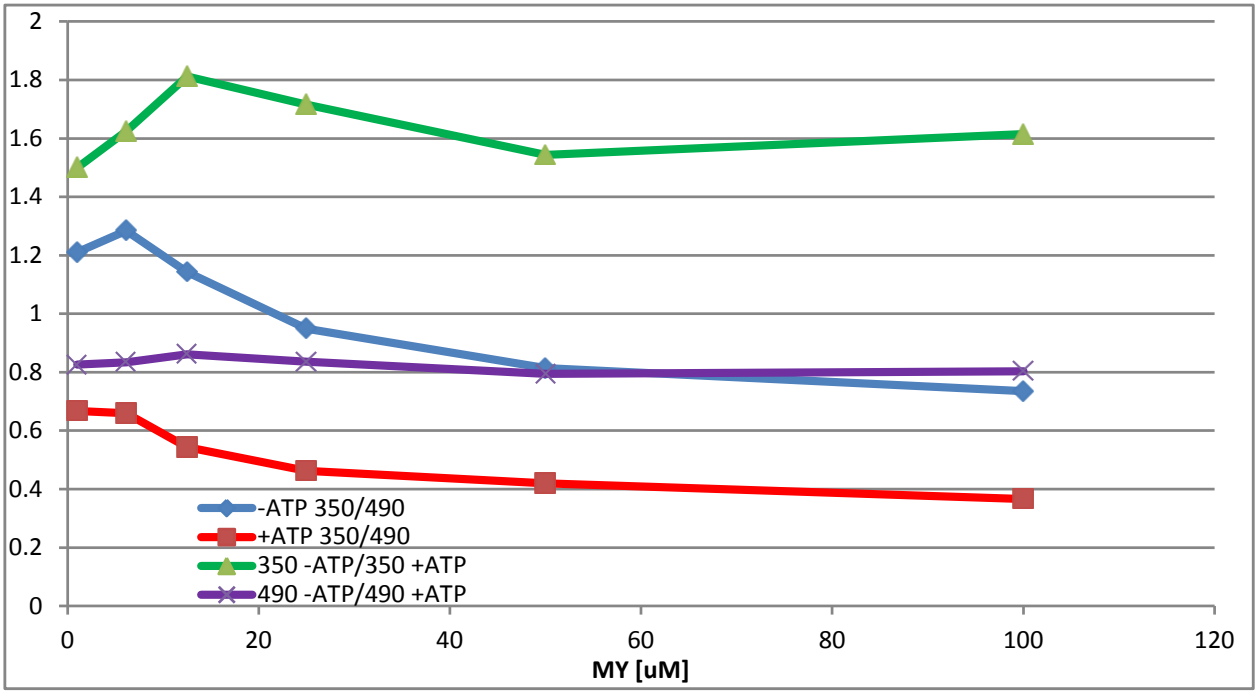

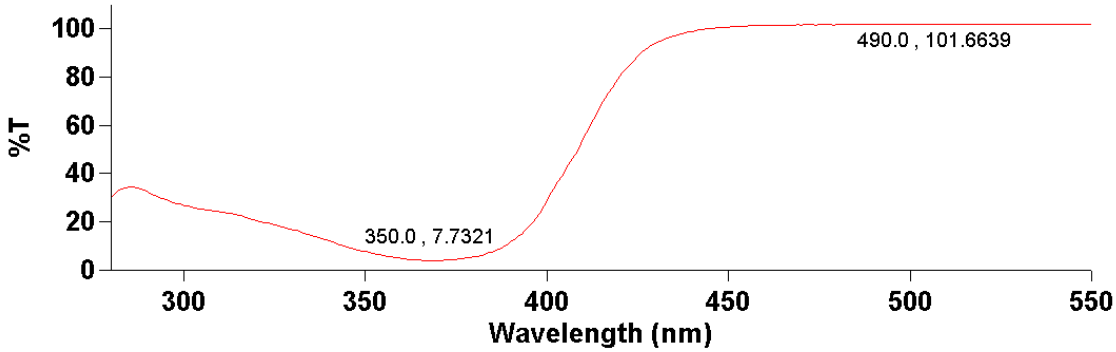

Figure 31. Effect of MY on conformational changes of DnaK assessed by FRET between W102 and R517C-IAEDANS. See Figure 30 for experimental details.

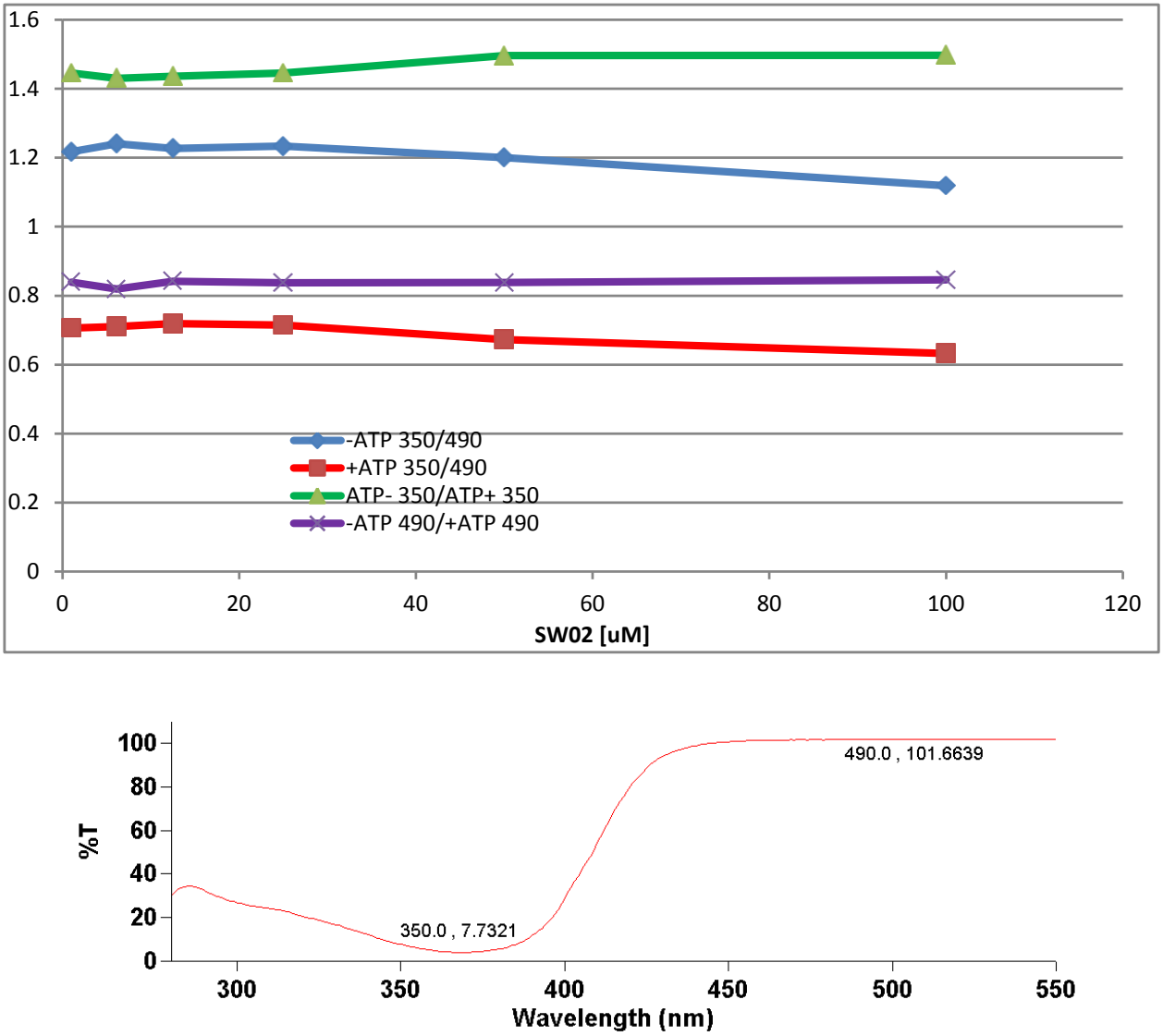

Figure 32. Effect of SW02 on conformational changes of DnaK assessed by FRET between W102 and R517C-IAEDANS. See Figure 30 for experimental details.

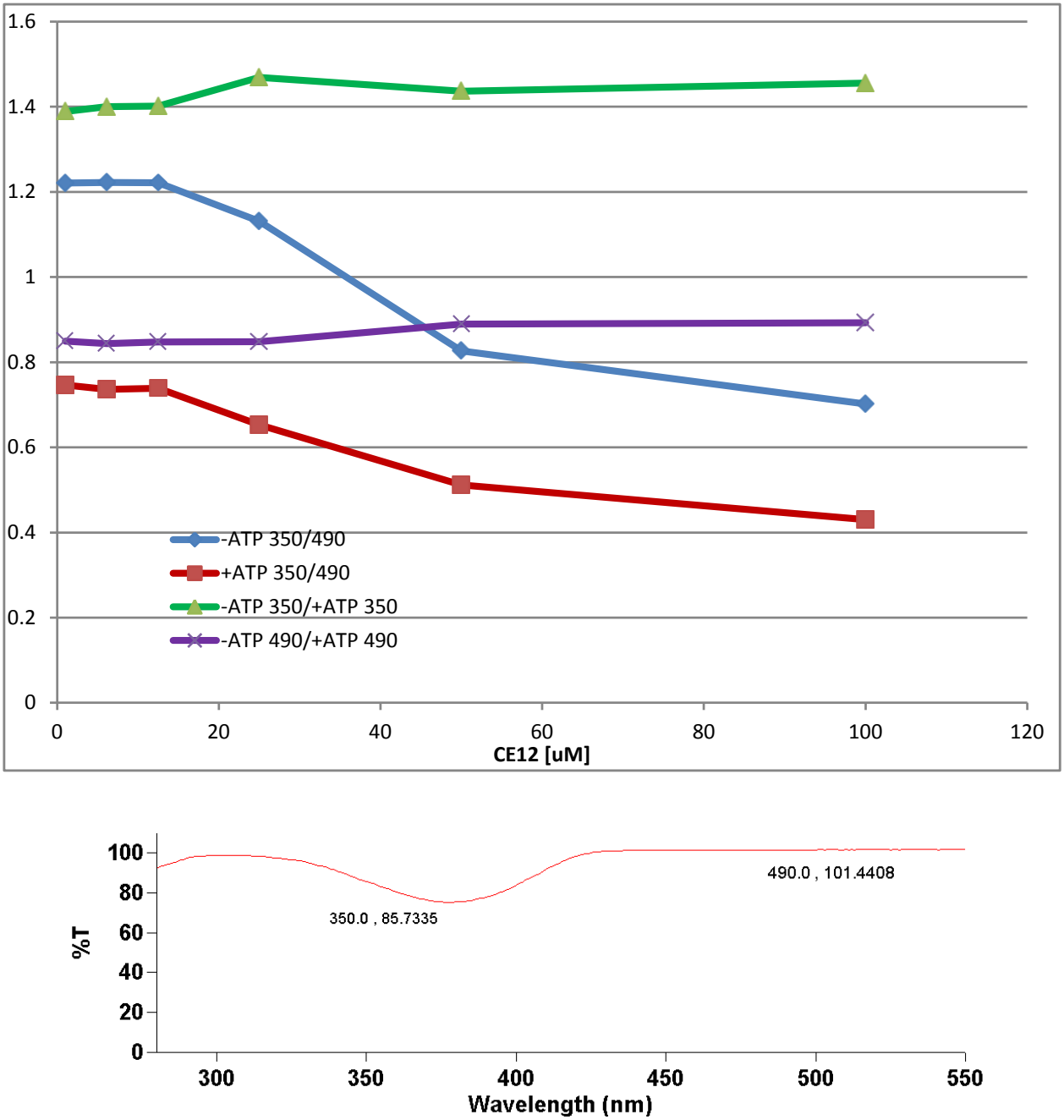

Figure 33. Effect of CE12 on conformational changes of DnaK assessed by FRET between W102 and R517C-IAEDANS. See Figure 30 for experimental details. Note that CE12 fluoresces significantly at 490 nm (see Appendix).

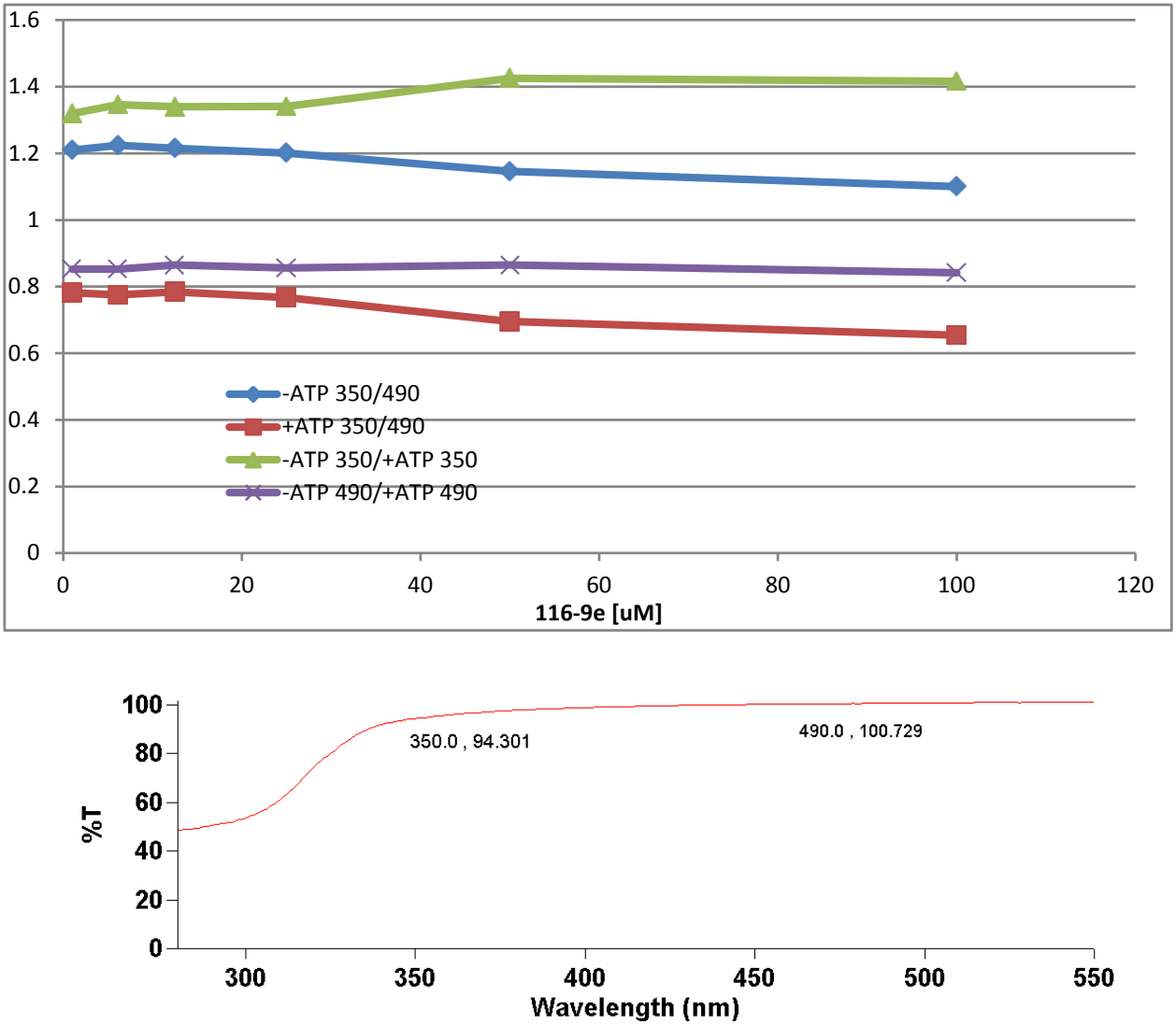

Figure 34. Effect of 116-9e on conformational changes of DnaK assessed by FRET between W102 and R517C-IAEDANS. See Figure 30 for experimental details.

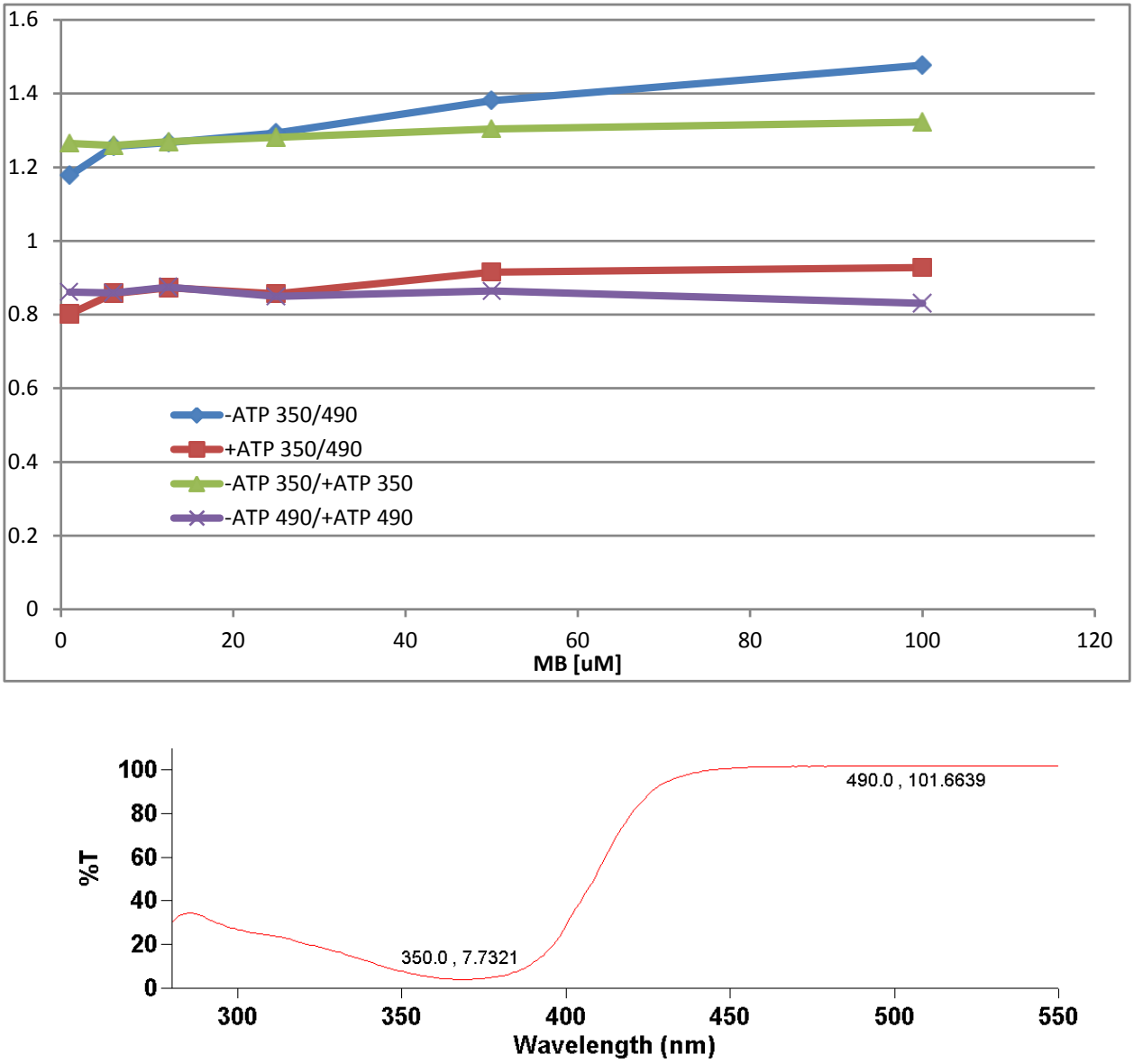

Figure 35. Effect of MB on conformational changes of DnaK assessed by FRET between W102 and R517C-IAEDANS. See Figure 30 for experimental details.

Finally, we utilized AF555-AF594 double-labeled DnaK to probe the effects of one Hsp70 activity modulator, MB, on DnaK's conformational shift. Due to MB's large absorbance at both the AF555 and AF594 emission wavelengths, we did not directly compare samples of labeled protein with and without MB present. Instead, we measured the change in AF555 donor fluorescence upon addition of ATP to DnaK in the presence of either MB or DMSO vehicle (Table 7). We found that the percent decrease in AF555 donor fluorescence with MB present (5.9%) was just over half the percent decrease with DMSO vehicle (10.8%). When DnaK was allowed to bind to 10 μM ADP before addition of a 100-fold excess of ATP, we observed an 8.0% decrease in AF555 donor fluorescence in the presence of MB but a

14.8% decrease with DMSO vehicle. These results indicate that MB restricts the conformational mobility of DnaK in response to nucleotides. It is impossible to know from this experiment, however, whether MB stabilizes the ATP-bound form of DnaK, the ADP-bound form, or some intermediate.

Table 7. Effect of MB on nucleotide-dependent conformational shift of DnaK assessed by AF555-AF594 FRET. Approximately 0.2 μM double-labeled DnaK with and without 10 μM ADP present was incubated with either 50 mM MB or DMSO vehicle for thirty minutes. Fluorescence emission spectra with excitation at 520 nm were taken before and 45 minutes after addition of a 100X ATP stock to a final ATP concentration of 1 mM, and the percent change in AF555 donor fluorescence at 567 nm was calculated.

Nucleotide	Compound	Percent decrease in AF555 donor fluorescence upon addition of 1 mM ATP
None	DMSO	10.8
None	MB	5.9
10 μM ADP	DMSO	14.8
10 μM ADP	MB	8.0

Chapter 4

Discussion

Characterization of protein cysteine residues using CPM

Of the twenty amino acids that make up proteins, cysteine residues are particularly interesting because they are common sites for post-translational modifications such as S-nitrosylation and S-palmitoylation, pairs of cysteines form disulfide bonds that are essential to protein tertiary structure, and cysteines are central players in redox chemistries associated with signaling pathways and oxidative stress. The reactivity of a cysteine to a certain molecule depends on many factors including solvent accessibility, thiol pK_a, the local electrostatic environment, the chemical nature of the thiol-reactive reagent, the interaction of the reagent with the cysteine's environment, and the stability of the bond formed (Forman et al., 2010; Paulsen and Carroll, 2010). Any tool that could be used to determine the reactivity of cysteines within proteins would be immensely useful to the study of cysteines' functional role. We have investigated the utility of thiol-reactive CPM as a probe for cysteine reactivity and examined whether a cysteine's reactivity to CPM can be used to judge its reactivity more generally.

We found that CPM reactivity depends on the position of a particular cysteine on the surface of DnaK, as different cysteine sites vary in CPM reactivity by greater than tenfold. Reaction of CPM to DnaK's endogenous cysteine at position 15, which is buried in the NBD, is very slow compared to solvent-exposed positions (data not shown), suggesting that CPM reactivity reflects solvent accessibility to some degree. For a range of solvent-exposed positions, however, we were unable to form a consistent correlation between CPM reactivity and accessibility of a cysteine calculated in Swiss PdbViewer or as estimated by hydrogen/deuterium exchange. In contrast, there is a correlation between the electrostatic potential of the surface surrounding the cysteine and the reactivity to CPM, with positive and neutral environments generally being conducive to faster CPM reaction rates, probably because negative environments disfavor deprotonation of the cysteine thiol. Thus, neighboring charged groups in addition to solvent accessibility are likely both important factors in determining CPM reactivity.

We hoped to demonstrate experimentally that solvent accessibility influences CPM reactivity by digesting DnaK with proteinase K and by denaturing DnaK with SDS before CPM labeling. Although small amounts of proteinase K increased slightly the CPM reaction rate for K446C/C15S, larger amounts of proteinase K led to a steady decline in CPM reactivity for T136C/C15S. We suspect that oxidation of cysteine thiols occurred during incubation with proteinase K, and in the future reduction with TCEP should be carried out

after digestion and before labeling with CPM. Measuring the reactivity of free reduced cysteine to CPM is another possible control to complement proteinase K digestion in demonstrating the effect of solvent accessibility. Small amounts of SDS (0.003-0.01%) increased CPM reactivity for DnaK single-cysteine variants, but circular dichroism showed that these concentrations of SDS do not significantly unfold DnaK, making it difficult to conclude that the increase in reaction rate was due to increasing accessibility of cysteine thiols. Transient unfolding could suffice to increase the CPM reaction rate without significantly affecting the circular dichroism spectrum. Larger concentrations of SDS (up to 2%) inhibited the CPM reaction, possibly because the net negative charge conferred on DnaK by SDS increased the thiol pK_a. Unfolding DnaK with other denaturants may prove more effective in maximizing CPM reactivity. The degree to which CPM reflects solvent accessibility will need to be further studied with other proteins and cysteines in a wide variety of solvent-exposed and solvent-buried locations.

Our studies with DnaK T136C/C15S and S423C/C15S demonstrated that CPM reactivity is strongly dependent on pH. For $pH \leq 9$, reaction rates increase with increasing pH in an S-shaped curve, and we could fit pH dependence of CPM reaction rate to deprotonation of T136C and S423C with pK_a values of 7.8 and 7.6, respectively. Free cysteine has a pK_a approximately equal to 8.0 that can be altered by surrounding charged groups, so the experimentally determined pK_a values are reasonable. Above pH 9 the CPM reaction rate increases again, probably because lysine residues become ionized and reactive. Although there is only a small difference in pK_a of T136C and S423C, we measured a nearly threefold difference in CPM reactivity at the two positions at pH 8.5. This suggests that steric hindrance may be greater surrounding S423C than T136C.

Our results indicate that CPM reactivity is influenced not just by solvent accessibility but by several competing factors. Nevertheless, CPM reactivity is predictive of relative reactivity to the Alexa Fluor maleimides, as T136C reacted approximately twentyfold faster than S423C to AF555 at pH 8.5. Interestingly, the reactivity of T136C to AF555 is fourfold slower than to CPM and reactivity of S423C to AF555 is thirtyfold slower than to CPM. This reactivity difference is probably due to the larger size of AF555, which has a molecular weight of approximately 1250 Da versus 402 Da for CPM, or to the several formal charges on the Alexa dyes that could interact unfavorably with the protein surface.

Alexa Fluor labeling kinetics

We used two methods to track labeling of DnaK with Alexa Fluor dyes. First we measured fluorescence anisotropy changes, allowing us to watch conjugation of AF555 or AF488 to DnaK in real time with minimal handling steps that might introduce error. With this method we obtained a reasonable progress curve for some DnaK variants, including T136C, with fluorescence anisotropy increasing over time and the reaction completing after about ten minutes. For other DnaK variants, including S423C, fluorescence anisotropy remained constant or decreased slightly during the conjugation reaction. We showed, however, that fluorescence anisotropy of purified AF488-DnaK complexes is about fivefold greater than free AF488, suggesting that unreacted free dye present during the labeling reaction may interfere with the expected increase in fluorescence anisotropy upon conjugation. One way to test this hypothesis is to add free dye back to purified AF488-DnaK complexes and see if fluorescence anisotropy decreases.

In contrast, our gel-based method of tracking labeling kinetics produces a reproducible rise in conjugation product over time for both DnaK T136C/C15S and S423C/C15S. The disadvantage of this method is that reaction aliquots must be quenched at the desired time points and run on an SDS-PAGE gel, with bands quantified by densitometry, steps at which errors could be introduced. Nonetheless, these reactions fit well to pseudo-first order kinetics (all Alexa Fluor labeling reactions were carried out with tenfold excess dye). Quantifying the amount of dye and protein in each time point may be made more precise by measuring light absorption due to the dye and tryptophan. Alternatively, each time point could be reacted with CPM to determine the amount of free thiol remaining.

Two pot double labeling method

Our initial method of double labeling DnaK involved first a short reaction with donor fluorophore to label fast-reacting T136C, purification of singly labeled DnaK by ion exchange or hydrophobic interaction chromatography, and last a long reaction with acceptor fluorophore to label slow-reacting S423C. The appeal of this method was the potential to remove unwanted unlabeled and double-labeled species between labeling reactions. We first attempted separation on a MonoQ anion exchange column. SDS-PAGE analysis suggested that early-eluting fractions contained small amounts of relatively pure DnaK single-labeled at S423C (Figure 20), but we were unable to achieve satisfactory separation of the major single-labeled species labeled at T136C from double-labeled and unlabeled protein by varying running buffer pH, decreasing the slope of the salt gradient, or adding 1 mM tryptophan to the

buffer. Although the Alexa Fluor dyes have multiple formal charges, in the context of a 70 kDa protein these charges may not be enough to influence elution in anion exchange. We next tried separation on the phenyl sepharose column, which when running at pH 9.0, room temperature, allowed us to attain some fractions that contained primarily DnaK single-labeled at T136C (Figure 21). Since hydrophobic interactions are generally reduced at higher pH values (Hydrophobic, 2000), pH 9.0 conditions may diminish DnaK's affinity for phenyl sepharose and permit discrimination of protein modified with the Alexa dyes. Another possible separation method that could be used in the future is thiol-disulfide interchange, as only single-labeled and unlabeled species would bind to sulfhydryls under oxidizing conditions. Bound protein could then be eluted with reducing agent such as β-mercaptoethanol (Idziorek et al., 1985).

Another problem we encountered during development of the labeling protocol was that fluorescently labeled DnaK was unstable and prone to precipitation in our original FL Buffer. This observation was surprising since the labeled proteins were at submicromolar concentrations, well below solubility limits for the individual DnaK protein and Alexa dye molecules. However, conjugation of two large fluorophores weighing approximately 1000 Da each, the weight of several amino acids, could result in alteration of DnaK's tertiary structure and exposure of hydrophobic surfaces, increasing vulnerability to precipitation. Our buffer screen showed that in the absence of detergents or hygroscopic adjuncts, the change in FRET upon addition of ATP is smaller or nonexistent compared to labeled protein in FL buffer containing 10% glycerol. Glycerol stabilizes proteins against denaturation and increases protein solubility by facilitating formation of a layer of structured water surrounding protein molecules that shields them from intermolecular interactions (Farnum and Zukoski, 1999). Preliminary tests indicated that in the presence of 10% glycerol DnaK does not bind to phenyl sepharose below 1.0 M ammonium sulfate. We also wished to minimize handling steps that could precipitate protein, so we decided to eliminate chromatographic purification of single-labeled species after the first labeling reaction. We moved to one pot labeling, with a 30-minute incubation of equal molar amounts of DnaK and donor fluorophore followed by addition of a tenfold molar excess of acceptor fluorophore and further two hour incubation. DnaK labeled according to this method with AF555 and AF594 shows a 16% decrease in donor fluorescence upon addition of ATP. The fact that we achieved a much larger change in FRET with two-step fluorophore addition than when we added equal molar amounts of the two fluorophores simultaneously (5.8% decrease in donor fluorescence, see buffer screen) verifies the difference in reactivity of T136C and S423C. If T136C and S423C reacted

equally to the Alexa dyes, then sequential fluorophore addition would have led to the same number of hetero-labeled species and the same change in FRET upon addition of ATP as adding both fluorophores simultaneously. Since we observed a nearly three-fold larger decrease in donor fluorescence after adding ATP to two-step-labeled DnaK, we produced approximately three times the number of hetero-labeled molecules and during the initial labeling reaction with AF555, conjugation at T136C was favored three to one over conjugation at S423C. Thus, our kinetics studies were worthwhile in identifying sites that reacted at different rates to fluorophores, thus improving our yield of hetero-labeled species.

Nevertheless, our labeling protocol could be improved by selecting better sites for fluorescent labeling. The largest change in FRET we observed upon addition of ATP to double-labeled DnaK was 16%, and more commonly we observed an approximately 10% change in FRET. Positions 136 and 423 are separated by 39 Å in the ADP-bound form according to the Bertelsen et al. NMR model, while the Förster radius for the AF555-AF594 dye pair is 47 Å. The sensitivity of the FRET sensor for DnaK's conformational change could be enhanced by choosing fluorophore conjugation positions separated by a distance closer to the Förster radii for Alexa dye pairs, which are 47 Å and greater.

The decrease in FRET we observed for the ATP-bound state compared to the apo and ADP-bound states indicates that the NBD and SBD are closer in the ATP-bound form of DnaK. This result is in agreement with SAXS, NMR, X-ray crystallography, and FRET studies indicating that with ATP bound, the NBD and SBD are docked, whereas with ADP bound, the NBD and SBD are disjoined (Wilbanks et al., 1995; Swain et al., 2006; Swain et al., 2007; Chang et al., 2008; Bertelsen et al., 2009; Mapa et al., 2010).

Analysis of Hsp70 activity modulators

We studied the effect of Hsp70 activity modulators on DnaK's conformational changes using four different methods: limited proteolysis, SAXS, FRET with single-labeled DnaK, and FRET with double-labeled DnaK. ATPase assays performed in the Gestwicki lab showed that SW02 and 115-7c are Hsp70 ATPase activators, while CE12, 116-9e, MB, and MY are ATPase inhibitors. Limited proteolysis of DnaK in the presence of the ATPase stimulator 115-7c resulted in a faint 70 kDa band characteristic of an ADP-like state in a reaction containing 10 μM ATP. It is possible that 115-7c increases the rate of ATP hydrolysis such that ATP begins to be exhausted in the protein/nucleotide/drug mixture in the approximately five minutes before proteinase K is added. Since DnaK intrinsically hydrolyzes ATP at a rate of about 0.1 to 1 ATP molecule per minute per monomer DnaK (Mayer and Bukau, 2005) and the reaction mix contains 10-fold excess ATP over DnaK, 115-

7c would need only to stimulate DnaK's ATPase activity approximately twofold for the amount of ATP present to decrease in five minutes below DnaK's K_d for ATP, which is submicromolar (Theyssen et al., 1996). Such an acceleration of ATPase activity is conceivable given the fact that DnaJ plus substrate protein stimulates DnaK's ATPase activity 1000-fold. Performing ATPase assays with DnaK and 115-7c present to determine the degree of ATPase stimulation would help determine whether this explanation is correct. In the presence of the other ATPase stimulator, SW02, the limited proteolysis banding pattern was similar to no compound present except for the appearance of a faint 70 kDa band with 1 mM ATP but not 10 μM ATP. This result is difficult to explain by SW02 stimulating ATPase activity, but it may have to do with SW02 stabilizing an ADP-like conformation. Small amounts of ADP-contamination in the ATP stock may permit SW02 to push DnaK's conformation equilibrium toward an ADP-bound form. With only 10 μM ATP, the amount of ADP-contamination may be insignificant. A limited proteolysis experiment with various intentional mixtures of ATP and ADP could shed light on this possibility.

Three of the ATPase inhibitors, CE12, 116-9e, and MY, also led to the appearance of a 70 kDa band when DnaK was digested with 1 mM ATP. MY caused the strongest ADP-characteristic 70 kDa band with 1 mM ATP, yet SAXS results suggested that MY stabilizes an ATP-like form of DnaK because it decreases DnaK's radius of gyration in the presence of ATP compared to no drug. CE12 also caused a decrease in DnaK's radius of gyration in the presence of ATP. Hsp70 inhibitors like MY and CE12 may interfere generally with DnaK's conformational change, and the particular conformation that is trapped may depend on experimental conditions. Indeed, FRET experiments with double-labeled DnaK showed that when the Hsp70 inhibitor MB is present, the change in FRET upon addition of nucleotide is smaller than without MB, suggesting that MB interferes with DnaK's conformational shift. Further experiments are required to determine the particular conformations that these drugs stabilize in different conditions. Isothermal titration calorimetry could be used to find the ΔG for binding of compound to DnaK in the presence of ATP or ADP, thus indicating which conformation(s) of DnaK the compounds interact with.

Future directions

One month before submission of this thesis, Mapa et al. published a study in *Molecular Cell* using intramolecular FRET to probe conformational changes of DnaK and Ssc1, a yeast Hsp70 localized to the mitochondrial matrix. Mapa et al. introduced cysteine residues at two pairs of locations in Ssc1 and DnaK. The first pair at positions 341 and 488 in Ssc1 (318 and 425 in DnaK) was used to measure distance changes between the NBD and the

SBD. The second pair of cysteines at positions 448 and 590 in Ssc1 (458 and 563 in DnaK) was used to monitor opening and closing of the SBD lid. Mapa et al.'s fluorescent labeling method was similar to ours in that protein was labeled in a single step with both donor and acceptor fluorophores, but they used Atto532 and Atto647N maleimides as FRET donor and acceptor, respectively. Consistent with our FRET studies on DnaK, single-molecule FRET with Ssc1 double-labeled at the (341, 488) positions showed a narrow distribution of molecules with FRET efficiency of 0.89 in the ATP-bound form, while the ADP-bound form had a wide distribution of conformations with lower FRET efficiency. smFRET experiments done with Ssc1 double-labeled at the (448, 590) positions showed a narrow distribution of molecules with low FRET efficiency of 0.20 in the ATP-bound form, but a broad distribution of molecules with higher efficiency in the ADP-bound form. These results suggest that in the ATP-bound state DnaK exists in a stable conformation with domains docked and lid open, whereas with ADP-bound DnaK is conformationally flexible with domains disjoined and lid closed. Mapa et al. went on to study the effects of substrate peptide P5 and the co-chaperone and J-domain protein Mdj1 on Ssc1 conformational dynamics. They found that Mdj1 plus P5 resulted in less FRET between positions 341 and 448 and greater FRET between positions 448 and 590 than in the ADP-only state, indicating stabilization of the domain-disjoined, closed lid form of Ssc1. Kinetics studies performed with fluorescently labeled Mdj1 showed that Mdj1 binds to Ssc1 only in the ATP-bound state and that Mdj1 is released from Ssc1 over a course of minutes after ATP hydrolysis. In FRET experiments performed with DnaK, Mapa et al. found that conformational dynamics of DnaK are similar to those of Ssc1 except that unlike Ssc1, DnaK appears not to undergo conformational changes on the 5 millisecond timescale in the ADP-bound state (Mapa et al., 2010).

The Mapa study demonstrates the utility in studying Hsp70 conformational dynamics by FRET and provides long-term direction for our work. It provides confirmation that our results with DnaK labeled at T136C and S423C are due to global conformational rearrangements rather than local fluorophore quenching or restriction in fluorophore rotation. Second, comparing the influence of co-chaperones and substrate peptides on DnaK to the effect of such factors on Ssc1 is a priority. It will be interesting to see if DnaJ interacts transiently to DnaK (Bukau and Horwich, 1998) or remains stably bound to DnaK over several minutes as is the case with Mdj1 and Ssc1. Third, it will be important to extend FRET studies to a range of prokaryotic and eukaryotic Hsp70s to determine their similarities and differences. Thus far it appears that while the ATP-bound state of all Hsp70 chaperones is similar, the ADP-bound state varies among homologs. FRET histograms made by Mapa et al.

indicate a certain degree of interdomain interaction in the ADP-bound form of Ssc1, and Jiang et al. observed an extensive interdomain interface for Hsc70 in the ADP state. In contrast, Mapa et al. found no evidence for interdomain interaction in DnaK with ADP bound, in agreement with NMR studies (Bertelsen et al., 2009; Swain et al., 2007). Fourth, it will be important to move to FRET measurements in cells, where we can observe the effects of cellular localization, protein crowding, and a variety of stressors on Hsp70 conformational dynamics.

The results of this thesis, however, segue into several short-term goals leading in the directions described above. To begin with, we should select new fluorophore conjugation sites whose separation distance is more similar to the Förster radii of Alexa dye pairs, leading to a more sensitive probe of conformational changes. Further screening for sites with CPM will facilitate this. Second, we will need to optimize a method for smFRET experiments. We were able to detect mobile AF488-labeled DnaK molecules with a total internal reflection microscope using a 488 nm excitation laser. In order to focus on single DnaK molecules, we will need to immobilize DnaK to a coverslip and can do this using a biotin-avidin linkage. We can use the HABA reagent, which binds to avidin to form a yellow-orange complex that absorbs at 500 nm, to quantify biotinylation of DnaK. We plan to coat a coverslip with biotinylated PEG, to which neutravidin binds, followed by biotinylated DnaK (Figure 36). Immobilization of DnaK will allow us to add and subtract variables by washing with reagents such as nucleotides, substrate peptides, co-chaperones, and Hsp70 activity modulators. Lastly, we will need to purify DnaJ and GrpE co-chaperones, the method for which we are currently optimizing.

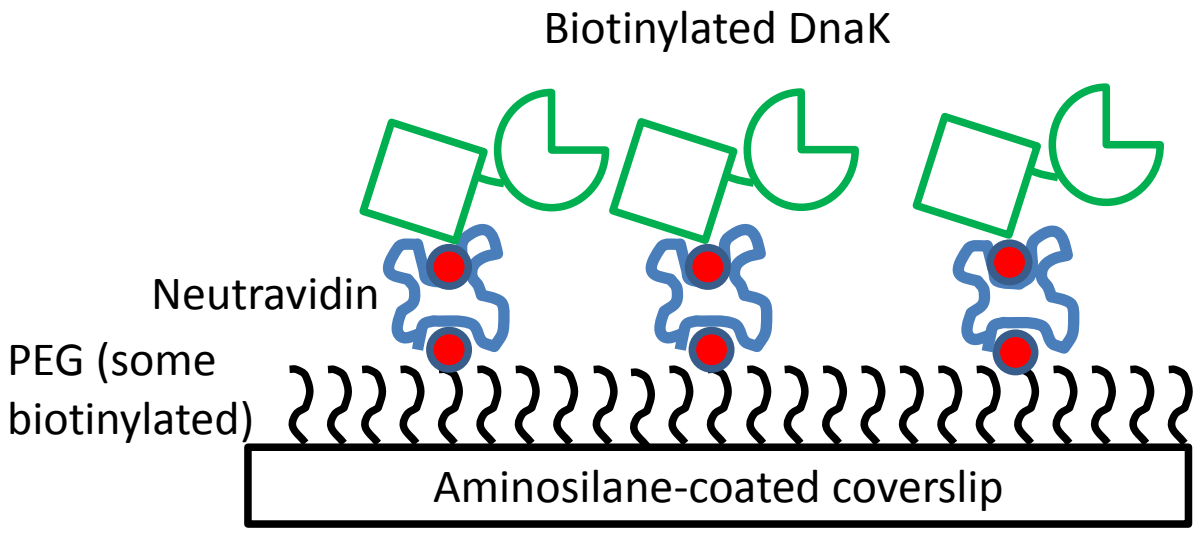

Figure 36. Proposed method for conjugation of DnaK to a glass coverslip. The coverslip is coated with aminosilane and allowed to bind to succinimide ester-derivatized PEG, a fraction of which contains a biotin group on the opposite end. Biotinylated PEG binds to tetravalent neutravidin, and neutravidin binds to biotinylated DnaK.

In summary, we have developed methods for measuring the reactivity of a variety of positions on DnaK using CPM, tracking Alexa Fluor labeling kinetics on SDS-PAGE gels, and double labeling of DnaK at two sites that react at significantly different rates to CPM and the Alexa Fluor maleimides. These methods led to creation of a double-labeled DnaK that allows real-time detection of DnaK's nucleotide-dependent conformational shift and confirms a model for DnaK function in which interdomain communication is facilitated by the NBD and SBD docking and disjoining in the ATP- and ADP-bound forms, respectively. We have shown preliminary data demonstrating the utility of double-labeled DnaK in the study of Hsp70 activity-modulating compounds, and our results provide the foundation for single molecule FRET studies.

References

Allen W.J., P.J. Rothwell, G. Waksman (2008). An intramolecular FRET system monitors fingers subdomain opening in Klentaq1. Protein Sci. 17:401-8.

Anfinsen C.B. Nobel lecture. Studies on the principles that govern the folding of protein chains. National Institutes of Health, Bethesda, MD. 11 Dec 1972.

Bertelsen E.B., L. Chang, J.E. Gestwicki, E.R. Zuiderweg (2009). Solution conformation of wild-type E. coli Hsp70 (DnaK) chaperone complexed with ADP and substrate. Proc. Natl. Acad. Sci. USA 106:8471-6.

Bolhassani A., S. Rafati (2008). Heat-shock proteins as powerful weapons in vaccine development. Exp. Rev. Vaccines 7:1185-1199.

Brown G.C. (1991). Total cell protein concentration as an evolutionary constraint on the metabolic control distribution in cells. J. Theor. Biol. 153:195-203.

Buchberger A., H. Theyssen, H. Schröder, J.S. McCarty, G. Virgallita, P. Milkereit, J. Reinstein, B. Bukau (1995). Nucleotide-induced conformational changes in the ATPase and substrate binding domains of the DnaK chaperone provide evidence for interdomain communication. J. Biol. Chem. 270:16903-10.

Bukau B. and A.L. Horwich (1998). The Hsp70 and Hsp60 chaperone machines. Cell 92:351-66.

Bukau B., J. Weissman, A. Horwich (2006). Molecular chaperones and protein quality control. Cell 125:443-51.

Bukau B., G.C. Walker (1990). Mutations altering heat shock specific subunit of RNA polymerase suppress major cellular defects of *E. coli* mutants lacking the DnaK chaperone. EMBO J. 9:4027-36.

Chang L., E.B. Bertelsen, S. Wisén, E.N. Larsen, E.R. Zuiderweg, J.E. Gestwicki (2008). High-throughput screen for small molecules that modulate the ATPase activity of the molecular chaperone DnaK. Anal. Biochem. 372:167-76.

Chang Y.W., Y.J. Sun, C. Wang, C.D. Hsiao (2008). Crystal structures of the 70-kDa heat shock proteins in domain disjoining conformation. J. Biol. Chem. 283:15502-11.

Davies, K.J.A. (1987). Protein damage and degradation by oxygen radicals. J. Biol. Chem. 262:9895-901.

Deuerling E., H. Patzelt, S. Vorderwülbecke, T. Rauch, G. Kramer, E. Schaffitzel, A. Mogk, A. Schulze-Specking, H. Langen, B. Bukau (2003). Trigger factor and DnaK possess overlapping substrate pools and binding specificities. Mol. Microbiol. 47:1317-28.

Dill K.A. (1990). Dominant forces in protein folding. Biochem. 29: 7133-55.

Ebeling W., N. Hennrich, M. Klockow, H. Metz, H.D. Orth, H. Lang (1974). Proteinase K from *Tritirachium album* limber. Eur. J. Biochem. 47:91-97.

El Khattabi M., P. Van Gelder, W. Bitter, J. Tommassen (2000). Role of the lipase-specific foldase of *Burkholderia glumae* as a steric chaperone. J. Biol. Chem. 275:26885-91.

Ellis R.J. (1991). Molecular chaperones. Ann. Rev. Biochem. 60:321-47.

Evans C.G., S. Wisén, J.E. Gestwicki (2006). Heat shock proteins 70 and 90 inhibit early stages of amyloid beta-(1-42) aggregation in vitro. J. Biol. Chem. 281:33182-91.

Farnum M. and C. Zukoski (1999). Effect of glycerol on the interactions and solubility of bovine pancreatic trypsin inhibitor. Biophys. J. 76:2716-26.

Flaherty K.M., C. DeLuca-Flaherty, D.B. McKay (1990). Three-dimensional structure of the ATPase fragment of a 70K heat-shock cognate protein. Nature 346:623-8.

Forman H.J., M. Maiorino, F. Ursini (2010). Signaling functions of reactive oxygen species. Biochem. 49:835-42.

Galvez E., M. Düser, M. Börsch, J. Wrachtrup, P Gräber (2008). Quantum dots for single-pair fluorescence resonance energy transfer in membrane-integrated EFoF1. Biochem. Soc. Trans. 36:1017-21.

Georgopoulos C.P. (1977). A new bacterial gene (groPC) which affects lambda DNA replication. Mol. Gen. Genet. 151:35-9.

Gupta R.S., G.B. Golding (1993). Evolution of Hsp70 gene and its implications regarding relationships between archaebacteria, eubacteria, and eukaryotes. J. Mol. Evol. 37:573-82.

Harrison C.J., M. Hayer-Hartl, M. Di Liberto, F.U. Hartl, J. Kuriyan (1997). Crystal structure of the nucleotide exchange factor GrpE bound to the ATPase domain of the molecular chaperone DnaK. Science 276:431-5.

Haugland R.P. (2005). Fluorescence Resonance Energy Transfer (FRET). The Handbook: A Guide to Fluorescent Probes and Labeling Technologies. Molecular Probes, Invitrogen. 29-30.

Haugland R.P. (2005). The Alexa Fluor dye series—peak performance across the visible spectrum. The Handbook: A Guide to Fluorescent Probes and Labeling Technologies. Molecular Probes, Invitrogen. 29-30.

Henderson B. (2010). Integrating the cell stress response: a new view of molecular chaperones as immunological and physiological homeostatic regulators. Cell. Biochem. Funct. 28:1-14.

Hettema E.H., C.C. Ruigrok, M.G. Koerkamp, M. van den Berg, H.F. Tabak, B. Distel, I. Braakman (1998). The cytosolic DnaJ-like protein djp1p is involved specifically in peroxisomal protein import. J. Cell. Biol. 142:421-34.

Hoffmann A., B. Bukau, G. Kramer (2010). Structure and function of the molecular chaperone trigger factor. Biochim. Biophys. Acta. In press, doi:10.1016/j.bbamcr.2010.01.017.

Hoffmann H.J., S.K. Lyman, C. Lu, M.A. Petit, and H. Echols (1992). Activity of the Hsp70 chaperone complex—DnaK, DnaJ, and GrpE—in initiation phage lambda DNA replication by sequestering and releasing lambda P protein. Proc. Natl. Acad. Sci USA 89:12108-11.

Hofmann G.E., B.A. Buckley, S. Airaksinen, J.E. Keen, G.N. Somero (2000). Heat-shock protein expression is absent in the Antarctic fish *Trematomus bernacchii* (family Nototheniidae). J. Exp. Biol. 203:2331-9.

Hydrophobic Interaction Chromatography: Principles and Methods. Amersham Pharmacia Biotech, 2000.

Idziorek T., B. Sablonniere, P. Formstecher, V. Dumar, M. Dautrevaux (1985). Covalent chromatography by thiol-disulfide interchange of the highly-purified non-transformed rat liver glucocorticoid-receptor. J. Steroid Biochem. 23:593-7.

Inoue H., H. Nojima, H. Okayama (1990). High efficiency transformation of *Escherichia coli* with plasmids. Gene 96:23-8.

Jiang J., K. Prasad, E.M. Lafer, R. Sousa (2005). Structural basis of interdomain communication in the Hsc70 chaperone. Mol. Cell 20:513-24.

Jinwal U.K., Y. Miyata, J. Koren 3rd, T.R. Jones, J.H. Trotter, L. Chang, J. O'Leary, D. Morgan, D.C. Lee, C.L. Shults, A. Rousaki, E.J. Weeber, E.R. Zuiderweg, J.E. Gestwicki, C.A. Dickey (2009). Chemical manipulation of hsp70 ATPase activity regulates tau stability. J. Neurosci. 29:12079-88.

Jones G.W., M.F. Tuite (2005). Chaperoning prions: the cellular machinery for propagating an infectious protein? Bioessays 27:823-32.

Karlin S., L. Brocchieri (1998). Heat shock protein 70 family: multiple sequence comparisons, function, and evolution. J. Mol. Evol. 47:565-77.

Kirkegaard T., A.G. Roth, N.H.T. Petersen, A.K. Mahalka, O.D. Olsen, I. Moilanen, A. Zylicz, J. Knudsen, K. Sandhoff, C. Arenz, P.K.J. Kinnunen, J. Nylandsted, M. Jäättelä (2010). Hsp70 stabilizes lysosomes and reverts Niemann-Pick disease-associated lysosomal pathology. Nature 463:549-53.

Konarev P.V., M.V. Petoukhov, V.V. Volkov, D.I. Svergun (2006). ATSAS 2.1, a program package for small-angle scattering data analysis. J. Appl. Cryst. 39:277-286.

Koren 3rd J., U.K. Jinwal, Y. Jin, J. O'Learly, J.R. Jones, A.G. Johnson, L.J. Blair, J.F. Abisambra, L. Chang, Y. Miyata, A.M. Cheng, J. Guo, J.Q. Cheng, J.E. Gestwicki, C.A. Dickey (2009). Facilitating Akt clearance via manipulation of Hsp70 activity and levels. J. Biol. Chem. 285:2498-505.

Lanneau D., A. de Thonel, S. Maurel, C. Didelot, C. Garrido (2007). Apoptosis versus cell differentiation: role of heat shock proteins Hsp90, Hsp70, and Hsp27. Prion 1:53-60.

Laskey R.A., B.M. Honda, A.D. Mills, J.T. Finch (1978). Nucleosomes are assembled by an acidic protein which binds histones and transfers them to DNA. Nature 275:416-20.

Laufen T., M.P. Mayer, C. Beisel, D. Klostermeier, J. Reinstein, B. Bukau (1999). Mechanism of regulation of Hsp70 chaperones by DnaJ co-chaperones. Proc. Natl. Acad. Sci. USA 96:5452-7.

Lindquist S. (1986). The heat-shock response. Ann. Rev. Biochem. 55:1151-91.

Liu Q., W.A. Hendrickson (2007). Insights into Hsp70 chaperone activity from a crystal structure of the yeast Hsp110 Sse1. Cell 131:106-20.

Magrané J., R.C. Smith, K. Walsh, H.W. Querfurth (2004). Heat shock protein 70 participates in the neuroprotective response to intracellularly expressed beta-amyloid in neurons. J. Neurosci. 24:1700-6.

Mapa K., M. Sikor, V. Kudryavtsev, K. Waegemann, S. Kalinin, C.A.M. Seidel, W. Neupert, D.C. Lamb, D. Mokranjac (2010). The conformational dynamics of the mitochondrial Hsp70 chaperone. Mol. Cell 38:89-100.

Mathew S.S., M.P.D. Selva, and A.D. Burch (2009). Modification and reorganization of the cytoprotective cellular chaperone Hsp27 during herpes simplex virus type 1 infection. J. Virol. 83:9304-12.

Mayer M.P. and B. Bukau (2005). Hsp70 chaperones: cellular functions and molecular mechanism. Cell. Mol. Life Sci. 62:670-684.

Montgomery D.L., R.I. Morimoto, L.M. Gierasch (1999). Mutations in the substrate binding domain of the *Escherichia coli* 70 kDa molecular chaperone, DnaK, which alter substrate affinity or interdomain coupling. J. Mol. Biol. 286:915-32.

Moro F., S.G. Taneva, A.Velázquez-Campoy, A. Muga (2007). GrpE N-terminal domain contributes to the interaction with Dnak and modulates the dynamics of the chaperone substrate binding domain. J. Mol. Biol. 374:1054-64.

Nettels D., S. Müller-Späth, F. Küster, H. Hofmann, D. Haenni, S. Rüegger, L. Reymond, A. Hoffmann, J. Kubelka, B. Heinz, K. Gast, R.B. Best, B. Schuler (2009). Single-molecule spectroscopy of the temperature-induced collapse of unfolded proteins. Proc. Natl. Acad. Sci. USA 106:20740-5.

Palleros D.R., L. Shi, K.L Reid, A.L. Fink (1993). Three-state denaturation of DnaK induced by guanidine hydrochloride. Evidence for an expandable intermidate. Biochem. 32:4314-21.

Paulsen C.E., K.S Carroll (2010). Orchestrating redox signaling networks through regulatory cysteine switches. ACS Chem. Biol. 5:47-62.

Pauwels K., I. Van Molle, J. Tommassen, P. Van Gelder (2007). Chaperoning Anfinsen: the steric foldases. Mol. Microbiol. 64:917-22.

Pedersen M., M. Carmosino, B. Forbush (2008). Intramolecular and intermolecular fluorescence resonance energy transfer in fluorescent protein-tagged Na-K-Cl cotransporter (NKCC1): sensitivity to regulatory conformational change and cell volume. J. Biol. Chem. 283:2663-74.

Pellecchia M., D.L. Montgomery, S.Y. Stevens, C.W. Vander Kooi, H.P. Feng, L.M. Gierasch, E.R. Zuiderweg (2000). Structural insights into substrate binding by the molecular chaperone DnaK. Nat. Struct. Biol. 7:298-303.

Ravagnan L., S. Gurbuxani, S.A. Susin, C. Maisse, E. Daugas, N. Zamzami, T. Mak, M. Jäättelä, J.M. Penninger, C. Garrido, G. Kroemer (2001). Heat-shock protein 70 antagonizes apoptosis-inducing factor. Nat. Cell Biol. 3:839-43.

Revington M., Y. Zhang, G.N. Yip, A.V. Kurochkin, E.R. Zuiderweg (2005). NMR investigations of allosteric processes in a two-domain *Thermus thermophiles* Hsp70 molecular chaperone. J. Mol. Biol. 349:163-83.

Rist W., C. Graf, B. Bukau, M.P. Mayer (2006). Amide hydrogen exchange reveals conformation changes in hsp70 chaperones important for allosteric regulation. J. Biol. Chem. 281:16493-501.

Rothman J.E., S.L. Schmid (1986). Enzymatic recycling of clathrin from coated vesicles. Cell 46:5-9.

Roy R., S. Hohng, T. Ha (2008). A practical guide to single-molecule FRET. Nature Methods 5:507-16.

Sakahira H. and S. Nagata (2002). Co-translational folding of caspase-activated DNase with Hsp70, Hsp40, and inhibitor of caspase-activated DNase. J. Biol. Chem. 277:3364-70.

Schwede T. and N. Guex. "Scripting Language." Swiss-Pdb Viewer DeepView v4.0. <http://spdbv.vital-it.ch/script_guide.html>.

Segal B.H., X.Y. Wang, C.G. Dennis, R. Youn, E.A. Repasky, M.H. Manjili, J.R. Subjeck (2006). Heat shock proteins as vaccine adjuvants in infections and cancer. Drug Discov. Today 11:534-40.

Shi L., M. Kataoka, A.L. Fink (1996). Conformation characterization of DnaK and its complexes by small-angle X-ray scattering. Biochemistry 35:3297-308.

Singh L.R., S. Gupta, N.H. Honig, J.P. Kraus, W.D. Kruger (2010). Activation of mutant enzyme function *in vivo* by proteasome inhibitors and treatments that induce Hsp70. PLoS Genet. 6:e1000807

Strunk J.J., I. Gregor, Y. Becker, P. Lamken, S. Lata, A. Reichel, J. Enderlein, J. Piehler (2009). Probing protein conformations by in sit non-covalent fluorescence labeleing. Bioconjug. Chem. 20:41-6.

Stryer L., and R.P. Haugland (1967). Energy transfer: a spectroscopic ruler. Proc. Natl. Acad. Sci. 58:719-726.

Summerer D., S. Chen, N. We, A. Deiters, J.W. Chin., P.G. Schultz (2006). A genetically encoded fluorescent amino acid. Proc. Natl. Acad. Sci. USA 103:9785-9.

Swain J.F., G. Dinler, R. Sivendran, D.L. Montgomery, M. Stotz, L.M. Gierasch (2007). Hsp70 chaperone ligands control domain association via an allosteric mechanism mediated by the interdomain linker. Mol. Cell 26:27-39.

Swain J.F., E.G. Schulz, L.M. Gierasch (2006). Direct comparison of a stable isolated Hsp70 substrate-binding domain in the empty and substrate-bound states. J. Biol. Chem. 281:1605-11.

Tautz D. and M. Renz (1983). An optimized freeze-squeeze method for the recovery of DNA fragments from agarose gels. Anal. Biochem. 132:14-9.

Terpetschnig E. (2005). "Fluorescence Polarization." Innovations in Fluorescence: Technical Notes. <http://www.iss.com/resources/tech2/Polarization.pdf>.

Teter S.A., W.A. Houry, D. Ang, T. Tradler, D. Rockabrand, G. Fischer, P. Blum, C. Georgopoulos, F.U. Hartl (1999). Polypeptide flux through bacterial Hsp70: DnaK cooperates with trigger factor in chaperoning nascent chains. Cell 97:755-65.

Theyssen H., H.-P. Schuster, L. Packschies, B. Bukau, J. Reinstein (1996). The second step of ATP binding to DnaK induces peptide release. J. Mol. Biol. 263:657-670.

Thiol-Reactive Probes. Molecular Probes, Invitrogen. Revised 10-April-2006.

Vogta G., S. Woella, P. Argos (1997). Protein thermal stability, hydrogen bonds, and ion pairs. J. Mol. Biol. 269: 631-43.

Wilbanks S.M., L. Chen, H. Tsuruta, K.O. Hodgson, D.B. McKay (1995). Solution small-angle X-ray scattering study of the molecular chaperone Hsc70 and its subfragments. Biochemistry 34:12095-106.

Wisén S., J.E. Gestwicki (2008). Identification of small molecules that the protein folding activity of heat shock protein 70. Anal. Biochem. 374: 371-7.

Witt S.N. (2010). Hsp70 molecular chaperones and Parkinson's disease. Biopolymers 93:218-28.

Xiang T.X., Y. Li, Z. Jiang, A.L. Huang, C. Luo, B. Zhan, P.L. Wang, X.H. Tao (2008). RNA interference-mediate silencing of the Hsp70 gene inhibits human gastric cancer cell growth and induces apoptosis *in vitro* and *in vivo*. Tumori. 94:539-50.

Xu Z., P.B. Sigler (1998). GroEL/GroES: Structure and function of a two-stroke folding machine. J. Struct. Biol. 124:129-41.

Zahn R., S. Perrett, G. Stenberg, A.R. Fersht (1996). Catalysis of amide proton exchange by the molecular chaperones GroEL and SecB. Scienct 271:642-5.

Zhu X., X. Zhao, W.F. Burkholder, A. Gragerov, C.M. Ogata, M. Gottesman, W.A. Hendrickson (1996). Structural analysis of substrate binding by the molecular chaperone DnaK. Science 272:1606-14.

Zimmermann R. (1998). The role of molecular chaperones in protein transport into the mammalian endoplasmic reticulum. Biol. Chem. 379:275-82.

Zylicz M., F.W. King, and A. Wawrzynow (2001). Hsp70 interactions with the p53 tumour suppressor protein. EMBO J. 20:4634-4638.

Appendix

Construction of pMSK

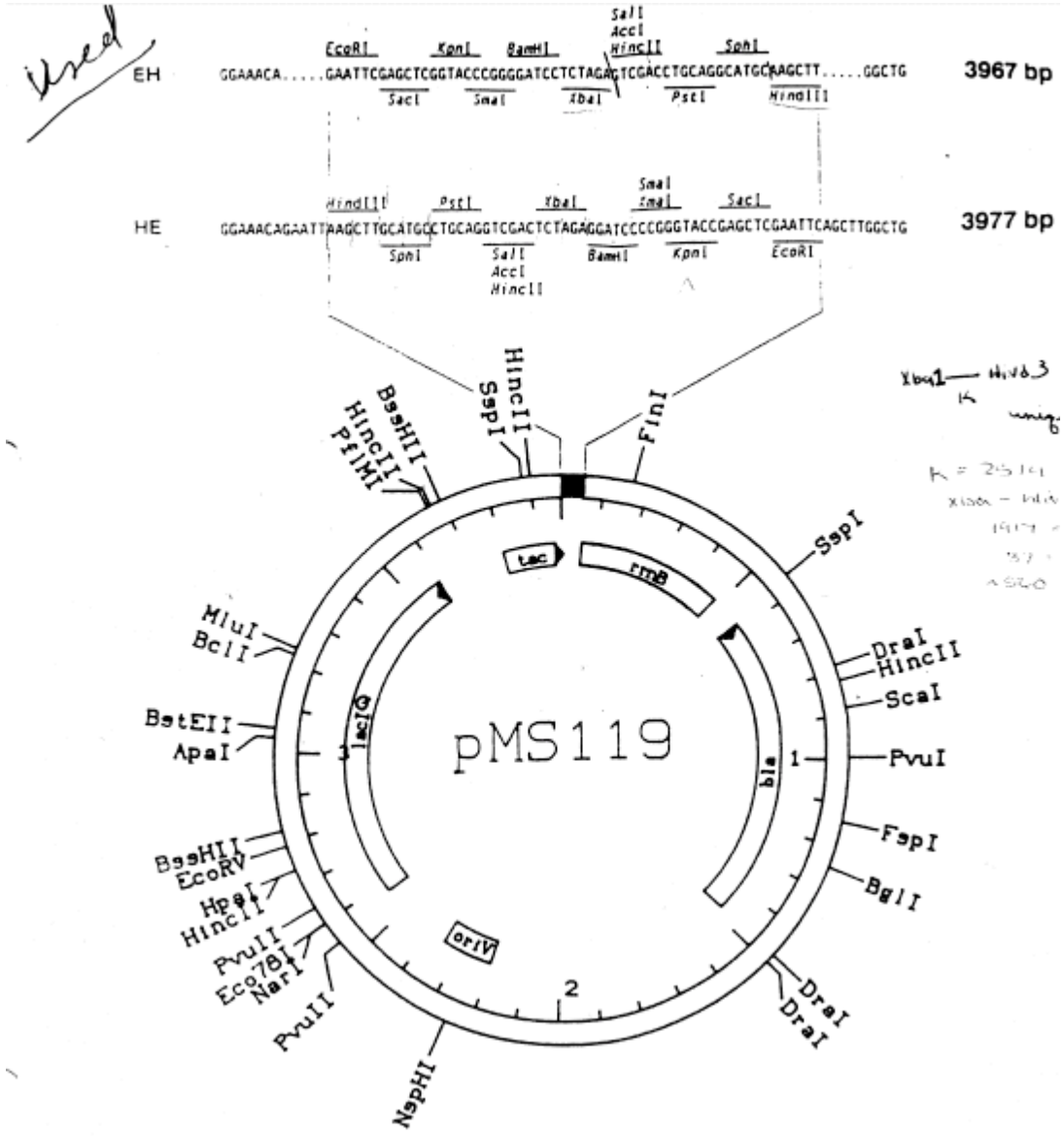

Figure 37. Map of pMS119-EH, the parent plasmid for pMSK. The DnaK gene was inserted using the 5' XbaI and 3' HindIII sites.

5' sequence of pMS119-EH

ATAACAATTTCACACAGGAAACAGAATTCGAGCTCGGTACCCGGGGATCCT…

5' untranslated region

…CTAGAAATAATTTTGTTTAACTTTAAGAAGGAGATATACAT…

WT DnaK sequence

…ATGGGTAAAATAATTGGTATCGACCTGGGTACTACCAACTCTTGTGTAGCGATT
ATGGATGGCACCACTCCTCGCGTGCTGGAGAACGCCGAAGGCGATCGCACCACG
CCTTCTATCATTGCCTATACCCAGGATGGTGAAACTCTAGTTGGTCAGCCGGCTA
AACGTCAGGCAGTGACGAACCCGCAAAACACTCTGTTTGCGATTAAACGCCTGAT

TGGTCGCCGCTTCCAGGACGAAGAAGTACAGCGTGATGTTTCCATCATGCCGTTC
AAAATTATTGCTGCTGATAACGGCGACGCATGGGTCGAAGTTAAAGGCCAGAAA
ATGGCACCGCCGCAGATTTCTGCTGAAGTGCTGAAAAAAATGAAGAAAACCGCT
GAAGATTACCTGGGTGAACCGGTAACTGAAGCTGTTATCACCGTACCGGCATACT
TTAACGATGCTCAGCGTCAGGCAACCAAAGACGCAGGCCGTATCGCTGGTCTGGA
AGTAAAACGTATCATCAACGAACCGACCGCAGCTGCGCTGGCTTACGGTCTGGAC
AAAGGCACTGGCAACCGTACTATCGCGGTTTATGACCTGGGTGGTGGTACTTTCG
ATATTTCTATTATCGAAATCGACGAAGTTGACGGCGAAAAAACCTTCGAAGTTCT
GGCAACCAACGGTGATACCCACCTGGGGGGTGAAGACTTCGACAGCCGTCTGAT
CAACTATCTGGTTGAAGAATTCAAGAAAGATCAGGGCATTGACCTGCGCAACGAT
CCGCTGGCAATGCAGCGCCTGAAAGAAGCGGCAGAAAAAGCGAAAATCGAACTG
TCTTCCGCTCAGCAGACCGACGTTAACCTGCCATACATCACTGCAGACGCGACCG
GTCCGAAACACATGAACATCAAAGTGACTCGTGCGAAACTGGAAAGCCTGGTTG
AAGATCTGGTAAACCGTTCCATTGAGCCGCTGAAAGTTGCACTGCAGGACGCTGG
CCTGTCCGTATCTGATATCGACGACGTTATCCTCGTTGGTGGTCAGACTCGTATGC
CAATGGTTCAGAAGAAAGTTGCTGAGTTCTTTGGTAAAGAGCCGCGTAAAGACGT
TAACCCGGACGAAGCTGTAGCAATCGGTGCTGCTGTTCAGGGTGGTGTTCTGACT
GGTGACGTAAAAGACGTACTGCTGCTGGACGTTACCCCGCTGTCTCTGGGTATCG
AAACCATGGGCGGTGTGATGACGACGCTGATCGCGAAAAACACCACTATCCCGA
CCAAGCACAGCCAGGTGTTCTCTACCGCTGAAGACAACCAGTCTGCGGTAACCAT
CCATGTGCTGCAGGGTGAACGTAAACGTGCGGCTGATAACAAATCTCTGGGTCAG
TTCAACCTAGATGGTATCAACCCGGCACCGCGCGGCATGCCGCAGATCGAAGTTA
CCTTCGATATCGATGCTGACGGTATCCTGCACGTTTCCGCGAAAGATAAAAACAG
CGGTAAAGAGCAGAAGATCACCATCAAGGCTTCTTCTGGTCTGAACGAAGATGA
AATCCAGAAAATGGTACGCGACGCAGAAGCTAACGCCGAAGCTGACCGTAAGTT
TGAAGAGCTGGTACAGACTCGCAACCAGGGCGACCATCTGCTGCACAGCACCCG
TAAGCAGGTTGAAGAAGCAGGCGACAAACTGCCGGCTGACGACAAAACTGCTAT
CGAGTCTGCGCTGACTGCACTGGAAACTGCTCTGAAAGGTGAAGACAAAGCCGC
TATCGAAGCGAAAATGCAGGAACTGGCACAGGTTTCCCAGAAACTGATGGAAAT
CGCCCAGCAGCAACATGCCCAGCAGCAGACTGCCGGTGCTGATGCTTCTGCAAAC
AACGCGAAAGATGACGATGTTGTCGACGCTGAATTTGAAGAAGTCAAAGACAAA
AAATAA…

560 bp of 3' untranslated sequence unknown, ending in Hind III site

3' sequence of pMS119-EH

…AAGCTTGGCTG

Creation of pMSK [T136C/S423C/C15S]: Sequencing

Figure 38. Segment of DNA sequence chromatogram for pMSK [T136C/S423C/C15S]. Sequencing was primed with DnaK 1021-1002 reverse primer. Thr→Cys (AGT→ACA) codon change at position 136 is labeled.

Characterization of Hsp70 activity modulators

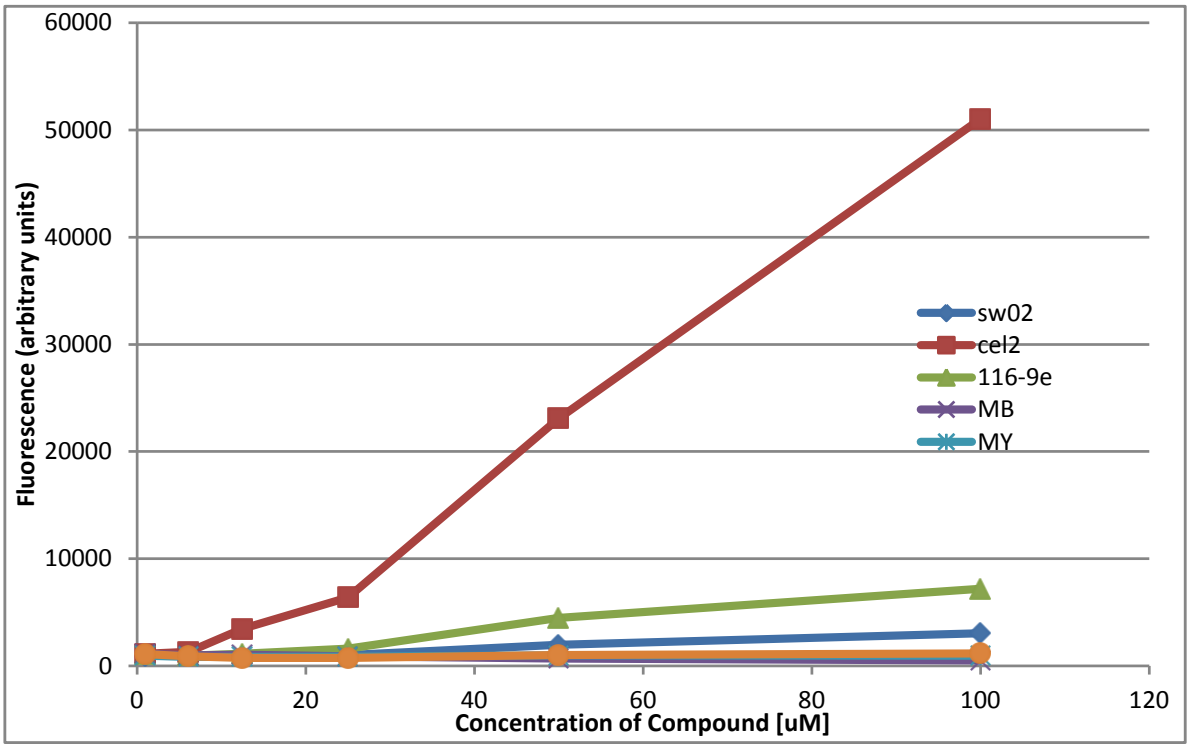

Figure 39. Fluorescence of Hsp70 activity modulators at various concentrations in gel filtration buffer. Experiment performed in 96-well plate format in the Polarstar fluorescence spectrophotomer.